Dynamics of passive mineral carbonation in ultramafic mining wastes and tailings

Thèse

Ali Entezari-Zarandi

Doctorat en génie chimique
Philosophiae doctor (Ph. D.)

Québec, Canada

Dynamics of passive mineral carbonation in ultramafic mining wastes and tailings

Thèse

Ali Entezari-Zarandi

Sous la direction de :

Faïçal Larachi, directeur de recherche

Georges Beaudoin, codirecteur de recherche

Benoît Plante, codirecteur de recherche

Résumé

L'élaboration de stratégies économiquement viables pour le stockage à long terme du dioxyde de carbone est devenue depuis quelques années un enjeu majeur en réponse aux préoccupations liées au réchauffement planétaire. Le captage et stockage du carbone (CSC) est considéré comme l'un des scénarios possibles visant à contrer le phénomène du réchauffement planétaire en ciblant le CO_2 atmosphérique. La carbonatation minérale – dans des plateformes de CCS – devrait être une option privilégiée pour la capture et le stockage permanent du carbone, connaissant la réactivité de matériaux alcalins tels que les silicates de magnésium et la brucite avec le dioxyde de carbone pour former des carbonates stables et respectueux de l'environnement. La carbonatation minérale passive des minéraux contenus dans les rejets ultramafiques pourrait être considérée comme une option économiquement attrayante en raison de la disponibilité de grandes quantités de rejets miniers riches en magnésium, de granulométrie très fine et hautement réactifs. De plus, les réactions impliquées dans la carbonatation minérale se font relativement facilement dans les conditions ambiantes. Le CO_2 est principalement dissous dans l'eau provenant de la pluie et de la fonte des neiges pour former des ions HCO_3^- et CO_3^{2-}. Des ions métalliques tels que le Mg^{2+} et le Ca^{2+} sont également lessivés dans l'eau permettant ainsi la formation de carbonates métalliques.

Des travaux expérimentaux de laboratoire ont été réalisés afin d'identifier la dynamique de la carbonatation minérale passive dans des conditions environnementales qui prévalent généralement dans les régions du Québec, au Canada. Une cellule de carbonatation à diffusion différentielle a été développée pour suivre la cinétique de carbonatation minérale

dans des conditions ambiantes. Les mesures cinétiques ont révélé le rôle complexe de l'eau à la fois dans le milieu réactionnel et en partie dans les processus de carbonatation. L'analyse par diffraction aux rayons X en fonction du temps et les observations au microscope électronique à balayage révèlent la formation de carbonates de magnésium intermédiaires, poreux et métastables qui ont ensuite évolué en couches de nesquehonite moins poreuses. Ces minéraux secondaires sont responsables de la passivation des surfaces malgré la disponibilité d'une partie de la brucite qui n'avait pas encore réagie. Cependant, les résultats ont montré que l'abrasion des surfaces de rejets préalablement carbonatés peut permettre l'exposition de surfaces fraiches permettant ainsi une carbonatation supplémentaire des résidus.

Des essais de carbonatation à température variable ont été effectués dans les plages de température chaude (35 ± 1 ° C), de laboratoire (23 ± 2 ° C), faible (5 ± 1 ° C) et de congélation (-5 ± 2 ° C) pour considérer les différences saisonnières. Les résultats suggèrent que la température a un effet notable sur la cinétique de carbonatation et une baisse de la température a provoqué un ralentissement de la réaction, bien que la carbonatation soit, d'un point de vue thermodynamique, définie comme une réaction exothermique. De plus, il a été observé que le séchage et les cycles de gel/ dégel étaient à l'origine d'un effet thermomécanique de "pelage" qui induit des microfractuations des couches de carbonates secondaires permettant à l'eau et au gaz de migrer et de réagir avec des sites donneurs de Mg.

L'analyse par spectroscopie FTIR a révélé que des carbonates de magnésium hydratés tels que la nesquehonite se forment parallèlement à la dissolution de la brucite pendant la carbonatation minérale des résidus miniers de nickel riches en brucite. Cependant, les résultats suggèrent aussi que la nesquehonite n'est pas le produit final de carbonate de magnésium hydraté. En effet, une surveillance à long terme (sur 2 ans) d'un matériau déjà carbonaté a révélé que la nesquehonite initiale a évolué en dypingite et en hydromagnésite, dépendamment de l'âge, des cycles de mouillage/séchage et de la profondeur où le carbonate initial s'est formé. Néanmoins, la nesquehonite pourrait maintenir sa stabilité sur des périodes prolongées si elle n'est pas soumise à des conditions humides.

Abstract

Developing economically feasible strategies for long-term storage of carbon dioxide has become over the past few years a major stake in response to the concerns over global warming. Carbon capture and storage (CCS) is widely believed to be one of the possible scenarios aimed in challenging the global warming phenomenon by targeting the atmospheric CO_2 content. Mineral carbonation – in the platform of CCS – is anticipated to be a premium option for permanent carbon capture and storage owing to the known reactivity of alkaline materials such as magnesium silicates and brucite with carbon dioxide to form stable and environmentally benign carbonates. Passive mineral carbonation of ultramafic mine waste and tailing minerals could be considered as an economically attractive option owing the availability of large amounts of magnesium-rich mining wastes, which are regarded to be virtually free, typically fine grained and highly reactive. Moreover, the energy input of nature is employed in passive mineral carbonation which is likewise free. In this way, CO_2 is mainly dissolved in water resulting from rain and snow season. Metal ions such as Mg^{2+} and Ca^{+} are also leached into the water allowing the formation of metal bicarbonate and consequently formation of metal carbonates.

Laboratory experimental works were done in order to identify the dynamics of passive mineral carbonation under environmental conditions prevailing the Quebec region, Canada. A differential diffusion carbonation cell was developed to monitor the kinetics of mineral carbonation under ambient conditions. The kinetic measurements revealed the

complex role of water both as reacting medium and moiety in the carbonation pathway. Time-dependent X-ray powder diffraction analysis and scanning electron microscopy reveal formation of transitional, metastable porous, flaky magnesium carbonates which subsequently evolved into less porous nesquehonite layers, which are shown to be responsible for surface passivation despite availability of unreacted brucite. However, surface abrasion was shown to liberate previously carbonated NIMT particles resulting in further carbonation on freshly exposed surfaces.

Temperature dependent carbonation tests were performed in the ranges of hot (35 ± 1 °C), laboratory (23 ± 2 °C), low (5 ± 1 °C), and freezing (-5 ± 2 °C) to mimic different seasonal conditions. Temperature had a notable effect on the carbonation kinetics and lowering temperature caused a reaction slowdown despite carbonation is thermodynamically defined as an exothermic reaction. Moreover, it was observed that drying and freeze/thaw cycles were at the origin of a thermomechanical "peel-off" effect which inflicted micro–fractures to the carbonate product layers enabling water and gas to engulf beneath and react with freshly unearthed Mg donor sites.

FTIR spectroscopy analysis revealed that hydrated magnesium carbonates such as nesquehonite are being formed parallel to brucite dissolution during mineral carbonation of brucite-rich nickel mining tailings. However, it was observed that nesquehonite is not the ultimate hydrated magnesium carbonate product. Long–term monitoring over 2 years of an already carbonated material revealed that the initial nesquehonite has evolved into dypingite and hydromagnesite depending on age, wetting/drying history and the depth where initial carbonate has been formed. Nonetheless, nesquehonite could maintain its stability over prolonged times if not being subjected to wet/ humid environmental conditions.

Table of contents

List of Tables

List of Figures

List of Abbreviations and Acronyms

[BG]	Gabbro rock sample
[Br]	Brucite
[CL]	Chrysotile/ Lizardite
[DU]	Dunite rock sample
[PD]	Peridotite rock sample
[VO]	Volcanic rock sample
BET	Brunauer-Emmett-Teller
Brg	Brugnatellite
BSE	Backscattered electron
CCS	Carbon capture and storage
CMR	Chrysotile Mining Residue
D	Dypingite
D80	80 W.%. of particles passing a giving sieve size
DNP	Dumont Nickel Project
EDX/EDS	Energy dispersive X-ray
FESEM	Field emission scanning electron microscope
G	Giorgiosite
GHG	Greenhouse Gases
H	Hydromagnesite
L	Lizardite
LC	Lower compartment
M	Magnetite

MS	Mass Spectrometer
N	Nesquehonite
NiMT	Nickel Mining Tailing
Q	Quartz
SEM	Scanning electron microscope
TDR	Time Domain Reflectometer
TGA	Thermogravimetric Analyzer
U	Unknown carbonates
UC	Upper compartment
XRD	X-Ray Diffraction

To my family

“The noblest pleasure is the joy of understanding.”

Leonardo da Vinci

“Nature and books belong to the eyes that see them.”

Ralph Waldo Emerson

Acknowledgment

I would like to express my gratitude to all those who have made this thesis possible. My deepest gratitude goes first and foremost to my supervisors, Professor Larachi, Professor Beaudoin and Professor Plante for giving me the opportunity to undertake this Ph.D. and for their scientific guidance during these years.

I would like to acknowledge the support of my parents, Mandana Hajjarian-Rezazadeh and Gholamreza Entezari-Zarandi for endless love and support during the time of this study. Furthermore, I would like to thank my sister Atena and my brother Amir and my extended family.

My sincere gratefulness to all my friends, an inspiring group of people especially Dariush Azizi, Shahab Boroun, Amir Motamed, Foroogh Abasian, Ommolbanin Ali Zadeh Sahraei, Olivier Gravel, Muhammad Khalid, Diana Aksenova, and Farnaz Ghoraishi. Special thanks to Dr. Gnouyaro Palla Assima for helping me in starting the project. I would like to thank El Hadji Babacar Kandji for his kindness in translating parts of this thesis into French and for helping with sample geochemical analysis.

I acknowledge all the people at Laval University, especially Jerome Nöel for his outstanding help in the fabrication and modification of different experimental setups. Marc Lavoie, Jean-Nicholas Ouellet and Yann Giroux.

I would like to thank for the financial support I received which enabled me to do this PhD. I am grateful for financial support from the Natural Sciences and Engineering Research Council of Canada (NSERC) and from RNC minerals (formerly Royal Nickle).

Finally, genuine appreciations to Professor Faïçal Larachi. It was an honor for me to be a part of your research group. Despite all the tough times to meet his high standards, I am deeply indebted for his guidance and patience.

Foreword

The work for this PhD thesis was carried out during 2014-2017 at the Département de génie chimique, Université Laval. This thesis comprises six chapters starting with the introduction, chapter 1, and ending with a conclusion, chapter 6. Chapters 2 and 3 represent articles published in scientific journals while chapter 4 is already submitted for publication (*International Journal of Greenhouse Gas Control*). Chapter 5 is an invited paper published in issue 50 of *Carbon Capture Journal* devoted to Leaders - CCS in Canada.

List of Publications

A. Entezari-Zarandi, F. Larachi, G. Beaudoin, B. Plante, M. Sciortino, Multivariate study of the dynamics of CO2 reaction with brucite-rich ultramafic mine tailings, International Journal of Greenhouse Gas Control 52 (2016) 110-119.

A. Entezari-Zarandi, F. Larachi, G. Beaudoin, B. Plante, M. Sciortino, Nesquehonite as a carbon sink in ambient mineral carbonation of ultramafic mining wastes, Chemical Engineering Journal 314 (2017) 160-168.

A. Entezari-Zarandi, F. Larachi, G. Beaudoin, B. Plante, M. Sciortino, Ambient Mineral Carbonation of Different Lithologies of Mafic to Ultramafic Mining Wastes/Tailings – A Comparative Study, International Journal of Greenhouse Gas Control 63 (2017) 392-400.

A. Entezari-Zarandi, F. Larachi, G. Beaudoin, B. Plante, B. Bussière, M. Sciortino, Ambient mineral carbonation of québec ultramafic mining wastes, Carbon Capture Journal 50 (Mar-Apr 2016) 8-11.

Part of the results were presented in the following conferences:

A. Entezari-Zarandi, F. Larachi, G. Beaudoin, B. Plante, Critical role of water during CO_2 sequestration in nickel mining residues under ambient conditions, 5th

International Conference on Accelerated Carbonation for Environmental and Material Engineering ACEME, 2015, New York City, USA.

A. Entezari-Zarandi, F. Larachi, G. Beaudoin, B. Plante, M. Sciortino, Hydrated Magnesium Carbonates, Formation and Stability in Ambient Conditions, 66th Canadian Chemical Engineering Conference, 2016, Quebec City, Canada.

Part of the results were presented in poster form in the following events:

- Sixth CGCC Annual Meeting, May 2015, Université Laval.
- Symposium 2015 sur l'environnement et les mines : de la science à la pratique, l'Université du Québec en Abitibi-Témiscamingue (UQAT)
- Seventh CGCC Annual Meeting, June 2016, Université de Montréal
- Colloque annuel de centre E4m, November 2016, Université Laval

Author's Contributions

Ali Entezari-Zarandi was responsible for design and modifications of experimental setup, planning and conducting the experiments, interpretation of the experimental results – in collaboration with Faïçal Larachi –, and for writing most of the text in the manuscript.

Chapter 1.

Introduction – State-of-the-Art and Objectives

1.1 A Global Warning – Global Warming

Six months before English naturalist (May 1859), geologist and biologist Charles Darwin publishes his *On the Origin of Species* to lay the foundation of evolutionary biology, a young Irish scientist John Tyndall experimentally established the physical basis for anthropogenic global warming. Researching on the Fourier's "theory of terrestrial temperatures" he brought evidences on higher energy absorption of water vapor, carbon dioxide and methane, in comparison to oxygen and nitrogen subjected to radiant heat [1]. Less than a century later, Charles D. Keeling could manage to start direct registering of atmospheric carbon dioxide concentrations (continued to this day) confirming the increasing trend in CO_2 accumulations in the atmosphere over the course of times [2]. Figure 1-1 presents the *Mauna Loa* record, or "Keeling Curve" of the atmospheric carbon dioxide concentration in background air.

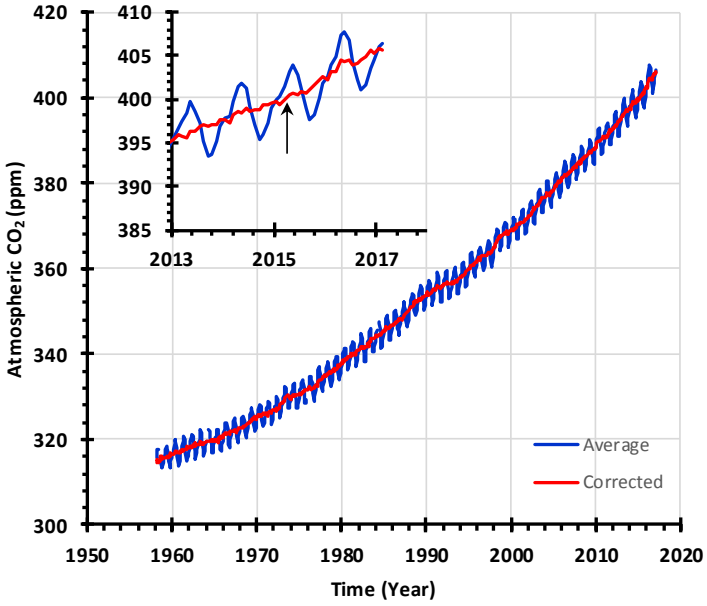

Figure 1-1. Monthly mean atmospheric carbon dioxide at Mauna Loa Observatory, Hawaii. **Blue line** accounts for mole fractions of carbon dioxide measured in dry air while **red line** represents the seasonally corrected data. Insert zooms on recent monthly mean measurements to date in which the black arrow pointes on the date when CO_2 concentration exceeded 400 ppm [3].

In 1990, Seifritz published a short scientific communication in Nature and proposed the idea of "Mineral carbonation" through carbonation of calcium silicates [4]. He warned about high energy requirements of the idea as well as possible slow kinetics of carbonation. Fortunately, the idea got attention and Lackner and coworkers investigated it in more detail at Los Alamos National Laboratory (LANL), USA [5, 6]. Identifying the reaction routes, Lackner and coworkers constructed a platform for future studies. Two approaches were considered: direct gas-solid carbonation and aqueous carbonation.

The Intergovernmental Panel on Climate Change published in its Fourth Assessment Report (AR4) "Most of the observed increase in global average temperatures since the mid-20th century is *very likely* due to the observed increase in anthropogenic greenhouse gases (GHG) concentrations" [7].

It is stated in the report that "human influence on the climate system is clear, and recent anthropogenic emissions of greenhouse gases are the highest in history." Figure 1-2 presents the total annual anthropogenic greenhouse gas emissions between 1970 and 2010.

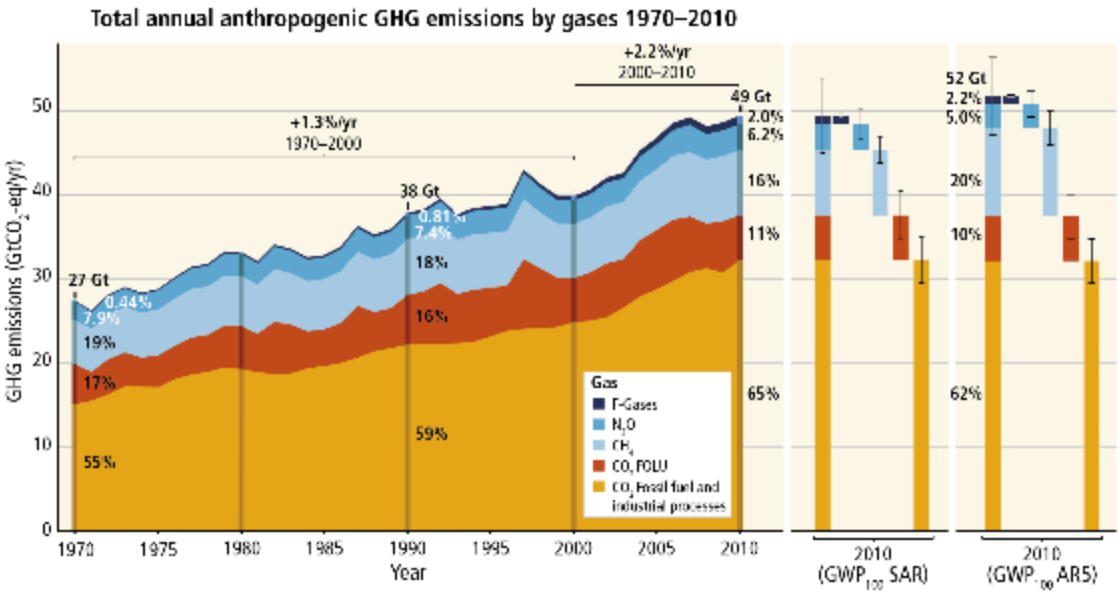

Figure 1-2. Total annual anthropogenic greenhouse gas emissions for 1970-2010 [8].

1.2 Mineral Carbonation

It is generally accepted that Carbon Capture and Storage (CCS) serves as a promising strategy to offset the anthropogenic CO_2 emission into the atmosphere. CO_2 sequestration in geological formations and mineral carbonation rank high among other strategies. While the former emphasizes on trapping gaseous, liquid, or supercritical carbon dioxide deep in geological formations, which requires monitoring of potential leakages into groundwater or back into the atmosphere, [9] the latter is implemented with minimal aboveground infrastructure to produce environmentally and chemically benign carbonates with no need for post-monitoring [10, 11].

Availability of large amounts of magnesium-rich mining wastes, which are regarded to be virtually free and typically fine grained could be considered as an economically attractive carbon capture and storage option [12]. Efforts are being made to introduce and optimize techniques on an industrial and global scale to permanently sequester atmospheric CO_2 in the form of stable mineral carbonates starting with mining and industrial residues [13-22]. Alkaline wastes such as steel slag [23-25], cement kiln dust [19, 26, 27], coal fly ash [28-30], saline waste water [31] and municipal solid wastes [32, 33] have been recently evaluated for their usefulness in carbonation. There are also a number of studies concerning the role of bacterial activity in mineral carbonation (Carbonate bio-mineralization) [34-36].

Mineral carbonation is defined as an exothermic reaction between a metal oxide bearing material and CO_2 [37]. The general reaction scheme can be written as:

$$MO + CO_2 \rightarrow MCO_3 + \text{Heat} \qquad (R-1)$$

Where M is a metal (alkaline earth), such as Mg. The released heat depends on the mineral being carbonated. Minerals of interest, reaction energy and the quantity required to sequester a unit weight of CO_2, assuming complete reaction of the mineral, is shown in Table 1-1 [38, 39].

Noticing the data in Table 1-1, in terms of volume of material required for the reactions, olivine group and especially its magnesium rich end member, forsterite (Mg_2SiO_4), is the most favored followed by brucite. In terms of volume of material produced (assuming

a final product porosity of 20%), olivine is outpaced by brucite with 4.09 and 2.92 cubic meters of product per tons of sequestered carbon, respectively [39]. Most of the carbonation reactions of minerals mentioned in Table 1-1 are thermodynamically favorable except for magnetite in which iron oxides have to be reduced to the divalent state. Brucite has the highest magnesium content than other raw materials, commonly used or considered for mineral carbonation. It is relatively soft (2.5 on the Mohs hardness scale) and has a low density (~2.40 g/cm^3) [40]. It is widely distributed in ultramafic rocks and its fibrous form, nemalite, coexists with chrysotile, the fibrous form of serpentine [41].

Table 1-1. Minerals of interest for mineral carbonation [38, 39]

Mineral	**Formula**	**Carbonation Products**	**Vol. min.* (m^3/ton C)**	**Heat gen.** (- kJ/mol CO_2)**	**Mg con.*** (wt. %)**
Olivine (Forstrite)	Mg_2SiO_4	$SiO_2 + 2MgCO_3$	1.82	88.65	25.4
Serpentine	$Mg_3Si_2O_5(OH)_4$	$2SiO_2 + 3MgCO_3 + 2H_2O$	2.98	64.13	26.3
Brucite	$Mg(OH)_2$	$MgCO_3 + H_2O$	2.02	81.10	41.7
Wollastonite	$CaSiO_3$	$CaCO_3 + SiO_2$	3.32	89.80	-
Basalt	Varies	$MgCO_3$, $CaCO_3$, $FeCO_3$	5.21	74.49	Assumed (11.5)
Magnetite	Fe_3O_4	$Fe_2O_3 + FeCO_3$	1.24	-9.50	-

* Volume of mineral reactant, ** Theoretical generated heat, *** Magnesium content.

The province of Quebec can be regarded as an important site for mineral carbonation because of the vast amounts of already mined and milled chrysotile wastes in southern parts as well as new working areas like Raglan Mine (ultramafic nickel) and the Dumont nickel

project in the northern part which will produce ultramafic tailings rich in chrysotile and brucite.

1.3 Mineral carbonation classification

Mineral carbonation of mafic and ultramafic (Alkaline) minerals mimics the natural weathering phenomena in which Ca-Mg-rich rocks react with atmospheric CO_2 (e.g. through dissolution in rain droplets) over geological timescales.

Mineral carbonation routes can be generally categorized in: a) ex-situ and b) in-situ carbonation. Figure 1-3 presents the suggested processes for mineral carbonation. The ex-situ process is the carbonation of alkaline minerals in mine tailings or wastes of other origin (e.g. slags and fly ashes) either in a direct or indirect manner. Direct carbonation refers to the process in which mineral is in direct contact with CO_2 (in an aqueous or dry medium) being carbonated in one step, but the idea behind indirect carbonation is the acid-, ammonium- or bio-aided extraction of the metal ions such as Ca or Mg from the material followed by a carbonation step (Figure 1-4). In situ carbonation involves CO_2 injection into a deep geological formation in order to produce carbonates. This route benefits from the high temperature/ pressure conditions of underground hydrothermal environments. A good indication of natural in situ mineral carbonation are the extensive outcrops of listvenite (fully carbonated peridotite) reported in *Samail Ophiolite*, Sultanate of Oman [42-44].

Direct and indirect carbonation can be divided into two schemes of gas–solid and aqueous carbonation. Gas–solid scheme was deemed to be the most straightforward carbonation pathway. It was soon understood that gas–solid carbonation may not be the best option due to very slow reaction rates for silicate minerals. This negative point is substantial to set aside advantages such as simpler process design and the possibility of reaction heat recovery (carbonation is an exothermic process). Few recent works in this field also do not seem to contribute in higher carbonation yields and technological advancements, although carbonation of Ca and Mg oxides or hydroxides seems to be more promising [45-47].

Typically, mafic rocks such as basalt and gabbro and ultramafic rocks such as serpentinite, peridotite, amphibolite and pyroxenite can be carbonated. However, the best candidates for large scale mineral carbonation are ferromagnesian minerals (e.g. olivine and

serpentine) as well as Ca rich minerals (e.g. plagioclase and amphibole), representing around 90% of ultramafic rocks [20].

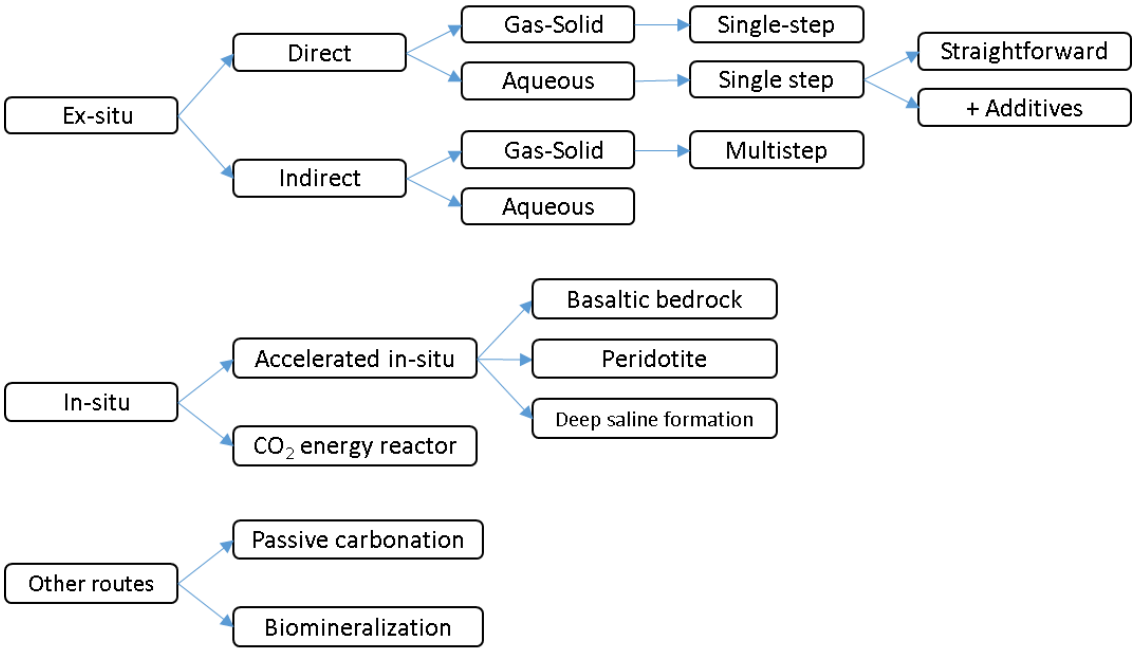

Figure 1-3. The summarization of researched and proposed mineral carbonation technologies [42].

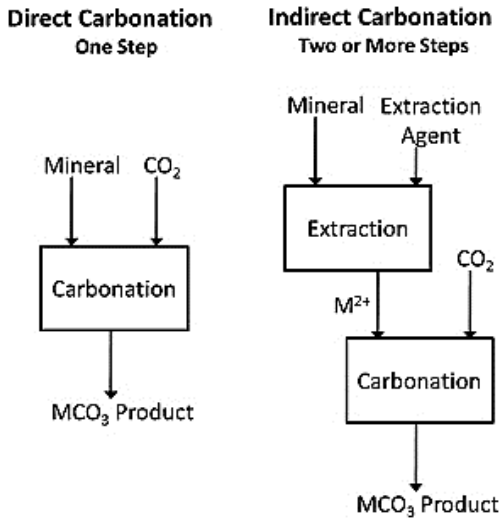

Figure 1-4. Direct and indirect mineral carbonation. M refers to metal ion [47].

1.4 Carbonation reaction and process chemistry

Increasing the reactive surface area and subsequently increasing the leaching rate of reactive metal ions (e.g. Mg^{2+} and Ca^{2+}) is possible by reducing the particle size. Since the size reduction process is highly energy intensive, the practical idea is to use already milled tailings from active process such ultramafic nickel ores or abandoned tailing dumps of asbestos mining. Particle passivation due to iron or silica gel formation can limit the diffusion of ions from and toward the particle surface. Different strategies like application of ultrasound or attrition aided reactions have been reported to be beneficial for driving the dissolution and extraction of metal species [17, 48].

Recent trends in strategy developments have proposed concepts accepting dilute CO_2 inputs, although not denying the necessity for chemical additives required for full metal ion recovery [49-51]. Thermal pretreatment (above ~600 °C) is another strategy to activate minerals such as serpentine group, expelling the chemically bound hydroxyls (OH) to consequently distort the crystal structure. The energy penalty associated with this scheme has been yet under debate.

Temperature positively affects mineral dissolution even though it hinders CO_2 dissolution. Sanna et al. used an ammonium salt to investigate the dissolution efficiency of olivine [52]. A dissolution efficiency of 77% during 3 hours of leaching at 100 °C (using 75–150 μm particle size) was achieved. It was found that formation of a passivation layer limits the diffusion. They calculated the apparent activation energy to be 62.8 kJ/mol.

Mineral carbonation is an example of a gas-solid-liquid system consist of different steps of solvation, hydration, reaction, dissolution and precipitation. In the case of brucite carbonation it can be presented as:

- Dissolution of CO_2 gas in pore water;
- Formation of H^+/H_3O^+, bicarbonate (HCO_3^-) and carbonate ions (CO_3^{2-});
- Diffusion of reactant H^+ through the liquid film to particles' surface;
- Reaction of H^+ ions with $Mg(OH)_2$;
- Dissolution of magnesium minerals into Mg^{2+} and OH^-;
- Diffusion/reaction of inorganic carbon with Mg^{2+} within liquid film.

The related reactions of mineral carbonation could be presented as [53]:

$$CO_2\ (q) \rightarrow CO_2\ (aq) \qquad (R-2)$$

$$CO_2\ (aq) + H_2O\ (l) \rightarrow H_2CO_3\ (aq) \qquad (R-3)$$

$$H_2CO_3\ (aq) \rightarrow H^+ + HCO_3^-\ (aq) \qquad (R-4)$$

$$HCO_3^-\ (aq) \rightarrow H^+ + CO_3^{2-}\ (aq) \qquad (R-5)$$

Serpentine

$$Mg_3Si_2O_5(OH)_4\ (s) + 3CO_2\ (aq) \rightarrow 3MgCO_3\ (s) + 2SiO_2\ (s) + 2H_2O\ (l) \qquad (R-6)$$

Olivine

$$Mg_2Si_2O_4\ (s) + 2CO_2\ (aq) \rightarrow 2MgCO_3\ (s) + SiO_2\ (s) \qquad (R-7)$$

Wollastonite

$$CaSiO_3\ (s) + CO_2\ (aq) \rightarrow CaCO_3\ (s) + SiO_2\ (s) \qquad (R-8)$$

Increasing pressure promotes the kinetics of CO_2 dissolution and increases the hydration of CO_2, thus shifting the reaction (R – 3) to the right. CO_2 solubility as well as solubility of carbonates in aqueous medium decreases with increasing temperature [54]. Steel et al. modeled the equilibrium concentrations of H_2CO_3, HCO_3^- and CO_3^{2-} in water as a function of CO_2 partial pressure (Figure 1-4) [55]. It can be inferred that despite increasing the CO_2 partial pressure, the concentration of carbonate ion stays at around 5×10^{-11} M and only the concentration of bicarbonate ion increases noticeably at higher CO_2 partial pressures.

While the near surface conditions are thermodynamically favorable for mineral carbonation, reaction kinetics are very slow [56]. Thus, various treatments have been examined to enhance reaction kinetics, such as: heat-pretreatment and pulverization [57]. These, however, are energy intensive operations and impose penalties on more CO_2 production. Enhanced reaction kinetics makes utilization of coarser-grained materials

possible (or comparatively higher carbonations for a given particle size), resulting in decreased total energy costs per net amount of CO_2 sequestered [56].

As it can be inferred from (R – 6), both dissolution and carbonate precipitation are pH-dependent processes. By increasing the acidity, minerals such as serpentine and olivine will be increasingly dissolved. However, carbonate formation will be possible only if the solution becomes supersaturated with respect to metal cations and bicarbonate (or carbonate) ions. As it can be seen in Figure 1-5, it is the H^+ that decreases the carbonate ion activity since protonation of the carbonate ion leads to the formation of bicarbonate. Further lowering the pH, bicarbonate ions will convert to carbonic acid, which decomposes into CO_2 and water.

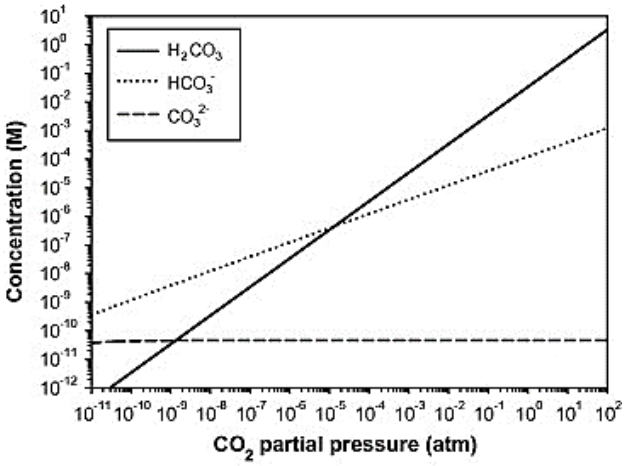

Figure 1-5. Effect of CO_2 partial pressure on carbonic acid dissociation [54].

Speaking of Nickel mining tailings (NiMT) as an example, they tend to increase the pH of the medium while the dissolution is only promoted by acidification. Conversely, high pH is required for efficient carbonate precipitation. In ambient conditions, environmental parameters such as temperature, CO_2 supply and water availability affects the formation of secondary carbonates such as nesquehonite ($Mg(HCO_3)(OH)\cdot 2H_2O$) and hydromagnesite ($4MgCO_3\cdot Mg(OH)_2\cdot 4H_2O$) which are reported to form normally on the surface of waste piles [21, 58-60].

1.5 Kinetics of mineral dissolution

A dissolution process is essential for releasing metal ions. Considering the general carbonation reaction of basic and ultrabasic rocks:

$$M_xSi_yO_{x+2y-t}(OH)_{2t} + x\,CO_2 \rightarrow x\,MCO_3 + y\,SiO_2 + t\,H_2O \qquad (R-9)$$

where M is divalent species, one may reach an idea about carbonation reactivity of minerals based on the standard Gibbs free energy of carbonation reactions listed in Table 1-2 (to be compared with acid minerals like albite feldspar) [61]. Energies are based on data from (1) Robie and Hemingway (1995) [62] and (2) Holland and Powell (1990) [63]. Chen and Brantley (2000) showed that the olivine dissolution is pH-temperature-dependent. In consistency with a surface protonation model, the dissolution rate becomes more pH-dependent, by increasing the temperature [64].

In contrast to salts which typically dissolve congruently, releasing stoichiometric amounts of elements, many silicates dissolve incongruently (at least for the initial step), leaving a silica skeleton depleted in alkalis and alkaline earths. Lasaga (1995) has proposed a general kinetic model for heterogeneous mineral-surface processes:

$$r = k_0 A_s e^{\frac{-E_a}{RT}} a_{H^+}^{n_H} \prod \left(a_i^{n_i}\right) g(I)\, f(A) \qquad (E-1)$$

where k_0 is the rate constant (mol/m^{2}s), A_s is the reactive surface area (m^2) which is not necessarily equivalent to surface area, $e^{-Ea/RT}$ accounts for effects of activation energy and temperature, $g(I)$ accounts for dependence of rate on ionic strength, $\Pi\,(a^{ni}{}_i)$ is the product of the activities of aqueous species such as H^+ for a given order n_i (e.g. $n = 1$ presents first order), and f(A) defines the dependence of rate on the distance from the equilibrium condition [65]. Particularly, the dissolution step is regarded to be the rate limiting step of the silicate minerals in carbonation processes [66].

Table 1-2. Standard Gibbs free energy of reaction for various carbonation reactions, adapted from Daval et al., (2009) [61].

Mineral	**Reaction**	**(1) *ΔGr* *(kJ/mol)***	**(2) *ΔGr* *(kJ/mol)***
Wollastonite	$CaSiO_3 + CO_2 \leftrightarrows CaCO_3 + SiO_2$	− 39.5	− 41.6
Olivine (forsterite)	$Mg_2SiO_4 + 2CO_2 \leftrightarrows 2MgCO_3 + SiO_2$	− 34.7	− 34.6
Basaltic glass	$MgSiO_3 + CO_2 \leftrightarrows MgCO_3 + SiO_2$	− 32.6	N.A.
Pyroxene (enstatite)	$MgSiO_3 + CO_2 \leftrightarrows MgCO_3 + SiO_2$	− 31.3	N.A.
Anorthite	$CaAl_2Si_2O_8 + CO_2 \leftrightarrows CaCO_3 + 2SiO_2 + Al_2O_3$	− 20.4	− 22.3
Magnetite	$Fe_3O_4 + CO_2 \leftrightarrows FeCO_3 + Fe_2O_3$	− 18.6	− 20.2
Serpentine (chrysotile)	$Mg_3Si_2O_5(OH)_4 + 3CO_2 \leftrightarrows 3MgCO_3 + 2SiO_2 + 2H_2O$	− 18.1	− 17.9
Talc	$Mg_3Si_4O_{10}(OH)_2 + 3CO_2 \leftrightarrows 3MgCO_3 + 4SiO_2 + H_2O$	− 14.0	− 14.9
Albite	$2NaAlSi_3O_8 + CO_2 \leftrightarrows Na_2CO_3 + 6SiO_2 + Al_2O_3$	52.4	N.A.
Brucite	$Mg(OH)_2 + CO_2 \leftrightarrows MgCO_3 + H_2O$	-35.06 [59]	
	$Mg(OH)_2 + CO_2 + 2H_2O \leftrightarrows MgCO_3 \cdot 3H_2O$	-38.73 [67]	

Kinetics of mineral dissolution/precipitation are mostly addressed by Transition State Theory (TST) assuming that: 1) reactants have to pass an energy barrier, referred to as the activated complex, to yield products; and 2) dissolution and precipitation is driven by the direct and reversible attachment of reactants at mineral surface sites. In the words of TST, (E – 1) can be thus rewritten as:

$$r = r_+ \left(1 - e^{\left(\frac{A}{\sigma RT}\right)}\right) \quad , A = RT.\ln\Omega \qquad \text{(E – 2)}$$

where r_+ is the forward rate, σ describes the Temkin's stoichiometric number which is the ratio of the destruction rate of the activated complex to the overall reaction rate, Ω stands for the degree of saturation, T is temperature, and R is the universal gas constant. Schott et al., (2012) report that due to possession of sufficient reactive sites, Brucite and hydromagnesite have dissolution and growth rates compatible with the classical TST rate law at close to equilibrium conditions (|ΔG| < 0.5 kJ/mol) [68].

For systems in which dissolution conditions are far from equilibrium, Krevor and Lackner [56] have used rate expression of:

$$r = k_0 a_i^{n_i} e^{(-E_a/RT)} \qquad \text{(E – 3)}$$

The solution species dependence, n, can be derived by obtaining dissolution rates in solutions with various species activities. They summarized the published values of proton promoted serpentine and olivine dissolution as provided in Table 1-3.

Table 1-3. Dissolution rates of olivine and serpentine [56].

Mineral	k_0 **[mol/cm^{2}s]**	n	E_a **[kJ/mol]**
Olivine	0.0854	0.46	52.9
Serpentine	0.028	0.24	70

1.6 Mineral carbonation of mining and mineral processing tailings

Transformation of (ultra)mafic mine tailings and wastes into carbonate precipitates in storage facilities may be regarded as the driving force for sustainable mining practice [69]. Abandoned asbestos mines (Chrysotile Mining Residues - CMR) as well as the widespread Mg-silicate rich rocks such as Ni-sulphide and Platinum-group element deposits of ultramafic complexes are the first targets. The alkaline mine tailings are appropriate candidates as they are already crushed and milled and can be regarded as virtually free and easy to access material [70].

Bodénan et al. outlined the results of the Carmex project (a four-year project concerned about the ex-situ mineral carbonation of different mafic/ultramafic mining wastes). They used GIS (Geographical Information System) to match significant and accessible waste points to CO_2 emission posts. In the framework of the project, three material types associated with mining sector were tested: harzburgite, wehrlite and lherzolite. Although they did not intend to follow ambient condition mineral carbonation, they were able to verify that different rocks present significantly different reactivities. They concluded that the degree of serpentinization should not be the only criterion affecting reactivity and parameters such as mineralogical composition differences are also of great importance [20].

While ex-situ carbonation of mining wastes in aqueous media is believed to be the most promising technique in permanent carbon sequestration, understanding the passive mineral carbonation in ambient conditions is of great importance. It has been shown in the literature that the surface of mining waste dumps undergoes passive carbonation by reaction with meteoric showers and atmospheric CO_2 [71-73]. Wilson et al. reported that passive atmospheric CO_2 uptake of Mount Keith NiMT offsets 11% of the mine's annual emissions [60]. Another example is the huge store of ca. 2 Gt of chrysotile mining residues accumulated in southern Québec with a potential to store up to 700 Mt of atmospheric CO_2 by mineral carbonation [74].

1.7 State of knowledge in mineral carbonation

Mine extraction and mineral processing tailings accrued in an open ground would encounter relatively faster weathering due to their higher surface area. In this manner, cations, such as magnesium and calcium as well as atmospheric carbon dioxide will go in rain water and metal carbonates will gradually precipitate. Presence of microorganisms can also promote carbonate formation. Power et al. proposed the use of *Acidithiobacillus* to enhance chrysotile dissolution by accelerating the oxidation of acid-generating material and lowering the pH [36, 75, 76].

They suggested a Geo-engineered design for tailing dumps in which rain waters firstly pass the acid-generating materials covering the ultramafic deposits. The run-off waters

could be drained into a closed pond where carbonate precipitation can be promoted to sequester CO_2 either by evaporation or by *cyanobacteria* (Figure 1-6). Cyanobacteria is proposed as it can induce the precipitation of carbonate species by making their micro-environment more alkaline.

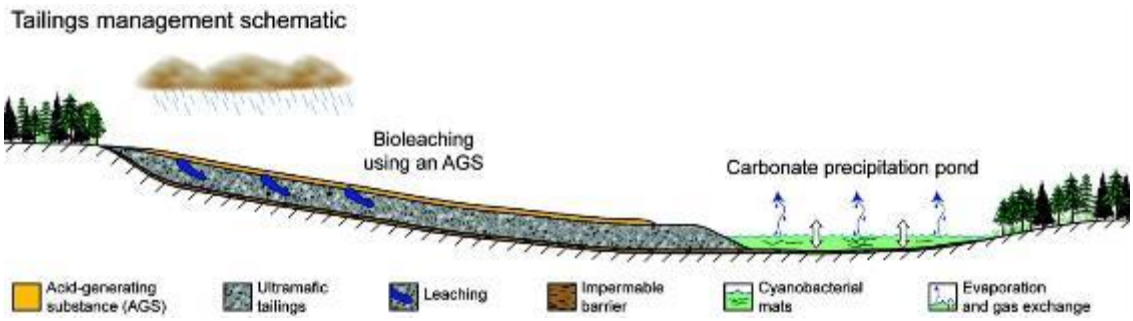

Figure 1-6. Schematic representation for a geo-engineered tailing site [36].

Room temperature carbonation of natural brucite at moderate partial pressures of carbon dioxide was studied by Zhao et al. in 2010 [59]. Brucite has the highest reactivity toward mineral carbonation, nonetheless it has got little attention mainly due to its scarcity, in comparison with serpentinite minerals. Although thermodynamically favorable, brucite carbonation in ambient conditions is slow. They studied brucite carbonation kinetics in an aqueous medium at room temperature and constant CO_2 gas pressure of 15 atm in headspace.

Employing Fourier Transform Infrared Spectrometry (FT−IR) and X-ray diffraction (XRD) to determine the mineral composition and observe the reaction, they could trace the carbonation in course of time. Time-dependent XRD revealed that the crystalline carbonate species start to appear within the first 30 minutes of reaction. About 95% of the carbonated material was estimated to be nesquehonite after 150 min of reaction (with the rest as hydromagnesite and dypingite). The reaction medium was composed of 20.88 g of brucite in 300 mL of distilled deionized water (DDW) or diluted HCl (0.39 mol/L). Surprisingly, in HCl solutions, lower concentration of nesquehonite was observed (78%) and chlorartinite ($Mg_2(CO_3)Cl(OH)\cdot 3H_2O$) was formed instead of hydromagnesite [59].

Gerdemann et al., 2007 have studied the aqueous mineral carbonation in an ex-situ mood. Employing the optimum conditions (185 °C with 150 bars of CO_2 in solutions of 0.64 M $NaHCO_3$ and 1 M NaCl), 80% carbonation rate for olivine after 6 h was reported. Magnesite ($MgCO_3$) was formed as the final carbonate. Comparing the composition and characteristics of freshly fractured olivine crystals with carbonated samples under different conditions of temperature and pressure they determined the secondary products formed and their differences by changing the reaction conditions [57].

An original method was developed by Pronost et al., in 2011 for real time monitoring of CO_2 consumption [15]. The experimental setup was composed of modified eudiometers (Figure 1-7), enabled them to follow the kinetics of the reaction and to determine the critical parameters controlling carbonation of ultramafic residues. Having a simple design, it was possible to utilize a number of eudiometers in order to follow the carbonation kinetics of several samples simultaneously.

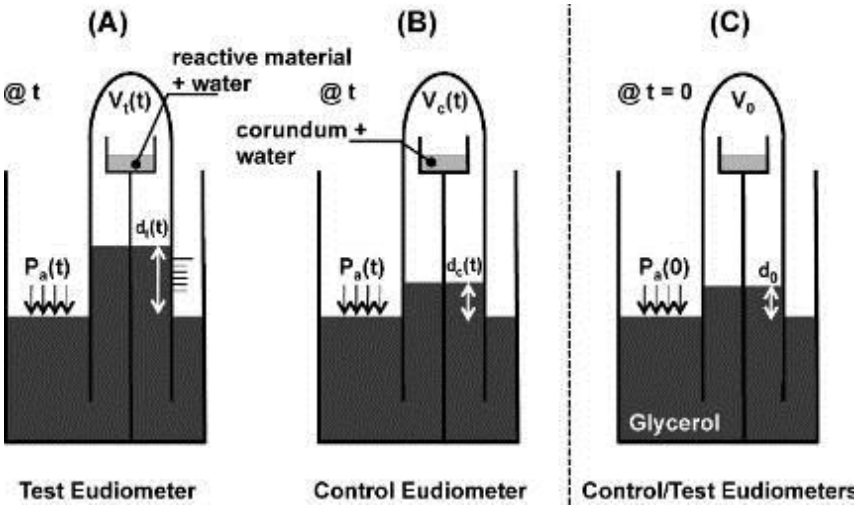

Figure 1-7. Schematic presentation of direct and indirect mineral carbonation [15].

Samples of ultramafic mining waste from the two different sites were studied under variable conditions of CO_2 partial pressure, particle size, relative humidity, and temperature, to determine optimal conditions for mineral carbonation. The CO_2 consumption was monitored in course of reaction while changes in mineralogy and identification of the

carbonate mineral products under various experimental conditions were determined after using XRD. Performing experiments in a temperature-controlled room (in two ranges of 21 °C and 33 °C) revealed that the mineralogy of neo-formed carbonates is dependent on the temperature. The XRD analysis confirmed nesquehonite ($Mg(HCO_3)(OH)\cdot 2H_2O$) and dypingite ($Mg_5(CO_3)_4(OH)_2\cdot 5H_2O$) as the dominant carbonation products at 21 °C and 33 °C respectively.

In 2014, Hemmati et al., studied carbon dioxide mineralization using a multi-step pH-swing process at different temperatures. They could similarly verify different forms of magnesium carbonate to be obtained at different reaction temperatures. While dypingite was obtained at higher temperatures (60 °C), in near ambient temperatures (10, 20, 30, 40, 50 °C), nesquehonite was the predominant form of magnesium carbonate obtained. However, hydromagnesite formation is reported to occur at low temperatures (10 °C) which seems not to be valid [77].

Normally, under ambient conditions, the metastable hydrated carbonate phases interfere with the production of magnesite because of a slower magnesite nucleation and crystal growth [78]. The formation of nesquehonite at ambient temperature and atmospheric CO_2 pressure, whether in aqueous media [59, 79] or with brucite-rich mining residues [16, 59, 80] is well documented in the literature. Lansfordite, $MgCO_3\cdot 5H_2O$ may form during low-temperature carbonation. However, it transforms into nesquehonite at temperatures over 10 °C [73, 81].

Swanson et al. reviewed different magnesium carbonate phases depending on Mg^{2+} source, e.g., magnesium salt or hydroxide [78]. They showed that seeding the carbonating medium with magnesite favored the formation of such anhydrous carbonate instead of nesquehonite and hydromagnesite [78]. Table 1-4 lists the common magnesium carbonates that may form at near ambient conditions while Table 1-5 presents the dependency of different (hydrated) carbonate formation on temperature and partial pressure of CO_2.

Table 1-4. Common magnesium carbonates forming near ambient conditions.

Carbonate mineral	**Formula**
Artinite	$Mg_2(CO_3)(OH)_2 \cdot 3H_2O$
Nesquehonite	$Mg(HCO_3)(OH) \cdot 2H_2O$
Hydromagnesite	$Mg_5(CO_3)_4(OH)_2 \cdot 4H_2O$
Dypingite	$Mg_5(CO_3)_4(OH)_2 \cdot 5H_2O$
Magnesite	$MgCO_3$

Research conducted by Assima et al. showed that carbonation is quite sensitive to water saturation and watering frequency of mineral layers. Columns packed with chrysotile mining residues (CMR) particles were used to study their carbonation behavior under environmental conditions [82].

These kind of residues are important potential sinks for carbonation as there are huge stores of already mined and crushed material in abandoned asbestos mines (e.g. the ca. 2 Gt waste heaps of CMR in Québec, 10 Mt deposit of Clinton Creek mine in Yukon or at least 17 Mt of CMR in Cassiar mine, British Colombia) [72, 74, 83]. The study was concerned with both mineral dissolution and carbonation. During leaching, the pH was allowed to freely drift until it stabilized. It was found that although brucite is the main soluble phase of the residue, chrysotile is also partially dissolved. Logically, Mg extraction was favored by lowering the initial pH. Surface passivation of the particles was reported due to the formation of a silica phase as a product of polymerization of fine silica as well as the appearance of a yellowish color deposit at pH 3 (supposed to be iron hydroxide). However, studying the carbonation of wollastonite at 90 °C and 250 bar Daval et al. proposed that the formation of a silica-rich layer over the silicate particles is not going to passivate the surface as such a layer is indeed porous [61].

Table 1-5. Dependency of magnesium carbonates to temperature and CO_2 partial pressure (modified after [78]).

Researcher	**Carbonate**	***p*CO₂ (atm)**	**Carbon source**	**Temp. (°C)**
Ming, 1985	Landsfordite	3.91×10^{-4}	CO_2	4
Smithson, 1973	Landsfordite	3.91×10^{-4}	CO_2	9
Cheng, 2009	Nesquehonite	3.91×10^{-4}	Na_2CO_3	10
Park, 2003	Nesquehonite	15	CO_2	20
Ballirano, 2010	Nesquehonite	1.00	CO_2	20
Montes-Hernandez, 2012	Dypingite	50	CO_2	20
Assima, 2012	Magnesite	1.00	CO_2	22
Assima, 2013	Nesquehonite	1.00×10^{-1}	CO_2	22
Hanchen, 2008	Nesquehonite	9.90×10^{-1}	Na_2CO_3, CO_2	25
Pronost, 2011	Dypingite	3.30×10^{-1}	CO_2	33
Cheng, 2009	Nesquehonite	3.91×10^{-4}	Na_2CO_3	40
Vagvolgyi, 2008	Nesquehonite	3.91×10^{-4}	HCO_3^-	45
Davis, 1973	Nesquehonite	3.91×10^{-4}	CO_2	60
Zhang, 2006	Nesquehonite	3.91×10^{-4}	K_2CO_3	75
Vagvolgyi, 2008	Hydromagnesite	3.91×10^{-4}	Na_2CO_3	45
Cheng, 2010	Hydromagnesite	3.91×10^{-4}	Na_2CO_3	50
Zhang, 2006	Hydromagnesite	3.91×10^{-4}	K_2CO_3	80
Cheng, 2010	Hydromagnesite	3.91×10^{-4}	Na_2CO_3	90
Schaef, 2011	Magnesite	81.2	CO_2	75
Swanson, 2014	Magnesite, hydro.	15	CO_2	80

A battery of quartz tubes served as carbonation cells where specified amounts of CMR were placed in each tube while a 10% CO_2 stream (balanced with air) was passing through the solid at room temperature. Different environmental conditions applied and results were compared to understand the carbonation behavior: 1) dry CMR, dry CO_2 stream; 2) dry CMR, humid CO_2 stream and 3) partially saturated CMR, humid CO_2 stream (rain shower imitation). No meaningful carbonation was inferred out of the first scenario indicating that passing dry CO_2 through a dry CMR bed (during 4 days) is not an option in environmental carbonation of this type of material. A humid CO_2 stream passing through a dry CMR bed was not promising as well. Pre-wetting of the CMR bed was effective and showed the stimulating role of water on mineral carbonation.

It was found that by increasing the pore water saturation, more carbonation was achieved. Speaking of total amount of added water, $MgCO_3$ conversion was positively correlated with watering frequency and in this manner, four episodes of 25% wetting was more beneficial in comparison with one shower episode of 100%. Following this logic, four episodes of 12.5% water saturation every 24 h were more beneficial, leading $MgCO_3$ conversion of 7.4 wt %. It is reasoned by the fact that Mg reaches the super-saturation state faster when the amount of water is reduced, which in turn leads to an increase in pH, which are both favorable for carbonate precipitation.

In conclusion, while there is virtually no carbonation of dry material in contact with dry gas (i.e., moisture free), the carbonation degree of partially wetted materials exposed to dry/humid gas was noticeable. Also, little carbonation was found in case of dry material traversed for several days by humid gas streams [82].

In 2009, Wilson and co-workers studied the Clinton Creek and Cassiar chrysotile waste deposits in western Canada, providing information on accelerated weathering of milled CMR in contact with air [72]. The dramatic increase in surface area due to ore milling was reasoned to be responsible for faster mineral carbonation. Different hydrated magnesium carbonate minerals were identified in the samples obtained from different parts of the tailings. It was understood from field observations and isotopic data that carbonates form in two main regions. Nesquehonite was formed on top of tailings (evaporative region) while dypingite and hydromagnesite were formed mainly deeper (subsurface region) with characteristics

similar to soil carbonate. Alongside with hydrated magnesium carbonate minerals such as nesquehonite, dypingite, and hydromagnesite, they also have detected small quantities of lansfordite, which is surprising. While the environmental conditions are favorable for its formation, they reported that the sampling was performed in the dry days of summer and the samples were dried for 48 hours under a drying hood. Lansfordite is known to be unstable in temperatures above 10 °C and gradually transform into nesquehonite. They could distinguish four distinct modes of hydrated magnesium carbonate and calcium carbonate minerals occurrence in their study area: 1) crusts on top and walls of the deposit, 2) disseminated precipitates cementing tailings grains together in the depth of the pile, 3) thin carbonate formations on the cobbles of serpentine (<1 mm in thickness), and 4) precipitates lining the beds of runoff waters (reported just in the Cassiar site). While nesquehonite, dypingite, hydromagnesite, and to much lesser extent lansfordite were typically found in the crusts, heavy cements of hydromagnesite (up to 10 wt. %) were observed within the pile (at a depth of 2 m). This suggests that hydromagnesite may precipitate preferentially and there is a hydrological control on its development [84]. They estimated that the annual sequestration capacity of a large mine like Mount Keith Nickel mine, Australia, exceeds the annual CO_2 emissions of the mine by more than a factor of ten.

Unluer and Al-Tabbaa characterized hydrated magnesium carbonates using thermal analysis. They put the minerals in two categories of so called “light” and “heavy” hydrated magnesium carbonates. *Light* hydrated magnesium carbonates refer to those with the empirical formula of $4MgCO_3 \cdot Mg(OH)_2 \cdot 4H_2O$, corresponding to hydromagnesite, while *heavy* hydrated magnesium carbonates refer to those having the empirical formula corresponding to dypingite: $4MgCO_3 \cdot Mg(OH)_2 \cdot 5H_2O$ [85].

As a result of microstructure and thermal decomposition characterization of seven different commercially produced hydrated magnesium carbonates by TG/DTA, SEM, XRD, and HCl acid testing, they were able to characterize light and heavy carbonates: heavies present a relatively non-porous structure while lights are more porous, probably due to more widely dispersed arrangement of particles. From TG results, it can be inferred that the chemical compositions of the hydrated magnesium carbonates (obtained by XRD) do not

exactly fit into the fixed stoichiometry in the $MgO–CO_2–H_2O$ system, suggesting the CO_2 presence in other types of carbonates (probably amorphous).

Different hydrated magnesium carbonates which may form in the $MgO–CO_2–H_2O$ system are listed in Table 1-6. Nesquehonite is stable at room temperature. There are different works reporting the formation of nesquehonite in the temperature range of 20-70 °C, however, nesquehonite tends to lose water to transform into a structure similar to hydromagnesite by heating above 50 °C. As Canterford et al. stated several decomposition mechanisms seem possible for nesquehonite and it is quite clear that hydromagnesite is the final product [86]. By further increasing the temperature (126 °C or higher) hydromagnesite transforms into magnesite.

Table 1-6. Compounds forming in the $MgO–CO_2–H_2O$ system (modified after [85]).

Chemical formula	**Compound**	**MgO moles**	**H_2O moles**	**CO_2 moles**
$MgCO_3·2H_2O$	Barringtonite	1	2	1
$MgCO_3·3H_2O$	Nesquehonite		3	1
$MgCO_3·5H_2O$	Lansfordite		5	1
$Mg_2(CO_3)(OH)_2·0.5H_2O$	Pokrovskite	2	1.5	1
$Mg_2(CO_3)(OH)_2·3H_2O$	Artinite		4	1
$Mg_5(CO_3)_4(OH)_2·4H_2O$	Hydromagnesite	5	5	4
$Mg_5(CO_3)_4(OH)_2·5H_2O$	Dypingite		6	4
$Mg_5(CO_3)_4(OH)_2·5\text{-}6H_2O$	Giorgiosite		6–7	4
$Mg_7(CO_3)_5(OH)_4·24H_2O$	Shelkovite	7	25	5
$Mg(OH)_2$	Brucite		1	–
$MgCO_3$	Magnesite		–	1

Beinlich and Austrheim did a field study in 2012 to investigate low temperature carbonate formation during weathering of ultramafic rocks [73]. The study site was chromite mine shafts in the Feragen ultramafic body, eastern Norway. Mining activities in this area were stopped in the mid-1920s indicating that the observed mineral carbonations were due to anthropogenic CO_2 sequestration. Millimeter to centimeter thick pure lansfordite was detected coating serpentinized peridotite host rock. Alongside with in situ rock analysis, samples of mine run-off waters and sub-aerial ponds were taken. It was found that upon infiltrating into the shafts, rainwater reacts rapidly with the brucite content of peridotites producing an alkaline water, which upon contact with cold and dry air circulation evaporates and forms thin films of carbonate mineral on walls and ceiling. Air circulation was determined as an important factor driving ambient carbonation to depth; mineral carbonation was found throughout the mines where natural ventilation (due to the presence of two or more entrances) caused air circulation. In contrast, in mines with only one entry, mineral carbonation was limited to the near entry area and not deeper (Figure 1-8).

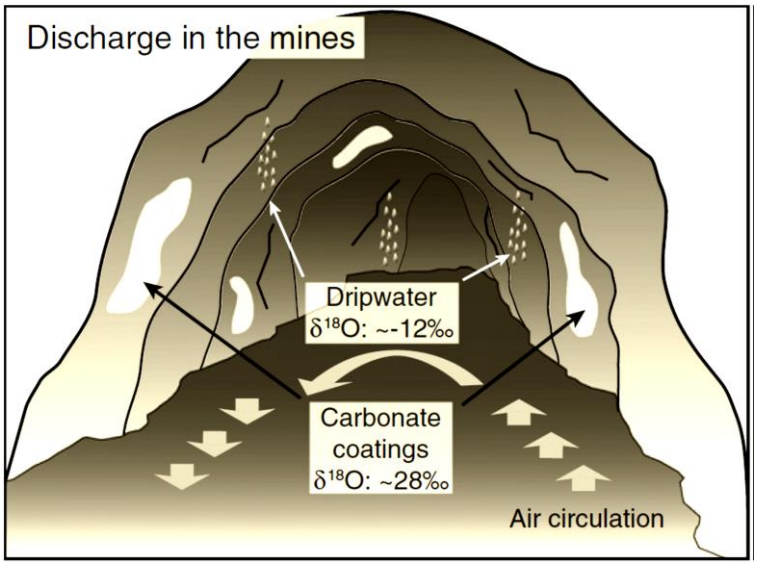

Figure 1-8. Surface carbonate formation in the Feragen chromite mines [73].

Another part of their study was the presentation of surface fragmentation and cracking due to: a) weakening caused by brucite dissolution and b) stress build-up owing to carbonate

formation and crystallization in fractures close to the surface. As authors claimed, the later "represents a positive feedback mechanism" because of providing fresh, reactive surface area during carbonation. Under atmospheric partial pressures of CO_2, the lansfordite–nesquehonite equilibrium was estimated to be between 8.5 and 12 °C. Above 20 °C lansfordite transforms rapidly into nesquehonite [87]. Having this in mind, the absence of nesquehonite in the samples gives a good estimation of the temperature regime in the mine shaft (barely exceeded 12 °C).

In 2013, Assima et al., assessed the impact of mining residue mineralogy and its grain size, gas composition, water saturation, and watering frequencies on carbonation. A fixed-bed reactor was designed and instrumented for online monitoring of the gas composition while solid samples were likewise taken for post-mortem analyses. As it was expected fines have the highest and the coarse fraction has the lowest carbon uptake. Post-mortem analysis of the reacted materials showed that chrysotile carbonation was controlled by fiber length. It was observed that the carbonation has a cementing action, keeping the particles together, preventing the fibers from being blown away by convective circulation of air in the packed-bed cell [88].

Another finding in this study was the effect of fiber length and brucite content on CMR carbonation. Short (38–53 μm) and long (800–1180 μm) chrysotile fibers were mixed with powdered brucite (under 2 mm), in different concentrations of 2, 5, 10, 15 and 20 wt.%. Generally speaking, addition of longer fibers promoted slightly carbonation while shorter fibers had inverse effect on carbonation. The effect of brucite doping was positive as it was highlighting its role in CMR reactivity. Gas composition had a direct effect on the extent of residue carbonation, higher the CO_2 content, higher the CMR carbonation. Periodic additions of water provided deeper carbonation probably due to alteration of silica polymerization thus the bulk of the CMR remains accessible for further reactions.

While ultramafic wastes are promising sinks for CO_2 sequestration, their alkaline nature upon contact with rain can pose serious concerns on alkaline rock drainage. Although high alkalinity of the medium is essential for the formation of carbonated species, high pH run-off waters can be harmful to the environment either because compounds which are sparingly soluble in neutral water may be become soluble in alkaline media, or, on the

contrary, being already dissolved in neutral pH may precipitate in the alkaline environment [89-93]. Furthermore, Canada's metal mining effluent regulations (MMER) stipulates that the discharge of alkaline waters with pH > 9.5 is prohibited. The mine effluent effects on the aquatic receiving environment such as fish habitat have to be evaluated under MMER [94]. Mineral carbonation includes consumption of metal and hydroxide ions for the formation of (hydrated) carbonates and water and in this manner may help the improvement of run-off waters.

Studying the accelerated carbonation of reactive MgO cements, it was concluded that brucite carbonation requires a sufficient supply of water and carbon dioxide [95]. Reactive MgO cements are the blend of MgO with a hydraulic cement, such as Portland cement and a pozzolan, such as pulverized fuel ash. The study considered exposing cement samples to 65% and 98% relative humidity with CO_2 concentrations of 5 and 20%. Upon hydration, MgO transforms into brucite which subsequently undergoes carbonation forming nesquehonite, while Portland cement produces calcite. An interesting behavior was noticed in their work regarding the role of water during accelerated carbonation on brucite. The highest carbonation rates of Portland based cements are found for intermediate water saturation degrees while MgO cements require high saturation degrees related to the high water consumption of brucite carbonation whereas Portland based cements carbonation liberates water.

Parallel to the convective carbonation tests in the packed bed cell, Assima et al., monitored the carbonation behavior of NiMT samples in a diffusion cell. A specially designed dual-compartment differential fixed-bed diffusion–carbonation reactor (Figure 1-9) was used to test the dynamics of mineral carbonation [12].

The carbonation reactor is composed of different parts and equipment to probe efficiently the evolution of carbonation: there are two hygrometers, CO_2 probes and fans in upper and lower compartments while a gate separates the sample holder which is equipped with a TDR probe and a pH-meter. Different CO_2 concentrations such as y_{CO2} = 0.5, 1, 2, 5 and 10 vol. % (balanced with N_2) were charged in the upper compartment and get contacted with NiMT of different water saturation degrees (dry, fully saturated and half saturated).

Figure 1-10 presents the experimental data on CO_2 diffusion across the NiMT bed in terms of evolution of CO_2 composition in upper (dotted line) and lower (solid line) compartments.

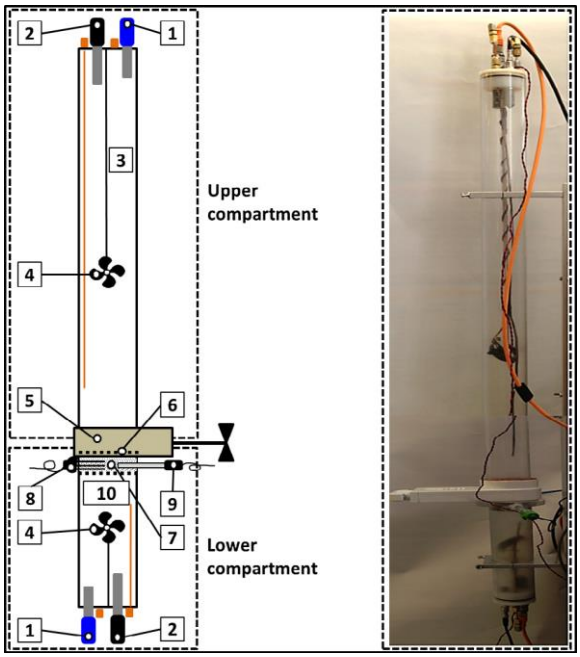

Figure 1-9. Schematic of differential fixed-bed diffusion/carbonation reactor. (1) hygrometer; (2) CO_2 probe; (4) fan; (5) gate; (6) sample holder; (7) NiMT layer; (8) TDR probe; (9) pH-meter; (3, 10) upper and lower compartments [12].

Low carbonation rates under both completely dry and fully saturated conditions were likewise observed. In the former case, the dry, open and interconnected pores act as corridors for rapid CO_2 advection through the layer leading to relatively fast CO_2 transfer from the upper compartment to the lower compartment. While water was found to be a crucial medium for supply of leached magnesium and dissolved CO_2, blockage of all pores by water in the latter case was found to be the main reason for the slow carbonation kinetics of a completely saturated medium. The presence of some liquid in the pores led the CO_2 to transfer from the gas mixture throughout the NiMT layer, taking advantage of a larger reservoir of potentially leachable Mg^{2+}. In case of fully saturated NiMT bed, although blockage of the pores abandons the bulk of material to get contact with the gas, however a continuation of CO_2 depletion from upper compartment is an indication of a carbonation regime much faster than dry carbonation scenario. Moreover, a sharp decline in water saturation was detected during

carbonation of brucite-rich nickel mining residues which was ascribed to the consumption of water in the formation of nesquehonite [12].

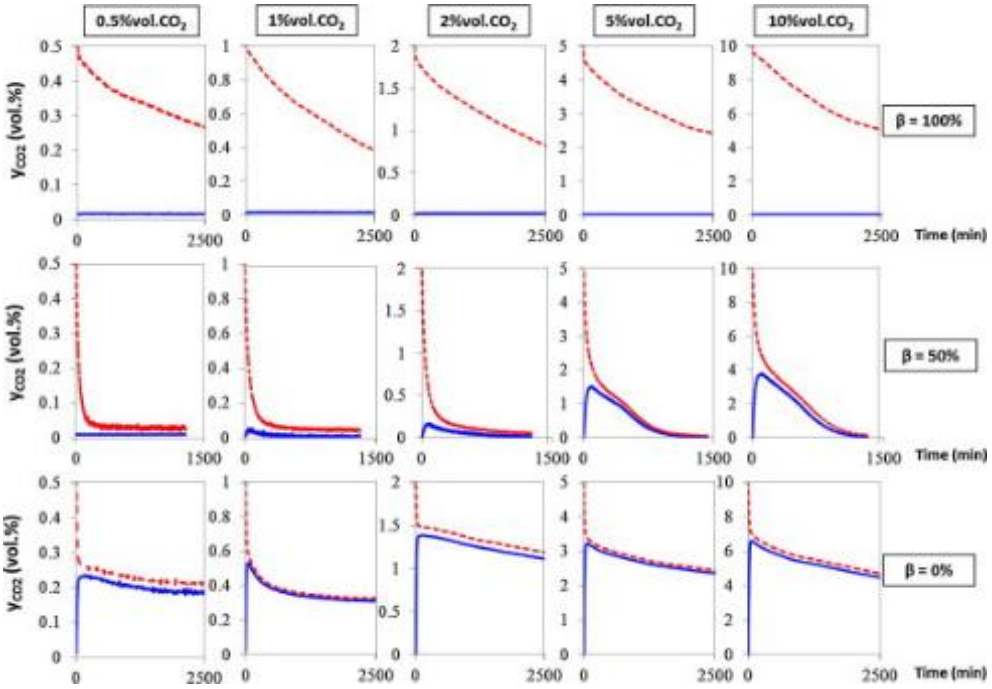

Figure 1-10. In situ monitoring of CO_2 diffusion across the NiMT bed in terms of CO_2 evolution in upper (dotted line) and lower (solid line) compartments [12].

In light of results obtained from their studies, Assima et al., proposed an engineered design, incorporating drainage systems into the mining residue storage piles in which air and run-off waters have facilitated pathways leading to higher contact of gas with moist solid. Using coarser-grained NiMT helps in providing permeable channels with low water retention to vent and drain the NiMT piles, thus air and water circulate deeper allowing Mg^{2+} and CO_2 to be dissolved across the whole structure.

Olsson et al., have studied olivine reactivity with CO_2 in the presence of water on a micro-scale [96]. They used atomic force microscopy (AFM), scanning electron microscopy (SEM) and X-ray photoelectron spectroscopy (XPS), before and after carbonation to explore the composition, structure and reactivity of olivine surfaces. To investigate the effect of

elevated CO_2 pressure (80 bars) and temperature (25 °C and 120 °C) experiments were carried out in pure water equilibrated with CO_2 in the absence and presence of oxygen. They noticed that even when oxygen is absent iron oxides form and olivine surfaces got oxidized suggesting hydrolysis, where water is converted to hydrogen and oxygen.

1.8 Objectives

One of the major environmental problems associated with mining activities is the production of significant quantities of solid waste mineral to be stored on the surface. Upon exposure to rain showers they can cause contamination of drainage water. These wastes are classified mainly as: mining operation waste rocks and mineral processing unit (concentrator) tailings. The former is made up of crushed rock (coarse grained) extracted during the operation, poor in minerals of economic value and are usually stored on the surface in the form of heaps. Mineral processing tailings result from the concentrator where finely ground ore is subjected to various treatments to concentrate and extract the minerals of interest. These tailings are often pumped in pulp form and stored in areas called tailings ponds. The various minerals present in the mining wastes are liable to react with water and ambient air (oxygen, carbon dioxide, moisture). Formation of mining wastes is inevitable, yet employing the engineering concepts they can be stored in a manner to harm less the environment or even be of help to it.

The main objective of the project is to improve the understanding of passive mineral carbonation in mining wastes and mineral processing tailing under environmental conditions. The specific objectives of this research can be summarized as follows:

- Study the mineral carbonation behavior in different conditions of temperature and water availability, mimicking the realistic environment found in southern Quebec. Emphasis on the effect of melting/ freezing cycles on mineral carbonation and possibilities of different mineralogical formations of the carbonated material.
- Identify carbonate forms at different temperature and water saturation conditions. Study of day/ night temperature variations corresponding to different seasons by programming the reactor to perform mineral carbonation in non-constant temperature regimes.

- Study the stability of different carbonates formed under environmental conditions. Study of natural weathering through wetting/ drying cycles to investigate the possibility of carbonate product detachment using natural thermomechanical stresses.
- Extending the study by monitoring carbonation behavior of extraction waste rocks (volcanic and gabbro) to get a good understanding of the total mineral carbonation potential of the Dumont nickel project.

1.9 References

[1] M. Hulme, On the origin of 'the greenhouse effect': John Tyndall's 1859 interrogation of nature, Weather 64 (2009) 121-123.

[2] C.D. Keeling, T.P. Whorf, C.S. Wong, R.D. Bellagay, The concentration of atmospheric carbon dioxide at ocean weather station P from 1969 to 1981, Journal of Geophysical Research: Atmospheres 90 (1985) 10511-10528.

[3] P. Tans, R. Keeling, NOAA/ESRL (www. esrl. noaa. gov/gmd/ccgg/trends/), 2017.

[4] W. Seifritz, CO_2 Disposal by Means of Silicates, Nature 345 (1990) 1.

[5] K.S. Lackner, C.H. Wendt, D.P. Butt, E.L. Joyce, D.H. Sharp, Carbon dioxide disposal in carbonate minerals, Energy 20 (1995) 1153-1170.

[6] F. Goff, K. Lackner, Carbon dioxide sequestering using ultramafic rocks, Environmental Geosciences 5 (1998) 89-101.

[7] R.K. Pachauri, A. Reisinger, D. Albritton, T. Barker, I. Bashmakov, O. Canziani, R. Christ, U. Cubasch, O. Davidson, H. Gitay, IPCC, 2007: Climate Change 2007: Synthesis Report. Contribution of Working Groups I, II and III to the Fourth Assessment Report of the Intergovernmental Panel on Climate Change. In: IPCC 104 (2008).

[8] The Core Writing Team, R.K. Pachauri, L.A. Meyer, IPCC, 2014: Climate Change 2014: Synthesis Report. Contribution of Working Groups I, II and III to the Fifth Assessment Report of the Intergovernmental Panel on Climate Change, IPCC, Geneva, Switzerland, 2014, pp. 151

[9] E.J. Wilson, T.L. Johnson, D.W. Keith, Regulating the ultimate sink: managing the risks of geologic CO2 storage, Environ Sci Technol 37 (2003) 3476-3483.

[10] L.-C. Pasquier, G. Mercier, J.-F. Blais, E. Cecchi, S. Kentish, Parameters optimization for direct flue gas CO2 capture and sequestration by aqueous mineral carbonation using activated serpentinite based mining residue, Applied Geochemistry 50 (2014) 66-73.

[11] A. Hemmati, J. Shayegan, J. Bu, T.Y. Yeo, P. Sharratt, Process optimization for mineral carbonation in aqueous phase, International Journal of Mineral Processing 130 (2014) 20-27.

[12] G.P. Assima, F. Larachi, J. Molson, G. Beaudoin, Emulation of ambient carbon dioxide diffusion and carbonation within nickel mining residues, Minerals Engineering 59 (2014) 39-44.

[13] A.-H.A. Park, L.-S. Fan, mineral sequestration: physically activated dissolution of serpentine and pH swing process, Chemical Engineering Science 59 (2004) 5241-5247.

[14] G.P. Assima, F. Larachi, J. Molson, G. Beaudoin, Impact of temperature and oxygen availability on the dynamics of ambient CO2 mineral sequestration by nickel mining residues, Chemical Engineering Journal 240 (2014) 394-403.

[15] J. Pronost, G. Beaudoin, J. Tremblay, F. Larachi, J. Duchesne, R. Hébert, M. Constantin, Carbon Sequestration Kinetic and Storage Capacity of Ultramafic Mining Waste, Environmental Science & Technology 45 (2011) 9413-9420.

[16] A.L. Harrison, I.M. Power, G.M. Dipple, Accelerated Carbonation of Brucite in Mine Tailings for Carbon Sequestration, Environmental Science & Technology 47 (2013) 126-134.

[17] C. Julcour, F. Bourgeois, B. Bonfils, I. Benhamed, F. Guyot, F. Bodénan, C. Petiot, É.C. Gaucher, Development of an attrition-leaching hybrid process for direct aqueous mineral carbonation, Chemical Engineering Journal 262 (2015) 716-726.

[18] N.A. Meyer, J.U. Vögeli, M. Becker, J.L. Broadhurst, D.L. Reid, J.P. Franzidis, Mineral carbonation of PGM mine tailings for CO2 storage in South Africa: A case study, Minerals Engineering 59 (2014) 45-51.

[19] D.N. Huntzinger, J.S. Gierke, L.L. Sutter, S.K. Kawatra, T.C. Eisele, Mineral carbonation for carbon sequestration in cement kiln dust from waste piles, Journal of Hazardous Materials 168 (2009) 31-37.

[20] F. Bodénan, F. Bourgeois, C. Petiot, T. Augé, B. Bonfils, C. Julcour-Lebigue, F. Guyot, A. Boukary, J. Tremosa, A. Lassin, E.C. Gaucher, P. Chiquet, Ex situ mineral carbonation for CO2 mitigation: Evaluation of mining waste resources, aqueous carbonation processability and life cycle assessment (Carmex project), Minerals Engineering 59 (2014) 52-63.

[21] H.C. Oskierski, B.Z. Dlugogorski, G. Jacobsen, Sequestration of atmospheric CO2 in chrysotile mine tailings of the Woodsreef Asbestos Mine, Australia: Quantitative mineralogy, isotopic fingerprinting and carbonation rates, Chemical Geology 358 (2013) 156-169.

[22] M. Bodor, R. Santos, T. Van Gerven, M. Vlad, Recent developments and perspectives on the treatment of industrial wastes by mineral carbonation — a review, Central European Journal of Engineering 3 (2013) 566-584.

[23] A. Kirchofer, A. Becker, A. Brandt, J. Wilcox, CO2 Mitigation Potential of Mineral Carbonation with Industrial Alkalinity Sources in the United States, Environmental Science & Technology 47 (2013) 7548-7554.

[24] O. Capobianco, G. Costa, L. Thuy, E. Magliocco, N. Hartog, R. Baciocchi, Carbonation of stainless steel slag in the context of in situ Brownfield remediation, Minerals Engineering 59 (2014) 91-100.

[25] M. Salman, Ö. Cizer, Y. Pontikes, R.M. Santos, R. Snellings, L. Vandewalle, B. Blanpain, K. Van Balen, Effect of accelerated carbonation on AOD stainless steel slag for its valorisation as a CO2-sequestering construction material, Chemical Engineering Journal 246 (2014) 39-52.

[26] C.W. Noack, D.A. Dzombak, D.V. Nakles, S.B. Hawthorne, L.V. Heebink, N. Dando, M. Gershenzon, R.S. Ghosh, Comparison of alkaline industrial wastes for aqueous mineral carbon sequestration through a parallel reactivity study, Waste Management 34 (2014) 1815-1822.

[27] D.N. Huntzinger, J.S. Gierke, S.K. Kawatra, T.C. Eisele, L.L. Sutter, Carbon Dioxide Sequestration in Cement Kiln Dust through Mineral Carbonation, Environmental Science & Technology 43 (2009) 1986-1992.

[28] G. Montes-Hernandez, R. Pérez-López, F. Renard, J.M. Nieto, L. Charlet, Mineral sequestration of CO2 by aqueous carbonation of coal combustion fly-ash, Journal of Hazardous Materials 161 (2009) 1347-1354.

[29] M.C. Mayoral, J.M. Andrés, M.P. Gimeno, Optimization of mineral carbonation process for CO2 sequestration by lime-rich coal ashes, Fuel 106 (2013) 448-454.

[30] J.-H. Wee, A review on carbon dioxide capture and storage technology using coal fly ash, Applied Energy 106 (2013) 143-151.

[31] R.M. Dilmore, B.H. Howard, Y. Soong, C. Griffith, S.W. Hedges, A.D. DeGalbo, B. Morreale, J.P. Baltrus, D.E. Allen, J.K. Fu, Sequestration of CO2 in Mixtures of Caustic Byproduct and Saline Waste Water, Environmental Engineering Science 26 (2009) 1325-1333.

[32] N. Um, S.-Y. Nam, J.-W. Ahn, Effect of Accelerated Carbonation on the Leaching Behavior of Cr in Municipal Solid Waste Incinerator Bottom Ash and the Carbonation Kinetics, MATERIALS TRANSACTIONS 54 (2013) 1510-1516.

[33] C.-L. Washbourne, E. Lopez-Capel, P. Renforth, P.L. Ascough, D.A.C. Manning, Rapid Removal of Atmospheric CO2 by Urban Soils, Environmental Science & Technology 49 (2015) 5434-5440.

[34] I.A. Bundeleva, B. Ménez, T. Augé, F. Bodénan, N. Recham, F. Guyot, Effect of cyanobacteria Synechococcus PCC 7942 on carbonation kinetics of olivine at 20 °C, Minerals Engineering 59 (2014) 2-11.

[35] I.A. Bundeleva, L.S. Shirokova, P. Bénézeth, O.S. Pokrovsky, E.I. Kompantseva, S. Balor, Calcium carbonate precipitation by anoxygenic phototrophic bacteria, Chemical Geology 291 (2012) 116-131.

[36] I.M. Power, G.M. Dipple, G. Southam, Bioleaching of Ultramafic Tailings by Acidithiobacillus spp. for CO2 Sequestration, Environmental Science & Technology 44 (2010) 456-462.

[37] M. Delgado Torróntegui, Assessing the mineral carbonation science and technology M. Sc, Thesis ETH Zürich, Switzerland, 2010.

[38] K.S. Lackner, Carbonate chemistry for sequestering fossil carbon, Annual review of energy and the environment 27 (2002) 193-232.

[39] D.M. Sturmer, D.D. LaPointe, J.G. Price, R.H. Hess, Assessment of the potential for carbon dioxide sequestration by reactions with rocks in Nevada, Citeseer2007.

[40] G.J. Simandl, S. Paradis, M. Irvine, Brucite - Industrial Mineral with a Future, 2007 (2007).

[41] S. Khan, K. Ali, S. Alam, Brucite deposits of Hindubagh (West Pakistan), Pakistan Journal of Scientific and Industrial Research 14 (1971) 542-545.

[42] A.A. Olajire, A review of mineral carbonation technology in sequestration of CO2, Journal of Petroleum Science and Engineering 109 (2013) 364-392.

[43] A. Azdarpour, M. Asadullah, E. Mohammadian, H. Hamidi, R. Junin, M.A. Karaei, A review on carbon dioxide mineral carbonation through pH-swing process, Chemical Engineering Journal 279 (2015) 615-630.

[44] E.S. Falk, P.B. Kelemen, Geochemistry and petrology of listvenite in the Samail ophiolite, Sultanate of Oman: Complete carbonation of peridotite during ophiolite emplacement, Geochimica et Cosmochimica Acta 160 (2015) 70-90.

[45] M.H. El-Naas, M. El Gamal, S. Hameedi, A.-M.O. Mohamed, CO2 sequestration using accelerated gas-solid carbonation of pre-treated EAF steel-making bag house dust, Journal of Environmental Management 156 (2015) 218-224.

[46] S. Veetil, L.-C. Pasquier, J.-F. Blais, E. Cecchi, S. Kentish, G. Mercier, Direct gas–solid carbonation of serpentinite residues in the absence and presence of water vapor: a feasibility study for carbon dioxide sequestration, Environmental Science and Pollution Research (2015) 1-10.

[47] E.R. Bobicki, Q. Liu, Z. Xu, H. Zeng, Carbon capture and storage using alkaline industrial wastes, Progress in Energy and Combustion Science 38 (2012) 302-320.

[48] R.M. Santos, D. François, G. Mertens, J. Elsen, T. Van Gerven, Ultrasound-intensified mineral carbonation, Applied Thermal Engineering 57 (2013) 154-163.

[49] M. Werner, S. Hariharan, M. Mazzotti, Flue gas CO2 mineralization using thermally activated serpentine: from single- to double-step carbonation, Physical Chemistry Chemical Physics 16 (2014) 24978-24993.

[50] H. Geerlings, R. Zevenhoven, CO2 Mineralization—Bridge Between Storage and Utilization of CO2, Annual Review of Chemical and Biomolecular Engineering 4 (2013) 103-117.

[51] X. Wang, M.M. Maroto-Valer, Integration of CO2 Capture and Mineral Carbonation by Using Recyclable Ammonium Salts, ChemSusChem 4 (2011) 1291-1300.

[52] A. Sanna, X. Wang, A. Lacinska, M. Styles, T. Paulson, M.M. Maroto-Valer, Enhancing Mg extraction from lizardite-rich serpentine for CO2 mineral sequestration, Minerals Engineering 49 (2013) 135-144.

[53] B. Metz, O. Davidson, H. De Coninck, M. Loos, L. Meyer, IPCC special report on carbon dioxide capture and storage. Prepared by Working Group III of the Intergovernmental Panel on Climate Change, IPCC, Cambridge University Press: Cambridge, United Kingdom and New York, USA 4 (2005).

[54] K. Alizadehhesari, Carbon dioxide sequestration by mineralization of serpentine, School of Chemical Engineering, The University of Queensland, 2013, pp. 143.

[55] K.M. Steel, K. Alizadehhesari, R.D. Balucan, B. Bašić, Conversion of CO2 into mineral carbonates using a regenerable buffer to control solution pH, Fuel 111 (2013) 40-47.

[56] S.C.M. Krevor, K.S. Lackner, Enhancing serpentine dissolution kinetics for mineral carbon dioxide sequestration, International Journal of Greenhouse Gas Control 5 (2011) 1073-1080.

[57] S.J. Gerdemann, W.K. O'Connor, D.C. Dahlin, L.R. Penner, H. Rush, Ex Situ Aqueous Mineral Carbonation, Environmental Science & Technology 41 (2007) 2587-2593.

[58] A.L. Harrison, G.M. Dipple, I.M. Power, K.U. Mayer, Influence of surface passivation and water content on mineral reactions in unsaturated porous media: Implications for brucite carbonation and CO2 sequestration, Geochimica et Cosmochimica Acta 148 (2015) 477-495.

[59] L. Zhao, L. Sang, J. Chen, J. Ji, H.H. Teng, Aqueous Carbonation of Natural Brucite: Relevance to CO2 Sequestration, Environmental Science & Technology 44 (2010) 406-411.

[60] S.A. Wilson, A.L. Harrison, G.M. Dipple, I.M. Power, S.L.L. Barker, K. Ulrich Mayer, S.J. Fallon, M. Raudsepp, G. Southam, Offsetting of CO2 emissions by air capture in mine tailings at the Mount Keith Nickel Mine, Western Australia: Rates, controls and prospects for carbon neutral mining, International Journal of Greenhouse Gas Control 25 (2014) 121-140.

[61] D. Daval, I. Martinez, J. Corvisier, N. Findling, B. Goffé, F. Guyot, Carbonation of Ca-bearing silicates, the case of wollastonite: Experimental investigations and kinetic modeling, Chemical Geology 265 (2009) 63-78.

[62] R.A. Robie, B.S. Hemingway, J.R. Fisher, Thermodynamic properties of minerals and related substances at 298.15 K and 1 bar (105 pascals) pressure and at higher temperatures, Bulletin, 1978.

[63] T.J.B. Holland, R. Powell, An enlarged and updated internally consistent thermodynamic dataset with uncertainties and correlations: the system K2O–Na2O–CaO–

MgO–MnO–FeO–Fe2O3–Al2O3–TiO2–SiO2–C–H2–O2, Journal of Metamorphic Geology 8 (1990) 89-124.

[64] Y. Chen, S.L. Brantley, Dissolution of forsteritic olivine at 65°C and 2 < pH < 5, Chemical Geology 165 (2000) 267-281.

[65] A. C. Lasaga, Fundamental approaches to describing mineral dissolution and precipitation rates, Reviews in Mineralogy Volume 31: Chemical Weathering Rates of Silicate Minerals, Mineralogical Society of America (1995) pp. 23-86.

[66] V. Prigiobbe, G. Costa, R. Baciocchi, M. Hänchen, M. Mazzotti, The effect of and salinity on olivine dissolution kinetics at 120°C, Chemical Engineering Science 64 (2009) 3510-3515.

[67] J. Davidovits, Geopolymer, Green Chemistry and Sustainable Development Solutions: Proceedings of the World Congress Geopolymer 2005, Geopolymer Institute2005.

[68] J. Schott, E.H. Oelkers, P. Bénézeth, Y. Goddéris, L. François, Can accurate kinetic laws be created to describe chemical weathering?, Comptes Rendus Geoscience 344 (2012) 568-585.

[69] J. McCutcheon, I.M. Power, A.L. Harrison, G.M. Dipple, G. Southam, A Greenhouse-Scale Photosynthetic Microbial Bioreactor for Carbon Sequestration in Magnesium Carbonate Minerals, Environmental Science & Technology 48 (2014) 9142-9151.

[70] A.D. Jacobs, M. Hitch, Experimental mineral carbonation: approaches to accelerate CO2 sequestration in mine waste materials, International Journal of Mining, Reclamation and Environment 25 (2011) 321-331.

[71] G. Beaudoin, R. Hébert, M. Constantin, J. Duchesne, E. Cecchi, F. Huot, S. Vigneau, R. Fiola, Spontaneous carbonation of serpentine in milling and mining waste, southern Québec and Italy, Accelerated Carbonation for Environmental and Materials Engineering (ACEME2008)Rome, Italy, 2008, pp. 73-82.

[72] S.A. Wilson, G.M. Dipple, I.M. Power, J.M. Thom, R.G. Anderson, M. Raudsepp, J.E. Gabites, G. Southam, Carbon Dioxide Fixation within Mine Wastes of Ultramafic-Hosted Ore Deposits: Examples from the Clinton Creek and Cassiar Chrysotile Deposits, Canada, Economic Geology 104 (2009) 95-112.

[73] A. Beinlich, H. Austrheim, In situ sequestration of atmospheric CO2 at low temperature and surface cracking of serpentinized peridotite in mine shafts, Chemical Geology 332–333 (2012) 32-44.

[74] F. Larachi, I. Daldoul, G. Beaudoin, Fixation of CO2 by chrysotile in low-pressure dry and moist carbonation: Ex-situ and in-situ characterizations, Geochimica et Cosmochimica Acta 74 (2010) 3051-3075.

[75] I.M. Power, S.A. Wilson, J.M. Thom, G.M. Dipple, G. Southam, Biologically induced mineralization of dypingite by cyanobacteria from an alkaline wetland near Atlin, British Columbia, Canada, Geochemical transactions 8 (2007) 13.

[76] I. Power, J. McCutcheon, A. Harrison, S. Wilson, G. Dipple, S. Kelly, C. Southam, G. Southam, Strategizing Carbon-Neutral Mines: A Case for Pilot Projects, Minerals 4 (2014) 399.

[77] A. Hemmati, J. Shayegan, P. Sharratt, T.Y. Yeo, J. Bu, Solid products characterization in a multi-step mineralization process, Chemical Engineering Journal 252 (2014) 210-219.

[78] E.J. Swanson, K.J. Fricker, M. Sun, A.-H.A. Park, Directed precipitation of hydrated and anhydrous magnesium carbonates for carbon storage, Physical Chemistry Chemical Physics 16 (2014) 23440-23450.

[79] M. Hänchen, V. Prigiobbe, R. Baciocchi, M. Mazzotti, Precipitation in the Mg-carbonate system—effects of temperature and CO2 pressure, Chemical Engineering Science 63 (2008) 1012-1028.

[80] L.N. Lammers, G.E. Brown Jr, D.K. Bird, R.B. Thomas, N.C. Johnson, R.J. Rosenbauer, K. Maher, Sedimentary reservoir oxidation during geologic CO2 sequestration, Geochimica et Cosmochimica Acta 155 (2015) 30-46.

[81] D.W. Ming, W.T. Franklin, Synthesis and Characterization of Lansfordite and Nesquehonite1, Soil Sci. Soc. Am. J. 49 (1985) 1303-1308.

[82] G.P. Assima, F. Larachi, G. Beaudoin, J. Molson, CO2 Sequestration in Chrysotile Mining Residues—Implication of Watering and Passivation under Environmental Conditions, Industrial & Engineering Chemistry Research 51 (2012) 8726-8734.

[83] J. Pronost, G. Beaudoin, J.-M. Lemieux, R. Hébert, M. Constantin, S. Marcouiller, M. Klein, J. Duchesne, J.W. Molson, F. Larachi, X. Maldague, CO2-depleted warm air venting from chrysotile milling waste (Thetford Mines, Canada): Evidence for in-situ carbon capture from the atmosphere, Geology 40 (2012) 275-278.

[84] S.A. Wilson, M. Raudsepp, G.M. Dipple, Verifying and quantifying carbon fixation in minerals from serpentine-rich mine tailings using the Rietveld method with X-ray powder diffraction data, American Mineralogist 91 (2006) 1331-1341.

[85] C. Unluer, A. Al-Tabbaa, Characterization of light and heavy hydrated magnesium carbonates using thermal analysis, Journal of Thermal Analysis and Calorimetry 115 (2014) 595-607.

[86] J. Canterford, G. Tsambourakis, B. Lambert, Some observations on the properties of dypingite, Mg5 (C03) iOH) 2· 5H20, and related minerals, Mineralogical magazine 48 (1984) 437-442.

[87] G.M. Marion, Carbonate mineral solubility at low temperatures in the Na-K-Mg-Ca-H-Cl-SO4-OH-HCO3-CO3-CO2-H2O system, Geochimica et Cosmochimica Acta 65 (2001) 1883-1896.

[88] G.P. Assima, F. Larachi, G. Beaudoin, J. Molson, Dynamics of carbon dioxide uptake in chrysotile mining residues – Effect of mineralogy and liquid saturation, International Journal of Greenhouse Gas Control 12 (2013) 124-135.

[89] C. Cravotta, III, Relations among pH, sulfate, and metals concentrations in anthracite and bituminous coal-mine discharges, Pennsylvania, 7th International Conference on Acid Rock Drainage (ICARD), American Society of Mining and Reclamation (ASMR), St. Louis, 2006, pp. 378-404.

[90] D. Banks, V.P. Parnachev, B. Frengstad, W. Holden, A.A. Vedernikov, O.V. Karnachuk, Alkaline mine drainage from metal sulphide and coal mines: examples from Svalbard and Siberia, Geological Society, London, Special Publications 198 (2002) 287-296.

[91] C. Cravotta, III, Passive aerobic treatment of net-alkaline, iron-laden drainage from a flooded underground anthracite mine, Pennsylvania, USA, Mine Water and the Environment 26 (2007) 128-149.

[92] B.W. Sung, K.H. Chu, S.L. Yun, J.Y. Ahn, J.H. Lee, S.S. Yoo, J.W. Lee, K.B. Ko, Removal of iron and manganese ions from abandoned neutral or alkaline mine drainage via ozone oxidation and micro-sand filtration: a pilot-scale operation, Desalination and Water Treatment 53 (2014) 2354-2362.

[93] C.D. Taylor, A.L. Meier, W.M. d'Angelo, J. Gray, J. Riehle, A reconnaissance study of the chemistry of natural waters draining chromite-bearing ultramafic complexes in Alaska, Geologic Studies in Alaska by the US Geological Survey, 1996 (1998) 9.

[94] N.E. Glozier, J.M. Culp, T.B. Reynoldson, R.C. Bailey, R.B. Lowell, L. Trudel, Assessing metal mine effects using benthic invertebrates for Canada's environmental effects program, Water quality research journal of Canada 37 (2002) 251-278.

[95] L.J. Vandeperre, A. Al-Tabbaa, Accelerated carbonation of reactive MgO cements, Advances in Cement Research, 2007, pp. 67-79.

[96] J. Olsson, N. Bovet, E. Makovicky, K. Bechgaard, Z. Balogh, S.L.S. Stipp, Olivine reactivity with CO2 and H2O on a microscale: Implications for carbon sequestration, Geochimica et Cosmochimica Acta 77 (2012) 86-97.

Chapter 2.

Multivariate study of the dynamics of CO2 reaction with brucite-rich ultramafic mine tailings

Ali **Entezari-Zarandi**,[1] Faïçal **Larachi**,[*,1] Georges **Beaudoin**,[2] Benoît **Plante**,[3] Michelle **Sciortino**[4]

[1]Department of Chemical Engineering, Université Laval, Québec, QC, Canada G1V 0A6

[2]Department of Geology and Geological Engineering Université Laval, Québec, QC, Canada G1V 0A6

[3]Université du Québec en Abitibi-Témiscamingue, Rouyn-Noranda, Québec, Canada J9X 5E4

[4]Senior Project Geologist, Royal Nickel, Toronto, Ontario, Canada

Abstract

Mineral carbonation of a nickel mine tailing (NiMT) was studied using a dual-compartment carbonation cell employing moderate CO_2 partial pressures for accelerating carbon uptake and to simulate outdoor temperature conditions prevailing in mining waste disposal sites. Time-dependent X-ray powder diffraction analysis and scanning electron microscopy reveal formation of transitional, metastable porous, flaky magnesium carbonates which subsequently evolved into less porous nesquehonite layers, which are shown to be responsible for surface passivation despite availability of unreacted brucite. However, the reactive cores could be turned into easily accessible regions following ex-foliation of carbonated materials. Moreover, it was demonstrated that slow carbonate nucleation events such as during carbonation of as-received ores may be significantly accelerated by means of carbonate pre-seeding strategies.

Résumé

La carbonatation minérale de résidus miniers nickélifères a été étudiée en utilisant une cellule à deux compartiments. Les essais ont été réalisés sous une pression partielle de CO_2 modérée dans le but d'accélérer la consommation du CO_2 et de simuler les conditions environnementales qui prévalent dans les sites d'entreposage des rejets miniers. La technique d'analyse de diffraction aux rayons X en fonction du temps et des observations au microscope électronique à balayage ont permis de mettre en évidence la formation de carbonates intermédiaires, instables et des carbonates de magnésium avec une structure floconneuse. Ces structures évoluent en couches de nesquéhonite moins poreuses qui induisent une passivation des surfaces malgré la disponibilité d'une certaine quantité de brucite qui n'avait pas encore réagi. Cependant, les noyaux réactifs pourraient être transformés en zones facilement accessibles après exfoliation des matériaux carbonatés. De plus, il a été démontré que la faible cinétique de nucléation des carbonates pendant la carbonatation de matériaux frais, peut être considérablement accélérée par des stratégies de pré-ensemencement des carbonates.

2.1 Introduction

Passive atmospheric mineral carbonation is an outcome of natural interactions between (ultra)mafic rocks and atmospheric CO_2 often involving meteoric water [1] to yield geologically stable and environmentally benign carbonates through kinetically slow processes [2-4]. There are numerous mining operations worldwide which produce, or hitherto have produced, large amounts of mafic- ultramafic mining wastes that are potentially suitable for atmospheric mineral carbonation. The Black Lake chrysotile mine at Thetford Mines in Québec [1, 5], the Clinton Creek asbestos mine in Yukon [6], the Cassiar asbestos mine in British Columbia [7], the Diavik Diamond Mine in Northwest Territories or the Mount Keith Nickel mine in Western Australia [6, 8] are a few examples of sites with easily accessible, finely ground and highly reactive mining waste with respect to atmospheric carbonation. Besides production of ultramafic mining wastes, nearly two billion tons of alkaline residues are annually produced in various metallurgical and power generation industries [9].

Particle size (or equivalent, specific surface area), temperature, and availability of liquid-state water, are amongst the factors which control the rate of mineral carbonation. Particle size directly controls the leaching rate of the reactive metal involved in solid carbon storage [10-12]. While comminution is an essential component of mineral processing due to its role in the liberation of valuable metal minerals from the matrix, it serendipitously confers a "second-life" advantage in the form of tailings with high specific surface areas to stimulate mineral carbonation reactions. Likewise, temperature directly impacts carbon mineralization by affecting gas, reactive and carbonated mineral solubility in water.

Coarse grained waste rocks from ultramafic mining operations, stored in large heaps, as well as fine grained mineral processing tailings deposited in impounded parks could be regarded as large man-made reactors active in carbon dioxide capture and sequestration. Such reactors exhibit highly heterogeneous spatiotemporal reactivity patterns which depend upon their contact with meteoric water, wind and exposure to solar radiation. The variability of these factors can result in the creation of dry, semi-saturated, and fully-saturated zones at different depth and temperatures. Understanding the carbonation behavior in correlation with the conditions prevailing in each zone is therefore a prerequisite to the precise quantification of the carbonation efficiency of mining wastes.

It has been well documented that water has an essential role in carbon uptake as a reaction medium in which both metal ions and CO_2 can dissolve as a prerequisite condition for the subsequent carbonate precipitations [5, 13-16]. Virtually no sign of carbonation is observed when desiccated materials such as MgO, Mg $(OH)_2$ or magnesium silicate minerals are contacted at ambient temperature with moisture-free CO_2-containing gas [17-19]. At the opposite end of the spectrum, carbonation of fully saturated (ultra)mafic minerals is also barely active as a result of the slow CO_2 diffusion rate in stagnant waters being a few orders of magnitude slower than its gas phase analog.

Hydrated magnesium carbonates have been observed to form at different temperatures contrary to the thermodynamically more stable magnesite ($MgCO_3$). Lansfordite ($MgCO_3 \cdot 5H_2O$) has been reported [20] to form at temperatures lower than 10°C while at room temperature, nesquehonite ($MgCO_3 \cdot 3H_2O$) is the most frequently observed carbonate product [21-23]. At higher temperatures (35-70 °C), hydromagnesite ($4MgCO_3 \cdot Mg(OH)_2 \cdot 4H_2O$) and dypingite ($Mg_5(CO_3)_4(OH)_2 \cdot 5H_2O$) form as the dominant solid carbonate species [8, 24-26]. The incipient formation of less stable hydrous carbonates in lieu of magnesite is usually explained by invoking the high hydration energy of solvated magnesium cations which prevents easy de-solvation during incipient formation of the solid carbonates [27]. This has also been rationalized in the form of Ostwald empirical rule of stages which implies that thermodynamically unstable phases start first to crystallize before evolving into thermodynamically stable recrystallized phases [28].

The province of Québec is the perfect location to assess the proof-of-concept of passive mineral carbonation given its long-standing history with the mining industry and its projected and current production of ultramafic wastes from the exploitation of mineral resources. As an example, the Dumont Nickel Project (DNP, Amos, Northwest Québec) is predicted to be the fifth largest nickel sulfide producer worldwide with ~1.18 billion metric tons of fine grained brucite-rich tailings (7-12 % Brucite, 80-88% total serpentine) as well as ~514 million metric tons of ultramafic waste rocks (0-5 % brucite) produced during the mining operations, pit opening and expansion over the mine's 31 year lifetime.

A multivariate study of the CO_2 fixation by brucite-rich ultramafic mining wastes was conducted for the assessment of the mineral carbonation potential of the DNP tailings. Pilot-

plant mineral processing tailings were submitted to various temperatures to mimic seasonal temperature conditions in hot, tempered, cold and freezing environments using a laboratory carbonation kinetic cell to gain insights on the corresponding evolution of carbon uptake and structure of the solid products being formed.

2.2 Materials and Methods

2.2.1 Experimental setup

The carbonation apparatus is shown schematically in Figure 2-1. It is an adaptation of our earlier setup [14, 29] but with an opportunity to monitor the carbonation kinetics at temperatures ranging from freezing to the hot summer conditions. It is a fixed-bed differential diffusion cell composed of 3 main parts: 1) CO_2 gas reservoir or lower compartment (LC), 2) gate and sample holder and 3) diffused gas reservoir or upper compartment (UC). A soft gas-bag was connected to LC to maintain, in spite of CO_2 consumption, isobaric pressure conditions inside the cell during the course of carbonation.

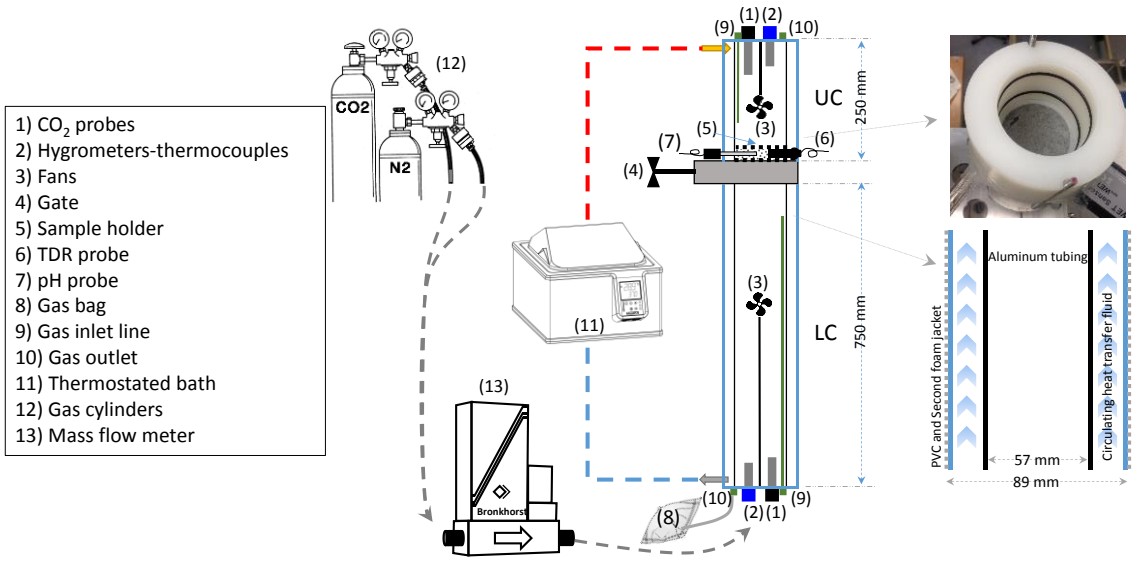

Figure 2-1. Schematic diagram of the experimental set-up. On the right side of the figure: core aluminum tubing having 3-mm wall thickness was jacketed in two insulating layers, 5 mm PVC and 12 mm polymer foam, for improved thermal insulation of the carbonation reactor. A heating/cooling fluid was pumped throughout the jacket to control temperature.

A thick PVC tube (ID = 78 mm and wall thickness of 6 mm) was employed to jacket the aluminum tubing of UC and LC (ID = 67 mm and wall thickness of 3 mm) replacing the original polycarbonate tubing of the cell. These modifications together with installing a thermostatically-controlled circulating bath (Cole-Parmer, Polystat 12101-00) enabled performing temperature-controlled carbonation tests simulating seasonal temperature variations. A second polymer foam jacket blanketed the whole reactor to ensure isothermal stability during the course of carbonation experiments.

The reactor was equipped with two sets of instrumentation: a) those installed within the solid layer, i.e., a time-domain reflectometry (TDR) probe (WET-2-K1, Delta-T) and a pH probe (HI 1053B, Hanna Instruments), and b) those installed in the upper and lower gas compartments, i.e., CO_2 probes (GMT221 0-10%, Vaisala) and moisture-temperature transmitters (HMT333, Vaisala). The CO_2 probes, moisture-temperature transmitters and pH probes were connected to a data logger to register signals at 5 min intervals (NI USB-6211, National Instruments). The WET-2 sensor was connected to its own data logger recording permittivity, bulk ionic conductivity and temperature of the solid layer at the same pace (GP1, Delta-T Devices Ltd.).

Opening the gate was assigned to the start of the reaction after which the carbonation tests continued until all the CO_2 was consumed or the reaction ceased to progress. To examine various carbonation regimes and the limiting carbonation capacity of the ore, several LC gas refills were applied by exposing the same aged sample (Table 2-1).

2.2.2 Materials characterization

The material used in this chapter was a nickel mine tailing, henceforth referred to as NiMT material, which resulted from preliminary batch flotation tests provided by Royal Nickel Corporation. The Dumont open-pit mining project is currently under development in the Abitibi-Temiscamingue region in Northwestern Québec (Canada) with the goal of exploiting nickeliferous deposits containing recoverable nickel sulfides (pentlandite: $(Fe,Ni)_9S_8$, and heazlewoodite: Ni_3S_2) and nickel-iron alloy (Ni_3Fe). From a mineralogical point of view, Dumont sill is composed of metamorphic rocks –highly serpentinized dunites– rich in lizardite with minor amounts of chrysotile, brucite, magnetite and antigorite [30, 31].

The serpentine dominant mineralogy of Dumont is a result of hydration of high Mg-olivine (Mg_2SiO_4) to serpentine. The serpentine family may undergo further hydration and carbonation forming talc and magnesite. CO_2 availability is an important control variable. The limiting case of depleted CO_2 results in hydration of olivine to serpentine and brucite [32]. This is the case of the Dumont sill where almost all the dunite body is well serpentinized with no trace of magnesite, though rich in brucite, and where only 4% of the dunite subzone contains over 20% olivine [31].

Table 2-1. Summary of the experimental campaign

	Run	Temperature (°C)	Water saturation (%)
Multiple contact	×1	23 ± 2	50
	×2	23 ± 2	50
	×3	23 ± 2	50
NiMT mixtures	Fresh (×1)	23 ± 2	50
	Alr. Carb.[&]	23 ± 2	50 (+3)
	50%:50%	23 ± 2	50
	3%	23 ± 2	50
Temperature sets	Freezing	−5 ± 2	50 (Iced)
	Cold	5 ± 1	50
	Room	23 ± 2	50
	Hot	35 ± 1	50

~ 35 g NiMT in contact with 10% CO_2 (balanced with N_2) used in each run, & = already carbonated

As summarized in Table 2-1, three experimental blocks are designed. The first focuses on the cyclic carbonation of as-received NiMT samples with replenished CO_2 environments under multiple contacts. In the second, carbonation of *already carbonated* NiMT samples mixed with as-received NiMT (50:50 wt%) is compared to that of as-received NiMT samples doped with 3% brucite. The already carbonated NiMT was obtained using *ca*. 70 g of as-received NiMT contacted over five successive cycles for a total duration of 3 weeks. Each cycle started with an initial gas mixture at 10% CO_2. The final product has been estimated to sequester ~ 20 mL of CO_2 per gram of NiMT. This product was then air dried and kept in closed plastic bags in laboratory conditions for about one week prior to be used in subsequent carbonation experiments. The brucite provided by Premier Chemicals LLC (USA) consisted of a ground powder (97 wt. % finer than 200 mesh) originating from naturally-occurring brucite ore (>95% $Mg(OH)_2$, 2% SiO_2, 2% CaO and minor amounts of Al_2O_3 and Fe_2O_3). In the third block, the effect of temperature on mineral carbonation was investigated where the selected temperatures were representative of seasonal changes.

Powdered samples, collected before and after carbonation, were analysed using X-ray diffraction (XRD), scanning electron microscopy (SEM) and energy dispersive X-ray (EDX) techniques. A Siemens D5000 diffractometer was employed to identify the crystalline minerals using Cu Kα radiation (λ = 1.54059 Å). The X-ray tube was operated at 40 kV, 30 mA and XRD data were collected at a 1°/min scanning rate over the 5–65° 2θ region (step size = 0.04°, dwell time = 1.2 s). The particle size and surface morphology of the as-received and carbonated NiMT powders were characterized using a dual-focused ion beam FEI Quanta 3D FEG field emission scanning electron microscope (FESEM) operated under 13.0 kV at high vacuum. Also, a FEI energy dispersive X-ray (Nano SEM 200) operated at 3.0 kV was used to examine powder compositions. A coupled TGA-MS apparatus (Perkin Elmer Pyris Diamond TGA-DTA and Thermostar Prisma QMS200, Pfeiffer Vacuum) was used to follow the mass loss of as-received NiMT in the range of 200-350°C to infer brucite content from the dehydroxylation patterns [33]. Specific surface area measurements were performed by means of a Micrometrics TRISTAR 3000 BET analyzer based on N_2 adsorption. Material bulk density was determined using an Ultrapyc 1200e gas pycnometer model (Quatachrome Instruments) where nitrogen was the gas phase and averaging out of three measurements.

Table 2-2 lists the chemical composition of NiMT and pure brucite samples as well as some other their physical properties.

2.2.3 Carbonation methodology

First, the as-received NiMT materials were thoroughly washed with deionized water to remove any residual chemical reagent, such as flotation collector or frother, and dried overnight in an oven at 110°C. The resulting powder was sieved on an 80-mesh sieve (D_{80} = 140 μm) to remove coarse grains before sealing in tight plastic containers.

Approximately 35 g of NiMT was placed on the sample holder in the form of a non-compacted layer 13-mm thick and 57 mm in diameter. Gentle hand tapping on the body of sample holder caused air cavity removal and flattening of the powdery surface. Afterwards, controlled amounts of deionized water were added in a stepwise manner until a liquid saturation of 50% was reached. This liquid saturation was shown to be the optimal level in the stimulation of a wet ambient carbonation [13, 14, 16]. In all cases, humidified gases were present in the cells to prevent water losses from NiMT bed due to evaporation.

Both LC and gas-bag were initially loaded with 10% CO_2 (balanced with N_2) gas mixtures while UC was loaded with pure N_2. Data acquisition was started with opening the gate and subsequent contact of the NiMT layer with the gas. The gas temperature was controlled by circulating a heating/cooling fluid from a thermostatically-controlled bath. The two fans mounted both in UC and LC helped not only to homogenize gas composition but also regulate temperature to ensure isothermal conditions over the entire cell.

2.3 Results

2.3.1 pH and CO_2 partial pressure evolution

Room temperature (23 ± 2°C) carbonation of NiMT was performed at the optimal water saturation identified previously [14]. Parallel to CO_2 consumption (Figure 2-2A), pH of the NiMT layer changed significantly (Figure 2-2B). Although similar depleting trends of CO_2 are shown for an as-received NiMT sample (×1) or an aged NiMT sample re-exposed

twice (×2) and thrice (×3) to a fresh CO_2 batch, yet subtle differences distinguish the dynamic behavior of $2^{nd}/3^{rd}$ cycles from first one. Each cycle is delineated by the time span between gate opening and closing (Figure 2-1) once CO_2 has been completely consumed in the gas mixture. Three distinct kinetic phases, namely, S1, S2 and S3, can be recognized during the carbonation of as-received NiMT sample (Figure 2-2): 1) fast pH drop/CO_2 removal (S1), 2) slow-paced pH restoration (S2) characterized by the emergence of a shoulder on the CO2 profile in Figure 2-2A and 2-3) increase in pH restoration/CO_2 removal (S3).

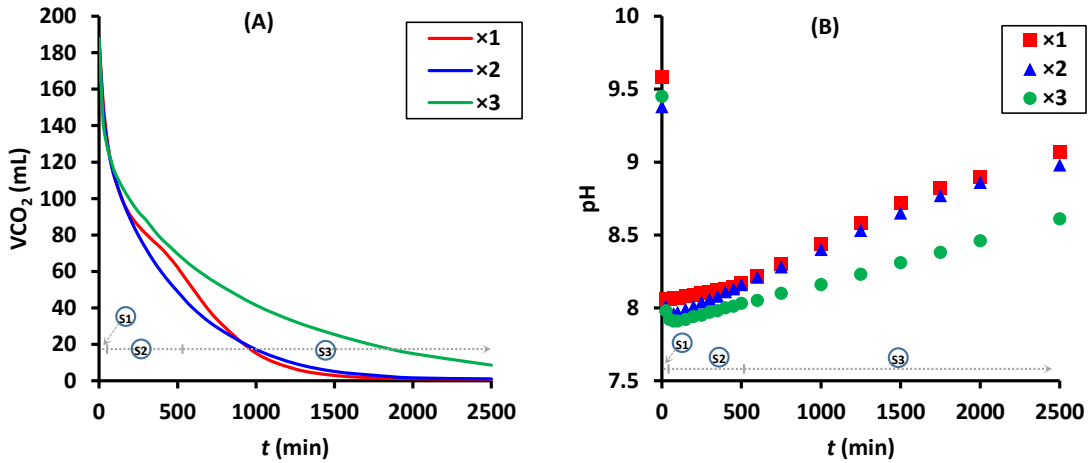

Figure 2-2. Mineral carbonation behavior of NiMT in terms of instantaneous A) volumetric consumption of CO_2 and B) pH evolution of pore water during first (×1) second (×2) and third (×3) contact with 10% CO_2 (balanced with N_2) gas mixture. S1, S2 and S3 correspond to three successive kinetic phases identified during the first contact with as-received NiMT: rapid phase S1 refers to early 60 min of carbonation where very fast CO_2 consumption mirrors sharp pH drops, S2 shoulder-type represents equal strength CO_2 acidification and brucite alkalization rates, S3 phase correspond to dwindling acidification rates.

The initial pH of NiMT wet layer was in the range 9.4 to 9.6. The rapid CO_2 uptake in the early minutes of reaction caused a sharp drop in pH of the poral water by nearly 1.5 unit. This phase was followed by a slower one where pH quietly increased to restore an alkaline region in conjunction with gradual depletion of carbon dioxide. The shoulder-like behavior characteristic of phase S2, which manifested during the carbonation of as-received

ore, was not observed in the subsequent carbonations of aged NiMT in twice and thrice re-exposures. In phase S1 lasting almost 60 min, fast CO_2 dissolution takes place implying reckless medium acidification to counteract alkalization due to brucite leaching. In phase S2 of as-received NIMT, CO_2 acidification and brucite alkalization of the medium come to be of the same strength thus leading to a shoulder as shown in Figure 2-2A. Afterwards, the dwindling acidification rates as a result of CO_2 impoverishment give rise to a slower S3 phase despite availability of unreacted brucite.

2.3.2 S2 shoulder and alteration of NiMT composition

During numerous tests performed in different conditions of water saturation, particle size and temperature, the same behavior of S2 shoulder occurring for the volumetric CO_2 consumption profile in conjunction with a low-paced pH restoration region – only in first contact – was observed. Thus, to gain insights on the phenomena occurring there, three different carbonation experiments using NiMT mixtures were carried out at ambient temperature: 1) already carbonated NiMT, 2) 50:50 wt. % mixture of already carbonated and as-received NiMT and 3) already carbonated NiMT doped with 3% of brucite powder. The already carbonated NiMT was obtained using as-received NiMT contacted over five successive cycles for a total duration of 3 weeks. As carbonation resulted in cementing together the NiMT grains, an agate mortar and pestle were employed to softly press and loosen the agglomerates. It was then set to 50% water saturation by adding de-ionized water. Figure 2-3 summarizes the acquired volumetric CO_2 consumption, pH, ionic conductivity and permittivity data for all three experiments plotted along with the corresponding profiles of as-received NiMT. The volumetric CO_2 consumption profiles of Figure 2-3A were derived from the instantaneous CO_2 mole evolution profiles from lower and upper cell compartments shown in Figure 2-4 for the three modalities of already carbonated and as-received NiMT samples. For instance, Figure 2-4A,B clearly show that higher amounts of CO_2 were able to enter the UC cell after crossing the NiMT bed layer, respectively, in the case of as-received and of already carbonated NiMT ore.

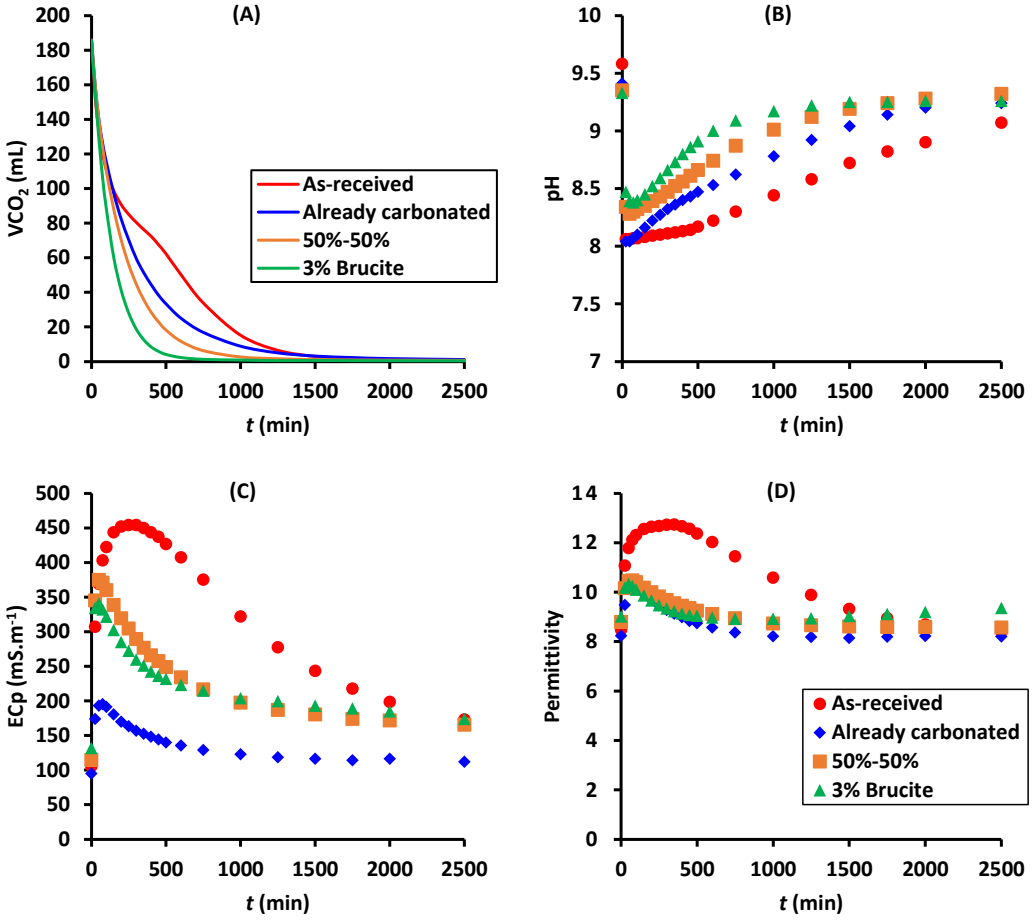

Figure 2-3. Carbonation behavior of NiMT in terms of synchronous transients of a) volumetric consumption of CO_2 b) evolution of pH of pore water, c) pore water electrical conductivity and d) medium permittivity: as-received NiMT, already carbonated NiMT, 50:50 wt.% mixture of as-received and already carbonated NiMT and mixture of 3% brucite powder with already carbonated NiMT.

Interestingly, none of the general trend of pH evolution or volumetric CO_2 consumption profiles of these three experiments showed any shoulder occurring or slow-paced pH restoration region. Furthermore, one may note the considerable carbonation reactivity of the already carbonated NiMT sample even after five exposure cycles (Figure 2-3A). Bearing in mind detachment of carbonates and exposure of new sites after gentle regrinding, the trend thus observed in Figure 2-3A is not in agreement with that depicted in Figure 2-2A for a steadily deactivating NiMT during carbonation. Indeed, reactivity of ×3

sequence (Figure 2-2A) was considerably lower than that of as-received NiMT. Assuming only the 11% brucite content in NiMT is prone to carbonation, indicate that 9 cycles would be necessary to convert all the NiMT brucite into magnesium carbonates. This suggests that magnesium carbonate product layer is loose enough to enable the peel-off of the product layer during gentle regrinding of the already carbonated NiMT sample. This interpretation supports this latter superior reactivity vis-à-vis that of Figure 2-2A conditions.

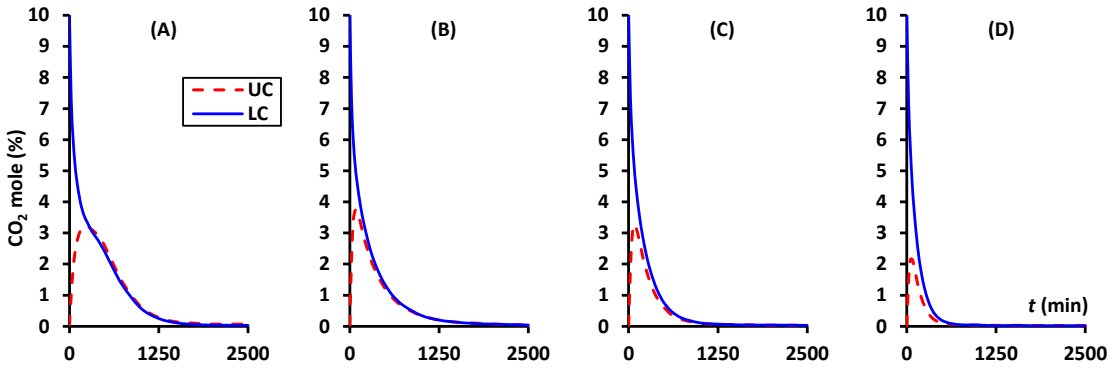

Figure 2-4. Instantaneous evolutions of CO_2 mole fractions in lower (LC) and upper (UC) cell compartments during the carbonation of A) as-received NiMT, B) already carbonated NiMT, C) 50%:50% mixture of as-received and already carbonated NiMT and D) mixture of 3% pure brucite powder with already carbonated NiMT. Note the difference in CO_2 diffusion through NiMT bed in different cases.

Figure 2-3 further illustrates the reactivity of already carbonated NiMT mixed compared to as-received NiMT or with 3% brucite. One may readily notice the higher reactivity, in comparison with as-received NiMT, of both powder mixtures in terms of CO_2 volumetric consumption. While this behavior may be ascribed to introduction of additional unreacted brucite in both mixtures, the case of already carbonated NiMT is yet remarkable as it is expected that much of its brucite content will be significantly converted over the five-cycle preparation phase.

2.3.3 Characterization of solid products

XRD patterns of reacted NiMT subject to different carbonation cycles are shown in Figure 2-5 together with coupled measurements with scanning electron micrographs (Figure 2-6). After 2500 min of first contact (×1), a weak signal stemming from nesquehonite (101) face is detected (Figure 2-5). Further contacts (×3 and ×5) to CO_2, after 7500 and 12500 min, strengthened even more the nesquehonite signatures as indicators of the buildup of increasing amounts of carbonates as shown from nesquehonite (002) and (103) faces. Likewise, brucite (001), (101) and (102) faces are expected to decline with the progress of carbonation. This is confirmed when comparing ×3 and ×5 XRD patterns, where one may note that brucite peaks are surviving. These peaks are assigned to unreacted brucite likely interlocked in the tailings particles or present as brucite encapsulated by nesquehonite coatings.

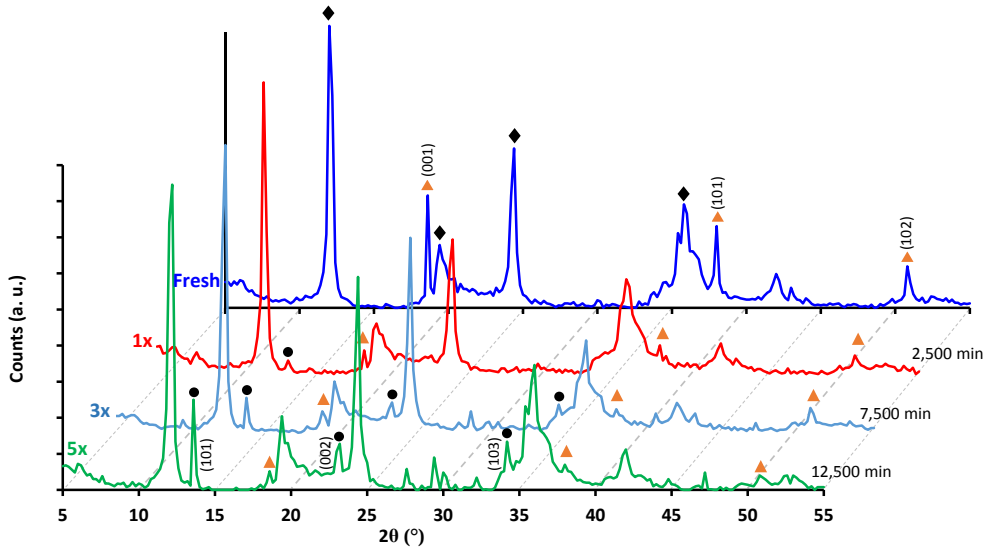

Figure 2-5. XRD patterns representing as-received and reacted NiMT for different cycles: as-received (fresh) NiMT, and after first, third and fifth contact with 10% CO_2. Diffraction peaks of lizardite/chrysotile (♦), brucite (▲) and newly formed nesquehonite (●).

FESEM images also deliver valuable information regarding the evolution of surface structure in the course of reaction. As-received NiMT is rich in hair-like fibers (~ 0.1 μm thick) which are rarely observed in carbonated samples (Figure 2-6A). Formation of an inter-grown porous flaky carbonate is visible after a first contact (Figure 2-6B). However, this

latter phase tends to evolve into elongated and dense nesquehonite crystals (Figures 2-6 C,D) in agreement with other previous studies [13, 16, 26, 34] It is plausible that, while gradually losing porosity, the newly formed, denser (Figure 2-6D), carbonate phases will cement (Figure 2-6C) the NiMT particles while retarding accessibility of protons to react with magnesium underneath or of carbon dioxide to react with leached Mg (II) cations.

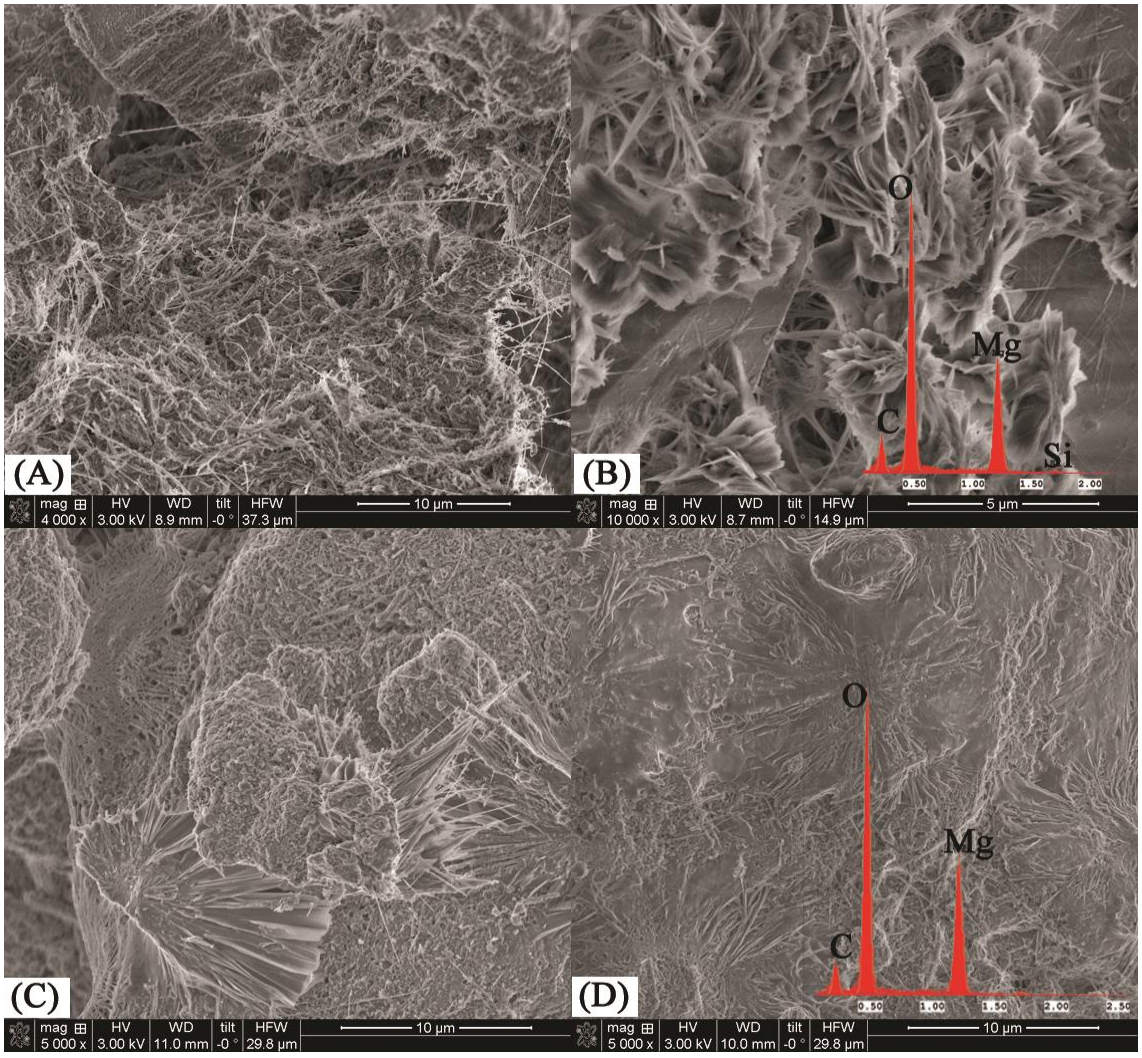

Figure 2-6. Scanning electron micrographs of surface structure details evolving during mineral carbonation showing A) as-received NiMT rich in long tiny fibers, B) flaky minerals formed after 2500 min carbonation, i.e., first contact (×1) of NiMT with 10% CO_2, C) elongated crystals of nesquehonite after 7500 min, i.e., third contact (×3) of material with CO_2 and D) dense nesquehonite coating bulk NiMT. (An SEM gallery of different carbonate formations witnessed in this work are gathered in Appendix A).

2.3.4 Effect of temperature on mineral carbonation

Mimicking environmental conditions of northern Québec, temperature dependent carbonation tests were performed in the ranges of hot (35 ± 1 °C), laboratory (23 ± 2 °C), low (5 ± 1 °C), and freezing (-5 ± 2 °C) conditions. Depicted in Figure 2-7 are the volumetric CO_2 residual profiles in solid lines (likewise illustrated in dotted lines as volumetric CO_2 consumption per gram of NiMT) and ionic conductivity variations of partially wetted NiMR samples subjected to different temperature conditions.

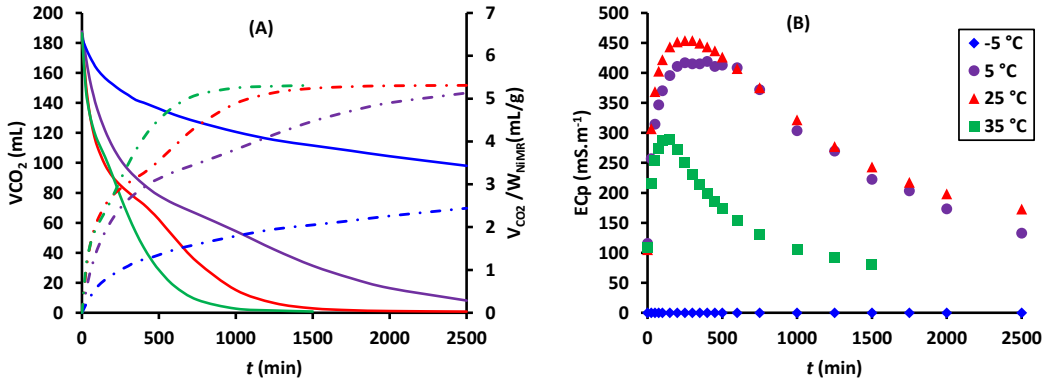

Figure 2-7. Transient evolution at different temperatures of A) CO_2 residual volume (solid lines) and sequestered CO_2 per grams of NiMT (dotted lines) and B) variations of ionic conductivity.

In agreement with previous observations [35], temperature had a notable effect on the carbonation kinetics. Lowering temperature caused a slowdown of NiMT reactivity. The largest uptake of CO_2 sequestered (~ 5.31 mL/g) was reached after 1500 and 2500 min at, respectively, high and laboratory temperatures. However, ionic conductivity change under high-temperature carbonation seems to reach a lower level in comparison with laboratory temperature. For the case of -5 °C, only zero values were recorded in response to a frozen ice layer.

2.4 Discussion

NiMT dissolution and precipitation of carbonates as the main contributors to carbonation are controlled by pH. It is accepted that mineral carbonation proceeds through a series of physicochemical events involving i) CO_2 dissolution (R1) and diffusive/convective transport promoting pore water acidification by way of ii) CO_2 hydration (R2) and subsequent deprotonation into bicarbonate/carbonate anions (R3,R4) followed by the iii) acidic dissolution of the metal-containing minerals liberating OH^- and metal ions (R5) iv) to ultimately culminate into the precipitation of carbonates (R6) depending on the local pH conditions [36, 37]. For the accomplishment of this last event, the nucleation of a carbonate phase requires super-saturation to be met including surfaces on which nuclei can form and grow:

$$CO_2\ (g) \rightarrow CO_2\ (aq) \quad \text{(R1)}$$

$$CO_2\ (aq) + H_2O\ (l) \rightarrow H_2CO_3\ (aq) \quad \text{(R2)}$$

$$H_2CO_3\ (aq) \rightarrow H^+\ (aq) + HCO_3^-\ (aq) \quad \text{(R3)}$$

$$HCO_3^-\ (aq) \rightarrow H^+\ (aq) + CO_3^{2-}\ (aq) \quad \text{(R4)}$$

$$Mg\ (OH)_2\ (s) + H^+\ (aq) \rightarrow Mg^{2+}\ (aq) + H_2O\ (l) + OH^-\ (aq) \quad \text{(R5)}$$

$$Mg^{2+}\ (aq) + HCO_3^-\ (aq) + OH^-\ (aq) + 2H_2O\ (l) \rightarrow Mg\ (HCO_3)\ (OH) \bullet 2H_2O\ (s) \quad \text{(R6)}$$

These events determine the pace at which the CO_2 profiles are depleted, e.g., Figure 2-2A. At t = 0, the hydroxide concentration in pore water is high (Figure 2-2B) mainly due to brucite dissolution (R5). Nonetheless, after the gate valve was opened, CO_2 is absorbed (R1) into the wet NiMT layer unleashing protons (R3, R4) to acidify the pore water during phase S1. A decrease is registered in LC simultaneously to an increase in UC in terms of CO_2 concentration in the gas compartments (Figure 2-4). Acidification results in increased metal extraction from the brucite-rich NiMT bed as brucite dissolution releases more OH^- ions as well as Mg^{2+} in pore water. This further promotes dissolution of CO_2 up to a stage where pore water reaches super-saturation to trigger precipitation of carbonate species. It was reported that nesquehonite cannot precipitate in under-saturated solutions even after 16 h [27].

Precipitation is greatly controlled by kinetic phenomena during nucleation and crystal growth [27, 28]. Over the first contact (×1) of as-received NiMT with CO_2, a shoulder clearly developed in phase S2 (Figure 2-2A) after pH started to raise above acidic levels (Figure 2-2B). This shoulder is attributed to delayed formation of new carbonate seeds presumably in the vicinity of free brucite particles (S2). Provided some carbonates are initially available, shoulders no longer form as shown in Figure 2-3A with the carbonation of already carbonated NiMT where carbonate seeds are being hosted from start. A monotonous regime of depletion of CO_2 is established reflecting crystal-growth controlled instead of nucleation-controlled CO_2 conversion into solid carbonates. This is corroborated by the lower ionic conductivities of poral water (Figure 2-3C) registered in the case of already carbonated NiMT. Also, stalling of pH (Figure 2-3B) during the early 500 min carbonation of the as-received NiMT is indicative of a dissolution rate of solids not fast enough to liberate sufficient amounts of hydroxide anions. During this step, a super-saturation state is developing into the pore water.

Although the change in global water content of the bed is minute, the TDR probe was sensitive enough to detect water proportion changes (Figure 2-3D). Hence, proton attacks resulting in water formation (R5) can be detected in the form of rising variations in medium permittivity during the course of carbonation. Likewise, the decreasing trends in permittivity are coherent with incorporation of water molecules into the lattice of the developing carbonate crystals. Furthermore, referring to the carbonation of already carbonated NiMT, the permittivity signals are clearly lower than in the case of as-received NiMT (Figure 2-3D).

The highest carbonation reactivity was attained with 3% brucite doping of an already carbonated NiMT (Figure 2-3A). This has to be contrasted with the carbonation response of the 50:50 wt. % of as-received and already carbonated NiMT to aide in understanding the role of mineral liberation on carbonation. The former case corresponds to addition of 1 g of virtually liberated brucite while in the latter 2 g of unreacted brucite were added by way of as-received NiMT presumably partially liberated and partially interlocked in the NiMT matrix. The BET surface areas of NiMT and brucite mineral powder being of the same order of magnitude (Table 2-2) cannot explain the boost in the carbonation response while the degree of liberation of the most reactive brucite is perhaps more plausible. Mineral liberation can indeed best be appreciated from the dynamics of CO_2 diffusion towards UC (red dashed

lines) as shown by lesser diffusion of CO_2 into UC (Figure 2-4D) across the brucite-doped NiMT wet layer in comparison with already carbonated (Figure 2-4C) or with 50:50 wt. % NiMT composite mixture (Figure 2-4C).

Carbonate seed formation is sensitive to temperature as shown in Figure 2-7A in terms of shifts and variations in the above described shoulder. Increasing temperatures prompt narrow-range shoulders to form earlier. The inflection points at 5°C and at room temperature were, respectively, located at ~750 and ~450 min, while at -5°C, no inflection point was observed. It is worthy of notice that though carbonation at low temperature is notably slower than at room temperature, the corresponding ionic conductivity profiles remain almost comparable as result of larger amount of dissolved and thus ionizable CO_2 (Figure 2-7B). While temperature rise negatively affects both CO_2 and brucite dissolution [38, 39], the faster CO_2 removal the higher the temperature indicates that the reduced saturation state is compensated by an increased rate constant [40].

Table 2-2. Chemical composition and physical properties of NiMT and pure brucite samples

		Unit	NiMT	Pure brucite
Analytes	**Mg**	(%w/w)	21	39.8
	Si	(%w/w)	19	1.8
	Ca	(%w/w)	0.03	1.4
	Fe	(%w/w)	3.5	0.15
	Ni	(%w/w)	0.3	-
Properties	**Brucite**	(%w/w)	11	>97
	B.E.T area	(m^2 g^{-1})	11.7	4.8
	Particle size, d_{80}	(μm)	140	90
	Organic carbon	(%)	<0.05	-
	Bulk density	(g cm^{-3})	2.67	3.04

Figure 2-8 illustrates a conceptual representation of NiMT carbonation in ambient conditions summarizing the abovementioned observations. The initial pH of wet NiMT bed is ~9.5 (Figures 2-2B,2-3B); however, upon introducing CO_2 (Figure 2-8A), the pH drops and acidification prompts leaching of metal ions. The yellow contour lines shown in Figure 2-8B delineate the high pH/metal ion region near the brucitic sites which are conjectured to be the main spots for carbonate nucleation. The flaky carbonate precipitates (Figure 2-6B), while colonizing brucite surface for growth and for cementing together the adjacent particles, do not impede further leaching of the brucite core. It is only after these flaky carbonate deposits evolve by further carbonation into the denser elongated nesquehonite structures (Figure 2-8C) that surface passivation gradually suppresses the progress of the reaction.

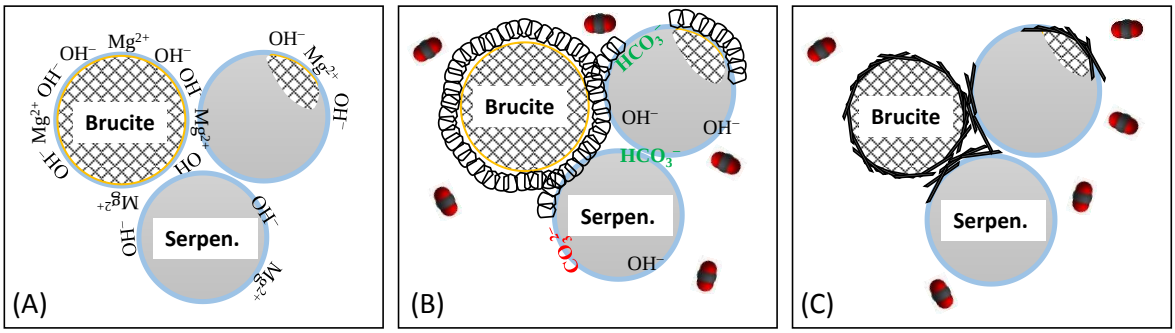

Figure 2-8. Conceptual representation of NiMT carbonation: A) driven by CO_2 acidity, metal and hydroxyl ions are being leached out mainly from brucitic regions; B) magnesium bicarbonates aggregate in the form flaky and highly porous hydrated magnesium carbonate structures nearby the high-pH brucite surfaces; C) As carbonation proceeds, the flaky phase evolves into more stable nesquehonite; being less porous these structures increasingly impeded metal leaching from unreacted mineral core.

2.4.1 Maturation of carbonate precipitates

Predominance of bicarbonate over carbonate at pH < 9 and nearly ambient conditions favors precipitation of nesquehonite (elongated crystals) $MgCO_3 \bullet xH_2O$ as reported in the pH-temperature morphology study of [41]. Despite magnesite being thermodynamically more stable in these conditions, nesquehonite is the commonly observed magnesium hydrated carbonate [41, 42].

The stoichiometric formula of nesquehonite is still debated in the literature opposing two formal transcriptions: Mg (HCO_3) (OH)•$2H_2O$ or $MgCO_3$•$3H_2O$ [43, 44]. However, bearing in mind predominance of bicarbonate in poral water and higher OH^- levels locally in water films over brucite surfaces, the former transcription of nesquehonite would be more plausible. This speculation is further reinforced by the detected presence of bicarbonate ions inside the elongated crystals of magnesium carbonates formed in near ambient conditions [41].

Examination of Figure 2-6 FESEM images unveils two significantly different precipitate types: 1) low-crystallinity flaky agglomerates (~ 0.05 μm thick and ~1-2 μm in diameter) such as those observed after *ca*. 41 h of reaction (Figure 2-6B) and 2) well-grown elongated crystals (10-20 μm long) forming after 105 h (Figure 2-6D). Similar morphologies during short and prolonged precipitation of nesquehonite were reported in the literature [41, 45]. Nucleation of the phase with the highest solubility is kinetically favored at the expense of more stable phases mainly due to the lower solid-solution interfacial tension of the less stable phase [46]. This might explain the earlier occurrence of carbonate flakes which subsequently transform into the more stable nesquehonite phase. EDX analysis shown in Figures 2-6B, D insets suggests an almost invariant C, O, Mg and Si composition (Table 2-3) between the flaky phase (1st contact) acting as a precursor and the well-grown elongated crystals (5th contact). Although it needs more detailed study, detection of nearly 3 wt.% of silicon in both cases may be taken as evidence of dissolution, though marginal, of serpentine during the carbonation process.

Table 2-3. EDX semi-quantitative elemental analysis of carbonates after 1st and 5th contact

		C	**O**	**Mg**	**Si**
×1	**(wt. %)**	8.1	40.5	48.4	3.1
	(at. %)	12.6	47.7	37.5	2.1
×5	**(wt. %)**	6.9	39.0	51.1	3.0
	(at. %)	10.8	46.7	40.4	2.0

2.5 Conclusion

Mineral carbonation of brucite-bearing serpentine tailings (NiMT) from the DNP was studied at temperatures reflecting ambient environmental conditions where these mining wastes are to be stored. It was shown that carbonate nucleation in as-received NiMT beds is a limiting step as exemplified through shoulder appearance during CO_2 uptake while pre-seeding carbonates in the beds led to noticeably faster carbonation kinetics with suppression of the shoulder. Carbonation proceeds through formation of a porous flaky carbonate phase topping mainly the high-pH brucite surfaces. This phase was gradually replaced by denser elongated nesquehonite crystals upon further carbonation. X-ray diffraction observations of the carbonation products confirmed that unreacted brucite was still present in the carbonated NiMT even after 200 h of carbonation suggesting that reactive brucitic cores may be buried underneath denser carbonate layers. Surface abrasion was shown to liberate previously carbonated NIMT particles resulting in further carbonation on freshly exposed surfaces.

2.6 References

[1] J. Pronost, G. Beaudoin, J.-M. Lemieux, R. Hébert, M. Constantin, S. Marcouiller, M. Klein, J. Duchesne, J.W. Molson, F. Larachi, X. Maldague, CO2-depleted warm air venting from chrysotile milling waste (Thetford Mines, Canada): Evidence for in-situ carbon capture from the atmosphere, Geology 40 (2012) 275-278.

[2] K.S. Lackner, A Guide to CO2 Sequestration, Science 300 (2003) 1677-1678.

[3] K.S. Lackner, Carbonate chemistry for sequestering fossil carbon, Annual review of energy and the environment 27 (2002) 193-232.

[4] K.S. Lackner, C.H. Wendt, D.P. Butt, E.L. Joyce, D.H. Sharp, Carbon dioxide disposal in carbonate minerals, Energy 20 (1995) 1153-1170.

[5] G.P. Assima, F. Larachi, G. Beaudoin, J. Molson, CO2 Sequestration in Chrysotile Mining Residues—Implication of Watering and Passivation under Environmental Conditions, Industrial & Engineering Chemistry Research 51 (2012) 8726-8734.

[6] S.A. Wilson, G.M. Dipple, I.M. Power, J.M. Thom, R.G. Anderson, M. Raudsepp, J.E. Gabites, G. Southam, Carbon Dioxide Fixation within Mine Wastes of Ultramafic-Hosted Ore Deposits: Examples from the Clinton Creek and Cassiar Chrysotile Deposits, Canada, Economic Geology 104 (2009) 95-112.

[7] J.G.M. Thom, G.M. Dipple, I.M. Power, A.L. Harrison, Chrysotile dissolution rates: Implications for carbon sequestration, Applied Geochemistry 35 (2013) 244-254.

[8] S.A. Wilson, A.L. Harrison, G.M. Dipple, I.M. Power, S.L.L. Barker, K. Ulrich Mayer, S.J. Fallon, M. Raudsepp, G. Southam, Offsetting of CO2 emissions by air capture in mine tailings at the Mount Keith Nickel Mine, Western Australia: Rates, controls and prospects for carbon neutral mining, International Journal of Greenhouse Gas Control 25 (2014) 121-140.

[9] H.I. Gomes, W.M. Mayes, M. Rogerson, D.I. Stewart, I.T. Burke, Alkaline residues and the environment: a review of impacts, management practices and opportunities, Journal of Cleaner Production 112 (2016) 3571-3582.

[10] A. Gras, G. Beaudoin, J.W.H. Molson, B. Plante, J.M. Lemieux, E.H.B. Kandji, Evidence for passive mineral carbonation from carbon isotope geochemistry of interstitial air in mine wastes from the Dumont Nickel Project (Abitibi, Quebec), AGU Fall Meeting, American Geophysical Union, Washington DC, United States, 2014.

[11] J.-j. Li, M. Hitch, Ultra-fine grinding and mechanical activation of mine waste rock using a high-speed stirred mill for mineral carbonation, International Journal of Minerals, Metallurgy, and Materials 22 (2015) 1005-1016.

[12] J.L. Linville, Y. Shen, M. Urgun-Demirtas, S.W. Snyder, Effect of particle size and doses of olivine addition on carbon dioxide sequestration during anaerobic digestion of sewage sludge at ambient and mesophilic temperatures, Process Biochemistry 51 (2016) 59-72.

[13] G.P. Assima, F. Larachi, G. Beaudoin, J. Molson, Dynamics of carbon dioxide uptake in chrysotile mining residues – Effect of mineralogy and liquid saturation, International Journal of Greenhouse Gas Control 12 (2013) 124-135.

[14] G.P. Assima, F. Larachi, J. Molson, G. Beaudoin, Emulation of ambient carbon dioxide diffusion and carbonation within nickel mining residues, Minerals Engineering 59 (2014) 39-44.

[15] K. Lechat, J. Lemieux, J. Molson, G. Beaudoin, R. Hebert, Monitoring CO2 Sequestration by Mineral Carbonation in Mine Tailings at Thetford Mines, Quebec, Canada, AGU Fall Meeting, American Geophysical Union, Washington DC, United States, 2014, pp. 4774.

[16] A.L. Harrison, G.M. Dipple, I.M. Power, K.U. Mayer, The impact of evolving mineral–water–gas interfacial areas on mineral–fluid reaction rates in unsaturated porous media, Chemical Geology 421 (2016) 65-80.

[17] H. Béarat, M.J. McKelvy, A.V.G. Chizmeshya, R. Sharma, R.W. Carpenter, Magnesium Hydroxide Dehydroxylation/Carbonation Reaction Processes: Implications for Carbon Dioxide Mineral Sequestration, Journal of the American Ceramic Society 85 (2002) 742-748.

[18] K.J. Fricker, A.-H.A. Park, Effect of H2O on Mg(OH)2 carbonation pathways for combined CO2 capture and storage, Chemical Engineering Science 100 (2013) 332-341.

[19] F. Larachi, I. Daldoul, G. Beaudoin, Fixation of CO2 by chrysotile in low-pressure dry and moist carbonation: Ex-situ and in-situ characterizations, Geochimica et Cosmochimica Acta 74 (2010) 3051-3075.

[20] A. Beinlich, H. Austrheim, In situ sequestration of atmospheric CO2 at low temperature and surface cracking of serpentinized peridotite in mine shafts, Chemical Geology 332–333 (2012) 32-44.

[21] P.J. Davies, B. Bubela, The transformation of nesquehonite into hydromagnesite, Chemical Geology 12 (1973) 289-300.

[22] G.P. Assima, F. Larachi, J. Molson, G. Beaudoin, New tools for stimulating dissolution and carbonation of ultramafic mining residues, Canadian Journal of Chemical Engineering 92 (2014) 2029-2038.

[23] A.L. Harrison, I.M. Power, G.M. Dipple, Accelerated Carbonation of Brucite in Mine Tailings for Carbon Sequestration, Environmental Science & Technology 47 (2013) 126-134.

[24] H.C. Oskierski, B.Z. Dlugogorski, G. Jacobsen, Sequestration of atmospheric CO2 in chrysotile mine tailings of the Woodsreef Asbestos Mine, Australia: Quantitative mineralogy, isotopic fingerprinting and carbonation rates, Chemical Geology 358 (2013) 156-169.

[25] I.M. Power, S.A. Wilson, J.M. Thom, G.M. Dipple, G. Southam, Biologically induced mineralization of dypingite by cyanobacteria from an alkaline wetland near Atlin, British Columbia, Canada, Geochemical transactions 8 (2007) 13.

[26] J. Pronost, G. Beaudoin, J. Tremblay, F. Larachi, J. Duchesne, R. Hébert, M. Constantin, Carbon Sequestration Kinetic and Storage Capacity of Ultramafic Mining Waste, Environmental Science & Technology 45 (2011) 9413-9420.

[27] M. Hänchen, V. Prigiobbe, R. Baciocchi, M. Mazzotti, Precipitation in the Mg-carbonate system—effects of temperature and CO2 pressure, Chemical Engineering Science 63 (2008) 1012-1028.

[28] J. Nývlt, The Ostwald Rule of Stages, Crystal Research and Technology 30 (1995) 443-449.

[29] G.P. Assima, F. Larachi, J. Molson, G. Beaudoin, Comparative study of five Québec ultramafic mining residues for use in direct ambient carbon dioxide mineral sequestration, Chemical Engineering Journal 245 (2014) 56-64.

[30] J. Duke, Petrology and economic geology of the Dumont sill: an Archean intrusion of komatiitic affinity in northwestern Quebec, Geological Survey of Canada, 1986.

[31] M. Sciortino, J.E. Mungall, J. Muinonen, Generation of High-Ni Sulfide and Alloy Phases During Serpentinization of Dunite in the Dumont Sill, Quebec, Economic Geology 110 (2015) 733-761.

[32] P.B. Kelemen, J. Matter, E.E. Streit, J.F. Rudge, W.B. Curry, J. Blusztajn, Rates and Mechanisms of Mineral Carbonation in Peridotite: Natural Processes and Recipes for Enhanced, in situ CO2 Capture and Storage, Annual Review of Earth and Planetary Sciences 39 (2011) 545-576.

[33] G.P. Assima, F. Larachi, J. Molson, G. Beaudoin, Accurate and direct quantification of native brucite in serpentine ores—New methodology and implications for CO2 sequestration by mining residues, Thermochimica Acta 566 (2013) 281-291.

[34] A.L. Harrison, G.M. Dipple, I.M. Power, K.U. Mayer, Influence of surface passivation and water content on mineral reactions in unsaturated porous media: Implications for brucite carbonation and CO2 sequestration, Geochimica et Cosmochimica Acta 148 (2015) 477-495.

[35] G.P. Assima, F. Larachi, J. Molson, G. Beaudoin, Impact of temperature and oxygen availability on the dynamics of ambient CO2 mineral sequestration by nickel mining residues, Chemical Engineering Journal 240 (2014) 394-403.

[36] L. Zhao, L. Sang, J. Chen, J. Ji, H.H. Teng, Aqueous Carbonation of Natural Brucite: Relevance to CO2 Sequestration, Environmental Science & Technology 44 (2010) 406-411.

[37] J. Sun, M.F. Bertos, S.J.R. Simons, Kinetic study of accelerated carbonation of municipal solid waste incinerator air pollution control residues for sequestration of flue gas CO2, Energy & Environmental Science 1 (2008) 370-377.

[38] N.P. Cheremisinoff, Chapter 2 - What Filtration is All About, Handbook of Water and Wastewater Treatment Technologies, Butterworth-Heinemann, Woburn, 2002, pp. 62-90.

[39] A.-H.A. Park, L.-S. Fan, mineral sequestration: physically activated dissolution of serpentine and pH swing process, Chemical Engineering Science 59 (2004) 5241-5247.

[40] Q. Gautier, P. Bénézeth, V. Mavromatis, J. Schott, Hydromagnesite solubility product and growth kinetics in aqueous solution from 25 to 75 °C, Geochimica et Cosmochimica Acta 138 (2014) 1-20.

[41] Z. Zhang, Y. Zheng, Y. Ni, Z. Liu, J. Chen, X. Liang, Temperature- and pH-Dependent Morphology and FT−IR Analysis of Magnesium Carbonate Hydrates, Journal of Physical Chemistry B 110 (2006) 12969-12973.

[42] D.W. Ming, W.T. Franklin, Synthesis and Characterization of Lansfordite and Nesquehonite1, Soil Sci. Soc. Am. J. 49 (1985) 1303-1308.

[43] E.E. Coleyshaw, G. Crump, W.P. Griffith, Vibrational spectra of the hydrated carbonate minerals ikaite, monohydrocalcite, lansfordite and nesquehonite, Spectrochimica Acta, Part A: Molecular and Biomolecular Spectroscopy 59 (2003) 2231-2239.

[44] R.L. Frost, S.J. Palmer, Infrared and infrared emission spectroscopy of nesquehonite Mg(OH)(HCO3)·2H2O–implications for the formula of nesquehonite, Spectrochimica Acta, Part A: Molecular and Biomolecular Spectroscopy 78 (2011) 1255-1260.

[45] J.T. Kloprogge, W.N. Martens, L. Nothdurft, L.V. Duong, G.E. Webb, Low temperature synthesis and characterization of nesquehonite, Journal of Materials Science Letters 22 (2003) 825-829.

[46] W. Stumm, J.J. Morgan, Aquatic chemistry: chemical equilibria and rates in natural waters, Third edition ed., John Wiley & Sons, New York, 1996.

Chapter 3.

Nesquehonite as a Carbon Sink in Ambient Mineral Carbonation of Ultramafic Mining Wastes

Ali **Entezari-Zarandi**,[1] Faïçal **Larachi**,[*,1] Georges **Beaudoin**,[2] Benoît **Plante**,[3] Michelle **Sciortino**[4]

[1]Department of Chemical Engineering, Université Laval, Québec, QC, Canada G1V 0A6

[2]Department of Geology and Geological Engineering Université Laval, Québec, QC, Canada G1V 0A6

[3]Université du Québec en Abitibi-Témiscamingue, Rouyn-Noranda, Québec, Canada J9X 5E4

[4]Senior Project Geologist, Royal Nickel, Toronto, Ontario, Canada

Abstract

X-ray diffraction of solid products combined with attenuated total reflection-Fourier transform infrared spectroscopy analysis reveals that during mineral carbonation of brucite-rich nickel mining tailings, parallel to brucite dissolution, hydrated magnesium carbonates such as nesquehonite are being formed. Wetting/drying cycles of the carbonation products revealed the important impact of temperature (25–70°C) oscillations on the stability of the primary carbonates. While nesquehonite was observed to transform into an amorphous phase during hot dry episodes, evidences are presented on nesquehonite transformation into hydromagnesite and dypingite on the surface of already carbonated layers during long-term contacts under occasional wetting and drying episodes. Such observations, made at controlled laboratory temperatures, suggest that even under environmental CO_2 partial pressures and over long periods, the hydrated magnesium carbonates act as precursors for the formation of more stable carbonate products. Moreover, it was observed that drying and freeze/thaw cycles were at the origin of a thermomechanical "peel-off" effect which inflicted micro–fractures to the carbonate product layers enabling water and gas to engulf beneath and react with freshly unearthed Mg donor sites. Results of an experimental campaign designed to evaluate the nature and stability of the ambient carbonation products are also discussed.

Résumé

Une analyse par diffraction aux rayons X combinée à la spectrométrie infrarouge à transformée de Fourier ont mis en évidence la formation de la nesquéhonite et la dissolution de la brucite pendant la carbonatation de résidus miniers nickélifères riches en brucite. Les cycles de séchage et de mouillage sur des matériaux déjà carbonatés ont permis de souligner l'impact des variations de températures (25–70 °C) sur la stabilité des carbonates primaires. Alors que la nesquéhonite se transforme en une phase amorphe pendant les périodes chaudes et sèches. Lors des cycles de séchage et de mouillage sur du matériel déjà carbonaté, la transformation de la nesquéhonite en hydromagnésite et en dypingite a été observée en surface. Ces résultats obtenus au laboratoire dans des conditions contrôlées suggèrent que même dans les conditions environnementales et sur de longues périodes de temps, les carbonates de magnésium hydratés sont les précurseurs de la formation de carbonates plus stables. De plus, le séchage et les cycles de gel/dégel sont à l'origine d'un effet thermomécanique qui induit des micro-fractures à la surface des carbonates, ce qui permet à l'eau et au gaz de pénétrer et de réagir avec les phases encore fraîches. Les résultats d'essais conçus afin d'évaluer la nature et la stabilité des carbonates ont été aussi discutés.

3.1 Introduction

Passive mineral carbonation consists of a carbon uptake process in which Nature's energy input is being exclusively taken advantage of during the fixation of atmospheric carbon dioxide through spontaneous transformation of suitable minerals into carbonates [1]. Mafic and ultramafic mining wastes, by virtue of their high calcium and magnesium content, are prone to forming numerous carbonate species upon contact with varying environmental conditions, such as sunlight which is a determinant of local temperature, or rain, snow and wind blows which are determining factors for water availability, and atmospheric partial pressures of CO_2. Chrysotile mine and processing waste stockpiles located in Thetford Mines (Québec, Canada) are examples of manmade carbonation reactors where, owing to passive mineral carbonation, *ca*. 120 Mt magnesium-rich ultramafic rocks have the potential to yearly bind with approximately 0.9 kt of atmospheric CO_2 on the basis of estimations of the heap area covered by vents [2].

Formation of various carbonate products (Table 3-1) is possible depending on the environmental conditions that prevail at the waste stockpiles, namely, the environmental mass and energy fluxes. However, if mineral carbonation of magnesium–rich minerals has been shown to yield hydrated magnesium carbonates, magnesite, *i.e*., anhydrous magnesium carbonate, on the contrary, has never been observed [3]. Lansfordite has been reported to form naturally at relatively low temperatures, namely < 10°C, although it is known to spontaneously and irreversibly evolve into the less hydrated nesquehonite as temperature rises [4-6]. Furthermore, the metastable nesquehonite was reported to be the dominant magnesium carbonate forming in ambient conditions [3, 7-12]. Upon rising the temperature above 50°C, nesquehonite evolves into thermodynamically more stable products with lower CO_2:Mg ratios [13-15]. Dypingite and hydromagnesite are attributed to precipitates formed from warm Mg–rich solutions in contact with carbon dioxide [16, 17], whereas magnesite, being the most stable magnesium carbonate [3], will nonetheless not form except at elevated temperatures and CO_2 partial pressures (~ >100°C, 100 bar) [3, 18, 19]. Interestingly, seeding reaction media with magnesite particles was shown to lead to particle growth in temperature conditions where normally hydromagnesite forms (80–150 °C) [3].

Table 3-1. Properties of (hydrated) magnesium carbonates

Mineral	Chemical formula	Molar ratio		Crystal habit
		CO_2:Mg	CO_2:H_2O	
Lansfordite	$MgCO_3 \cdot 5H_2O$	1	0.2	Short tabular, Monoclinic
Nesquehonite	$Mg(HCO_3)(OH) \cdot 2H_2O$	1	0.33	Elongated, Orthorhombic
Dypingite	$Mg_5(CO_3)_4(OH)_2 \cdot 5H_2O$	0.8	0.2	Globular aggregates, Monoclinic
Hydromagnesite	$Mg_5(CO_3)_4(OH)_2 \cdot 4H_2O$	0.8	1	Platy crystal, Pseudo–orthorhombic
Magnesite	$MgCO_3$	1	–	Massive Trigonal

The thermal decomposition of nesquehonite has attracted the attention of several research groups with contradictory figures on the limiting temperatures for its thermal integrity. Nesquehonite transformation into hydromagnesite reported to be "exceedingly rapid" above 52°C [14], while other authors stated that its crystal structure remains virtually intact up to *ca*. 80°C [20] or *ca*. 99 °C [8]. The phase transformation sequence during the course of thermal decomposition of nesquehonite is likewise debated [21]. Upon drying nesquehonite at 80, 100 and 120°C, it was found that an unidentified product supplanted the decomposing nesquehonite [17]. Detailed examination of nesquehonite and the intermediate phases through XRD and FT–IR techniques during thermal decomposition revealed that nesquehonite transforms at 115°C into an amorphous material the chemical composition of which is very close to that of hydromagnesite. However, a forced heating of the nesquehonite over short periods of time (at 460°C for 5-10 minutes), results in formation of crystalline hydromagnesite [22]. It is worthy to note that nesquehonite loses its bound water before its bound CO_2 [20]. The presence of humidity was found to promote nesquehonite stability perhaps by retarding crystal dehydration and decomposition [23]. On the assumption that thermal decomposition is not at the expense of a CO_2 loss, nesquehonite may be regenerated through rehydration of the amorphous phase suggesting that the structure of nesquehonite remains partially preserved during dehydration [21].

Although the effect of water saturation and temperature on the formation of different magnesium carbonates is well documented in the literature [10, 19, 24, 25], environmental parameters, such as freeze/thaw (F/T) and wetting/drying (W/D) cycles and their incidence on the stability of carbonate minerals is deemed to be of great importance because of the cyclic episodes in outdoor conditions. Thus, the knowledge gained from reproducing these conditions in a laboratory is important to shed light on our understanding of the dynamics of passive mineral carbonation which may be advantageously exploited in waste stockpile engineering and design in order to optimize the mineral–water–air contact and subsequently maximize the carbonation yields. In this regard, we studied the formation and stability of hydrated magnesium carbonates under various ambient and near–ambient mineral carbonation scenarii and mimicking environmental conditions, such as raining seasons or cyclic freeze/thaw phenomena which are likely to manifest at inter–season transitions. Two different experimental setups were used to monitor carbonation of brucite–rich nickel mine tailings and wastes at CO_2 mole fractions starting from the ambient concentration up to several percent. Furthermore, monitoring of spent materials helped understanding on the stability of pre–carbonated materials exposed to the atmosphere over a 2-year period of time.

3.2 Materials and Methods

3.2.1 Mine Tailing and Waste Materials

Two different samples were provided by RNC Minerals from its Dumont open–pit mining project in the Abitibi– Témiscamingue region in Northwestern Québec (Canada) with the perspective to exploit a deposit containing recoverable nickel sulfides and a nickel–iron alloy [26]. The main solid waste streams generated during the mining operations would consist of nickel mine tailings (NiMT) produced from bench–scale metallurgical tests of dunite rocks (first sample), and of mining wastes of low economic value (second sample). The NiMT sample was delivered in tight packages resting beneath water to minimize contacts with atmospheric carbon dioxide. Where needed, a part of the material was oven–dried (110°C) overnight and subsequently passed through a 150 μm sieve prior to the carbonation experiments. The NiMT is mainly composed of chrysotile and lizardite, with brucite and magnetite as minor minerals, as verified by XRD. The second sample, referred to as waste

sample, was in the form of half cores of peridotite rocks obtained during exploration of the mine site. The core samples were crushed and milled, and the particle size range between 200 and 300 microns was isolated for the reactional tests. The sample is likewise composed of chrysotile and lizardite as the main minerals, and brucite, magnetite and clinochlore as minor minerals. It is worth mentioning that NiMT and waste materials each have different disposal planning. The former is disposed of in fine grained tailing ponds while the latter is stocked in typically coarse grained waste rock stockpiles. Because of the highly reactive brucite present in both tailing and waste samples, technical grade single–mineral brucite diluted in a quartz matrix was also studied for carbonation. The brucite sample (Premier Chemicals LLC, USA), was a ground powder (97 wt. % finer than 200 mesh) originating from naturally–occurring brucite ore (>95% $Mg(OH)_2$, 2% SiO_2, 2% CaO and minor amounts of Al_2O_3 and Fe_2O_3). The pure silica sand was purchased from Sigma Aldrich.

3.2.2 Materials Characterization

Mineral identification was performed on dry fine powders obtained from gentle mechanical grinding of the carbonation products. Samples were analysed using X–ray powder diffraction (XRD) and Fourier transform infrared spectroscopy (FTIR) in the attenuated total reflection (ATR) mode. All analyses were conducted at laboratory temperature. A Siemens D5000 was employed to identify the crystalline minerals using Cu Kα radiation (λ = 1.54059 Å). The X–ray tube was operated at 40 kV/30 mA and data were collected at a 1°/min angular sweep. The 2θ angular range recorded was 5°–65° with a 0.02° step size. Scanning electron micrographs (SEM) were recorded using a JEOL JSM–840–A SEM in backscattered electron (BSE) and energy dispersive spectroscopy (EDX) modes with an acceleration voltage of 15 kV. The samples were coated with an Au/Pd film before analysis. FTIR spectroscopy was carried out on a Magna 850 Fourier transform spectrometer (Thermo Scientific) equipped with a mercury cadmium telluride detector cooled with liquid nitrogen and a potassium bromide coated germanium beam splitter. A golden–gate attenuated total reflection module (Specac Ltd.) was used to record attenuated total reflection spectra on a diamond crystal (mid–IR, from 750 to 4000 cm^{-1}).

3.2.3 Carbonation with Atmospheric CO_2 in Through–flow Cell

Convection due to wind pressure (or thermal gradients) is a critical contributor to the transport of CO_2 inside waste rock stockpiles [27]. Hence, the depth of penetration of convective streams can be limited to the edges of the waste stockpile or extend to some distance inside the structure's core. Thus, CO_2 convective transport *via* air circulation through the waste rock stockpiles affect the overall rate of mineral carbonation of the structure depending on the coarseness of the stockpile material, the pore water saturation, the wind speed and/or temperature gradient. These natural mineral carbonation conditions are simulated in the laboratory with a stream of ambient air, at room temperature and atmospheric pressure, flowing through porous media of NiMT and waste materials exposed to occasional wetting episodes to mimic the outdoor W/D cycles of raining and drying (Figure 3-1).

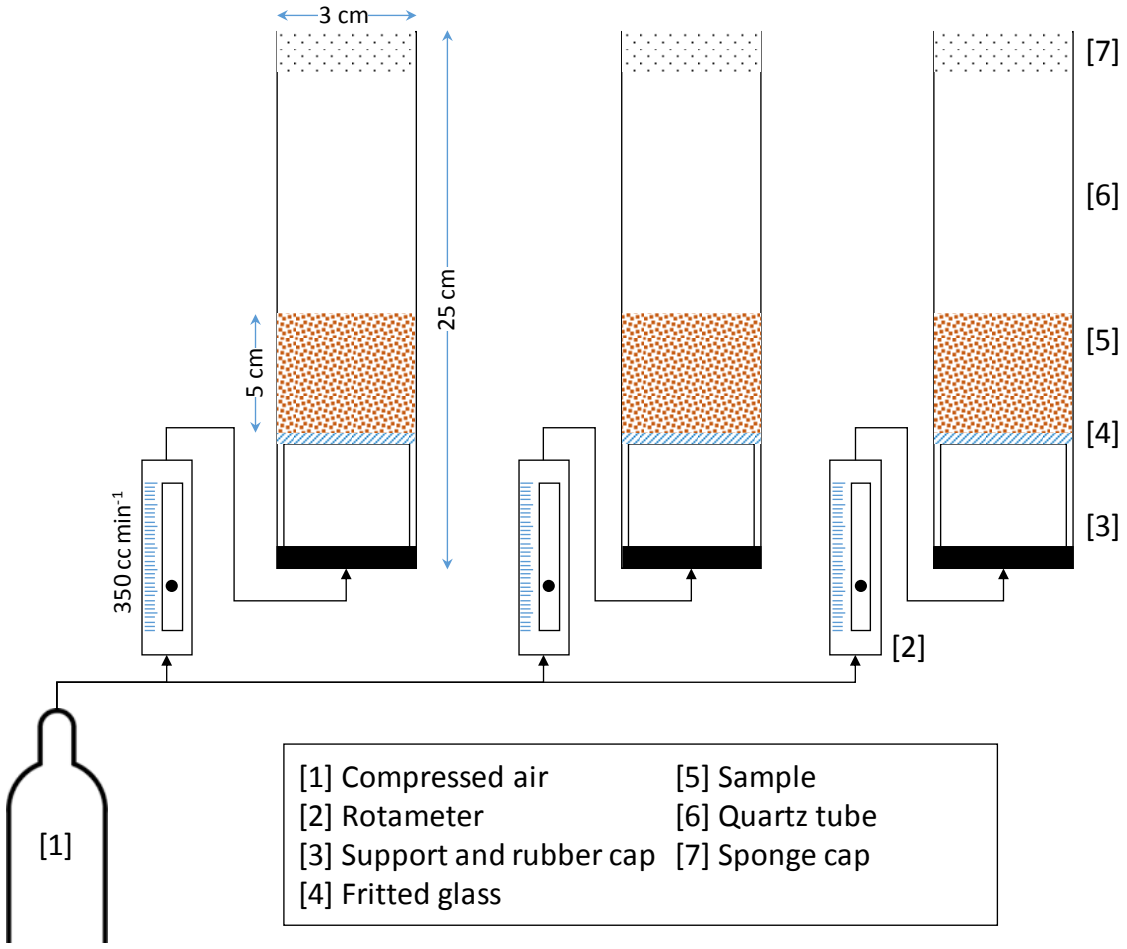

Figure 3-1. Through–flow experimental cell for the carbonation with atmospheric CO_2.

Experiments were carried out using a battery of three fixed–bed cells (25 cm length × 3 cm inner diameter) connected to a cylinder of compressed air to deliver, *via* a pressure regulator, a gas stream at quasi–atmospheric pressure. The gas was fed through a fritted disc at the bottom of each cell serving both as a sample holder and a gas distributor. Cells were labeled and hosted about 25 g of nickel mine tailing, nickel mining waste and a mixture of brucite (11 wt. %) with quartz respectively. This amount of brucite corresponds to the NiMT brucite content which was determined by means of a thermogravimetric analyses (TGA) method [28]. Water was periodically added to the fixed–bed cells to achieve varying but controlled degrees of saturation to emulate the behavior of carbonation in environmental conditions over a time horizon of 30 days. The cell inventories were periodically discharged, dried overnight at room temperature and sampled for further analyses before transfer back into their corresponding cells and rewetted to pursue the carbonation until the next sampling. Table 3-2 summarizes the particle size, height and porosity for each bed inventory associated with the through–flow carbonation tests.

Table 3-2. Summary of the experimental procedures trailed in ambient mineral carbonation approach

	Major mineral phases*	**Particle size (µm)**	**Bed Height (mm)**	**Porosity**	**Product (14 days)***	**Product (30 days)***
NiMT**	Chrysotile Lizardite Brucite Magnetite	150	25	0.47	–	Nesquehonite
Peridotite	Chrysotile Lizardite Magnetite	200–300	28	0.51	Giorgiosite	Nesquehonite, Giorgiosite
B + Q*** (11wt.%)	–	140–200	23	0.50	–	Nesquehonite

* Confirmed by XRD analysis. ** Nickel mining tailing tested as received without further grinding. *** Brucite + Quartz

3.2.4 Carbonation with Enriched CO_2 in Batch Cell

Parallel to the above through–flow carbonation tests, a differential thin–bed carbonation cell was also designed to investigate the course of carbonation in batch conditions with gas diffusion as the main transport process through a thin (~1 cm) porous mineral layer. The diffusive batch cell consists of 3 main modules: a batch gas reservoir containing the reacting binary CO_2/N_2 mixtures with varying mole fractions, a sample holder to retain the thin porous mineral layer, and the diffusion compartment (Appendix B, Figure S1). Approximately 35 g of powdery material was placed on the sample holder which was gently hand–tapped to help eliminate trapped air and to level the surface. To accelerate the carbonation kinetics, synthetic CO_2–rich mixtures (10%v/v CO_2, balance N_2), instead of atmospheric air, were monitored in the cell by means of two gas–phase CO_2 probes located in the gas reservoir and the diffusion compartment. A syringe was used to allow stepwise addition of controlled amounts of deionized water until an overall liquid saturation of 50 % v/v was attained. To control the start of the reaction, the sample holder was initially isolated from the gas reservoir by means of a gate valve. After the batch carbonation was initiated, it continued until exhaustion of all the CO_2 contained in the gas reservoir. To assess the decline in carbonation reactivity due to magnesium consumption and hindrance effects by the neo–formed carbonate layers, the gas reservoir was refilled with fresh gas mixtures.

The carbonate products and their stability were investigated following a series of W/D and F/T stress cycles. For this purpose, the partially reacted mineral layers were delicately removed from the diffusive cell and placed either to an oven or a freezer for predetermined drying or freezing times before their reintroduction into the cell for further carbonation experiments.

A W/D stress cycle was comprised of the following steps: i) sample wet carbonation, ii) sample drying in an oven for 15–18 h at 40°C, 60°C and 70°C, iii) sample cooling to room temperature, iv) sample rewetting to regain the original water saturation, and v) then sample reintroduction in the cell for additional room–temperature carbonation experiments at the same water saturation and initial CO_2 composition in the gas reservoir. Similarly, a F/T stress cycle consisted of i) wetting an already wet (50% saturation) carbonated sample, ii) sample freezing at *ca*. –18°C for 24 h, iii) gradual sample unfreezing at room–temperature for 24 h,

iv) water adjustment up to 50% saturation and repetition of steps ii) & iii) up to 10 times, iii) then sample reintroduction in the cell for room–temperature wet carbonation.

3.2.5 Long-term Nesquehonite in Contact with Atmospheric CO_2

The spent NiMT materials of *ca*. 70 room–temperature wet carbonation runs were successively collected from the diffusive batch cell and disposed of in an open–wide neck plastic container (Appendix B, Table S1). The cumulative materials amounted to *ca*. 70 runs × 35 g/sample ≈ 2450 g of carbonated NiMT. They were occasionally watered up to full saturation for a day or two and then left to dry at ambient temperature for a few weeks. Collection continued for over a couple of years piling up layer–wise and without mixing the spent materials so that the bottommost layers represent the oldest samples with the youngest laying atop (Appendix B, Figure S2).

After two years, thin layers were sliced off the cumulative spent material at different depths for XRD analyses. FTIR analyses were also performed on the white surface formations occurring on the top layer in order to discriminate different forms of carbonates.

3.3 Results and Discussion

3.3.1 Carbonation with Atmospheric CO_2 in Through–flow Cell

The carbonation of reactive mine tailing, peridotite waste, and a brucite/quartz control sample in through–flow cells under atmospheric CO_2 upflow streams is illustrated in Figure 3-2. The temporal distribution of water saturation over 30 days of the carbonation, based on daily additions of deionized water, is shown in Figure 3-2a along with the temperature history of the ambient air fed to the cells in the course of carbonation (Figure 3-2b). Reacted samples from the cells were withdrawn after 14 (Figure 3-2c) and 30 (Figure 3-2d) days, dried at room temperature for 24 h before performing X–ray diffraction (XRD) according to the procedures described in sections 2.2 and 2.3 above.

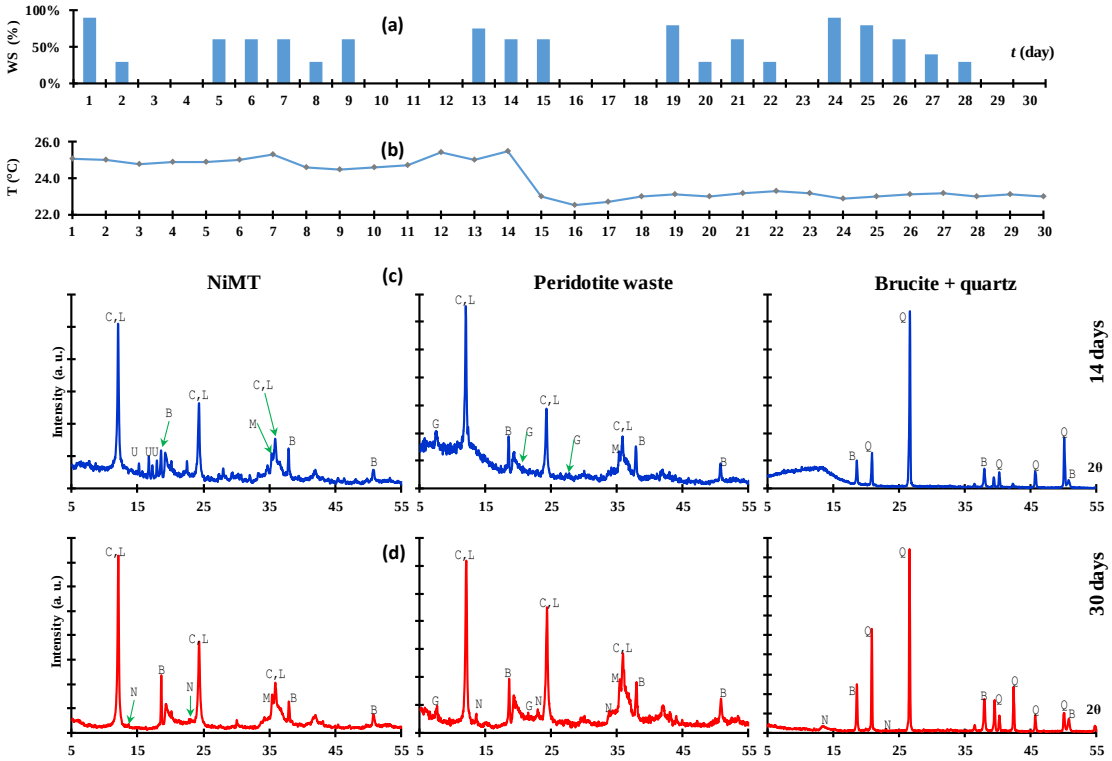

Figure 3-2. Carbonation of NiMT, peridotite waste, and brucite/quartz control sample with atmospheric CO_2 in through–flow cell mode: a) temporal distribution of water saturation over 30 days of the carbonation cells based on daily additions of deionized water, b) temperature history of ambient air fed to the cells in the course of 30–day carbonation, c) 14–day, d) 30–day XRP diffractograms of analyzed samples. Diffraction peaks of brucite (B), chrysotile (C), giorgiosite (G), lizardite (L), magnetite (M), nesquehonite (N), quartz (Q), unknown (but presumably) carbonates (U).

XRD of the NiMT samples, taken after 14 days of carbonation, did not reveal any evidence for the formation of crystalline magnesium carbonate products (Figure 3-2c). However, even if the several peaks emerging in the 15–20° range could not be related to any well–known hydrated carbonate phase, visual inspection of the carbonation cells revealed the formation of white deposits at the bottom of the layers, i.e., specifically where the air streams first impinge on the cells (Supplementary information, Figure S3). Unlike NiMT, crystalline carbonates could be recognized in the form of giorgiosite with stoichiometry ($Mg_5(CO_3)_4(OH)_2 \cdot 5{-}6H_2O$) for the peridotite waste sample after 14–day carbonation (Figure

3-2c). The brucite/quartz control sample, despite its highly reactive brucite, did not reveal, over the same time period, carbonate crystalline signatures presumably due to the overwhelming quartz XRD peaks. Inspecting the samples' X–ray diffraction patterns after 30 days of carbonation under atmospheric CO_2 exposure confirmed inception of nesquehonite (101) and (002) faces in all three columns with giorgiosite still being recognizable in the case of peridotite waste sample (Figure 3-2d). Nesquehonite identification as the hydrated magnesium carbonate species matches pervious results where elevated concentrations of CO_2 was employed for the sake of reaction acceleration, implying that the CO_2 concentration does not necessarily change the product carbonated being formed in ambient conditions of temperature and pressure [9-12].

3.3.2 Carbonation with Enriched CO_2 in Batch Cell

The carbonation kinetics was followed in terms of instantaneous residual CO_2 volume in the diffusive batch cell (Figure 3-3). Specifically, the long–term behavior of the materials was mimicked under accelerated carbonation conditions by allowing successive contacts of fresh humidified 10% CO_2–containing gas mixtures with the same *ageing* and partially saturated solid sample. This latter was left undisturbed on the sample holder with no correction of water saturation while humidification of the loaded gas prevented evaporative water losses from the wet mineral sample. As seen in Figure 3-3a, successive exposures of the same mineral sample to a fresh gas load led to CO_2 consumption profiles which slowed down after each one of the 9 refill sequences. Such gradual deactivation of the mineral was ascribed to a morphological evolution of the carbonate products during the course of carbonation and not to Mg depletion as its availability outweighed by far that of CO_2 [12].

Indeed, over the first exposures, a porous flaky carbonate phase started to grow on the surface of the mineral particles. The morphology of these young porous carbonates then evolved into denser and less porous needle–like nesquehonite layers. These layers, by sealing the surface of the reacting particles, and more noticeably the brucitic sites, tended to interfere with the leaching of magnesium cations and their subsequent uptake by the metal carbonate precipitation/crystallization steps [12].

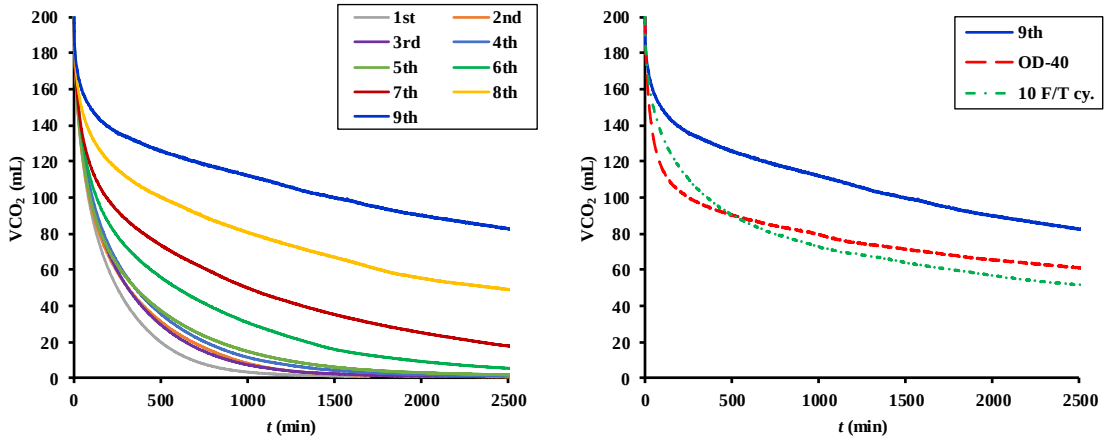

Figure 3-3. Carbonation kinetics of NiMT at ambient temperature in terms of instantaneous residual CO_2 volumes a) for 9 successive exposures of the NiMT sample to fresh 10% v/v CO_2 loads, b) for assessing after 9th contact the effect of drying and freeze/thaw (F/T) cycles of the aged mineral on its carbonation kinetics. OD-40 stands for oven drying at 40°C.

Environmental parameters such as water availability have dramatic impacts on the progress of mineral carbonation [9, 12, 24, 29]. Nevertheless, the carbonation tests just described, being carried out with constantly wet samples, captured one of the instances reflecting environmental conditions. However, W/D and F/T cycles exemplify actual environmental variabilities and reflect the alternating seasons which are believed to be crucial factors to control the mineral carbonation kinetics of the materials disposed of in the mining site. For instance, seasonal changes are accompanied by thermomechanical stresses which might alter the physical integrity of developing carbonate layers thus leading to an enhancement on carbonation capacity of the mining wastes.

3.3.3 Wetting/Drying Cycles

The reactivity and morphology evolution was examined as wet carbonated minerals undergo complete drying before resumption of wet carbonation. Hence, a 10th exposure to a fresh gas load of the spent mineral sample was conducted after removing the sample from the cell, and drying it in an oven for 24 h at 40°C. The dried pre–carbonated sample was then transferred back to the batch diffusive cell and room–temperature carbonation was resumed

under the same water saturation and CO_2 composition as for the previous 9 exposures. Referring to the "OD-40" profile of Figure 3-3b, a much more active material was revealed with CO_2 consumption outperforming that from the 9th exposure and nearly equaling the one reached under the 8th exposure. This experiment shows that carbonate–buried Mg donor sites could be activated by drying and by getting exposed, stimulate carbonation activity after mineral's rewetting. This stimulation can naturally occur for example in summer, after alternating rain and dry episodes. It may be attributed to thermomechanical stresses during drying which causes micro–fractures to the carbonate product layers and enable water and gas to penetrate across the layer and react with Mg donor sites. This is confirmed from the abundant cracks (10 to 50 μm long and *ca*. 0.5 to 3 μm wide) which are shown on the scanning electron microscopy photograph of the dried sample (Figure 3-4a). Micro-fractures also can be observed on the body and tip of elongated crystals (Figure 3-4b).

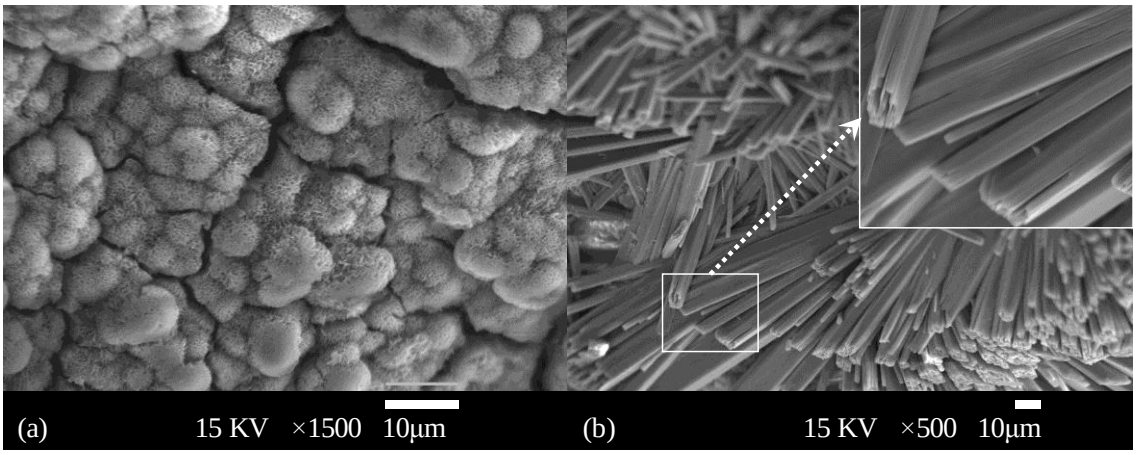

Figure 3-4. Scanning electron micrographs of surface structure details a) deep cracks on the surface of flaky carbonate product layer covering NiMT particles, b) well–grown elongated nesquehonite crystals for a 10-exposure carbonated sample after drying for 24 h at 40°C.

An additional set of ambient wet carbonation experiments scrutinized more systematically the impact of drying temperature on the sample mineralogy after five repeated W/D stress cycles as described earlier in section 2.4. It is worth reminding that the sample was removed after each one of the five wet ambient carbonation sequences, dried at the

prescribed temperature, re–transferred to the cell and re–wet before resumption of the next ambient carbonation sequence. The evolution of the sample mineralogy as a function of the drying temperature, exemplified in the case of NiMT, is shown in Figure 3-5 using X–ray diffractograms after the drying step of the fifth W/D cycle.

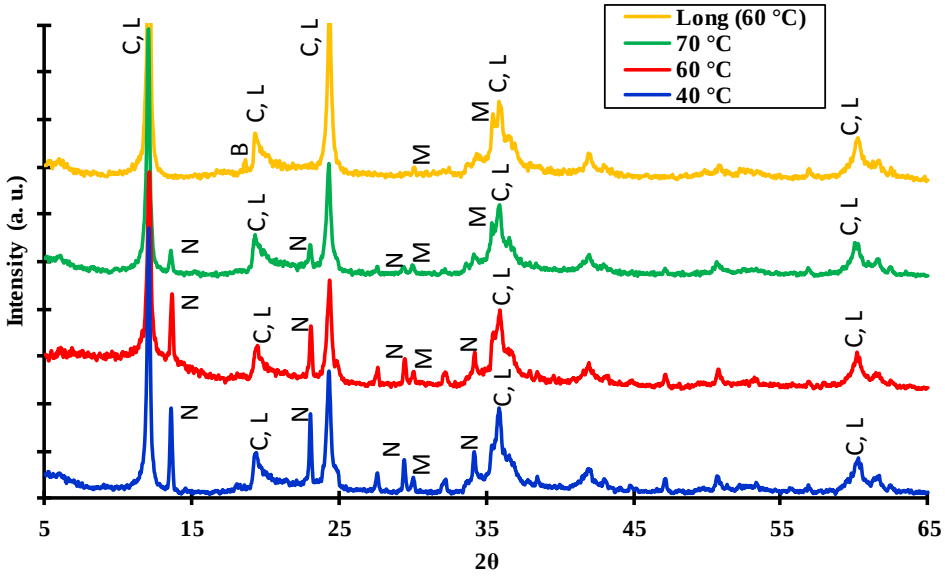

Figure 3-5. X–ray powder diffractograms after the drying step of the 5th wetting/drying cycle of ambient wet carbonated NiMT samples. Drying temperatures 40°C for 5×18 h, 60°C for 5×18 h, 70°C for 5×18 h, and 60°C for 4×18 h + 7×24 h. Diffraction peaks of chrysotile/ lizardite (C,L), brucite (B), magnetite (M) and nesquehonite (N).

Apart from nesquehonite being the only detectable crystalline carbonate phase, the intensity of its (101) and (002) peaks exhibits a decreasing trend as the temperature increases. Partial loss of the nesquehonite crystalline signature may be ascribed to the carbonate phase either becoming amorphous or undergoing decomposition during the cumulative drying steps (5×18 h = 90 h). To make sure amorphisation is not a slow interlude preceding recrystallization of the carbonate phase, an aged NiMT sample after the 5th cycle was dried under 60°C for an entire week (5×18 h + 7×24 h = 258 h). The corresponding X–ray diffractogram, referred to as "Long (60°C)" in Figure 3-5, reveals no indication of new carbonate crystalline phases while crystalline nesquehonite is no longer detectable.

Interestingly, a peak emerging near 2θ ≈ 20°, matching brucite (001) face, indicates that, without ruling out nesquehonite amorphisation, the decomposition of carbonates during the drying step was also possible. Coexistence of amorphous carbonates with solid by–products of decomposed carbonates is confirmed from the TGA shown in Figure 3-6.

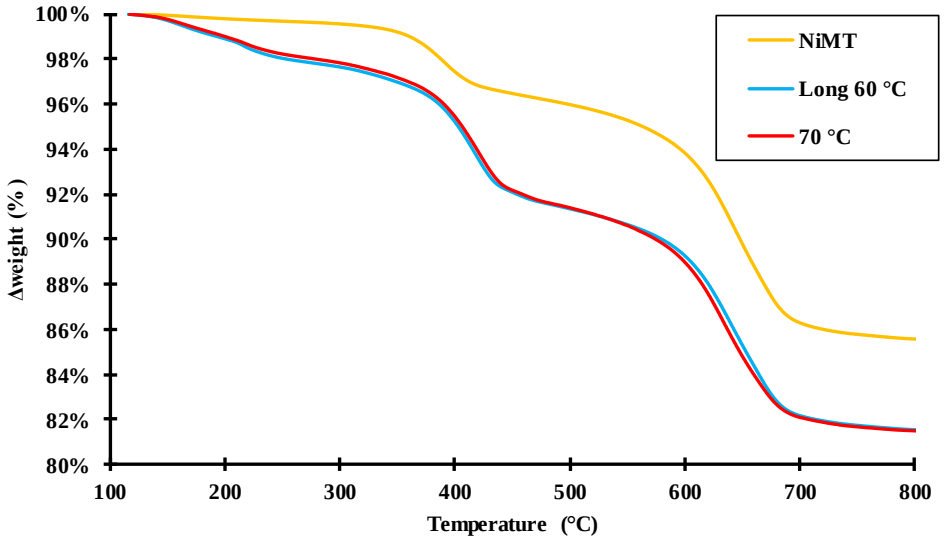

Figure 3-6. TGA profiles of as–received NiMT and of ambient wet carbonated NiMT samples corresponding to the same "L-60" and "70°C" samples analyzed with XRD. Heating rate: 10°C min^{-1} from 25°C to 800°C under N_2 stream. The region between two arrows represents the mass loss region due to brucite de-hydroxylation and hydrated carbonate species de-hydroxylation/de-carbonation.

Comparison of the TGA profiles unveils indeed a more important mass loss activity over the 330–460°C temperature range for the "Long (60°C)" and "70°C" samples as compared to the as–received NiMT sample. This activity is the result of interfering brucite dehydroxylation and carbonate decomposition [28]. However, since the mass loss kinetics of the two "Long (60°C)" and "70°C" samples are almost coincident, and on account of the crystalline nesquehonite evidenced for the latter sample (Figure 3-5), it is much likely that the mass loss accompanying the decomposition of amorphous carbonates outweigh that associated with the dehydroxylation of the neo–formed brucite which result from the decomposition of nesquehonite.

3.3.4 Freeze/Thaw Cycles

Apart from summer W/D, colder seasons cause solidification of pore water followed by melting. Thus, F/T cycles are a potential source for mechanical stresses which alter the integrity of the product carbonates providing another path for stimulation of carbonation reactions. Referring to Figure 3-3 again, the wet sample after a 10^{th} carbonation was taken out of the diffusive cell and placed in a freezer at *ca*. –18°C for 24 h to ensure complete solidification of water. It was then subjected to a series of F/T stress cycles as described earlier in section 2.4 before transfer into the batch cell for room–temperature wet carbonation under the same water saturation and CO_2 composition as for the previous 10 exposures. Referring to the "10 F/T cy." profile of Figure 3-3b, it can be seen that the material's reactivity was marginally improved with respect to the one achieved for the 10^{th} test after sample drying at 40°C. One would have expected the carbon uptake for the 11^{th} exposure to be lesser than during the 10^{th} exposure considering the deactivation trend shown in Figure 3-3a. The F/T cycles appear thus to have reversed deactivation, suggesting that the ensuing exfoliation of the product layer is a naturally occurring process enabling surface regeneration for additional carbonation experiments. The comparison could be extended by examining the consumption/diffusion profiles corresponding to Figure 3-3b (Supplementary information, Figure S4) where one may note the considerable change in time needed for CO_2 to diffuse through the NiMT layer subjected to F/T cycles. Moreover, the scanning electron microscopy photographs of the sample after oven drying reveal both flaky and elongated carbonate crystals (Figures 3-4a,b). Thus, although micro-fractures have formed during the drying episode, persistence of the less porous nesquehonite layers on the Mg–donor mineral substrate explain the limited carbonation improvements following the F/T cycles.

3.3.5 Fate of Nesquehonite in Contact with Atmospheric CO_2

Nesquehonite ($MgCO_3 \cdot 3H_2O$) is known to be a metastable carbonate form [13]. Its transformation into thermodynamically more stable carbonates such as the less hydrated and lower –CO_2:Mg– ratio dypingite ($4MgCO_3 \cdot Mg(OH)_2 \cdot 5H_2O$) or hydromagnesite ($4MgCO_3 \cdot Mg(OH)_2 \cdot 4H_2O$) and even magnesite ($MgCO_3$) is probable. The long-term stability of nesquehonite which was built up as described in section 2.5 over the two-year wet carbonation campaigns under enriched CO_2 in the diffusive cell was therefore examined

in detail. Thin layers were sliced off the cumulative spent material and XRD analyses were performed at the following depths from oldest to youngest: 0–2 mm (*ca*. 2 y old); 20–23 mm; 39–40 mm; 50–51 mm; 59–61 mm and the youngest atop (a few weeks old) referred to as "Newly carb.", in addition to the X–ray diffractogram of as-received NiMT (Figure 3-7). The spent carbonated NiMT subjected to long–term contact with atmospheric CO_2 and varying degrees of water saturation underwent changes in the structure of the carbonate products as a function of sample depth. The mineralogy of the youngest carbonated NiMT slice was somehow similar to that of the initial NiMT material except for nesquehonite forming as the major carbonate product at the expense of brucite which was dissolved early because of its high reactivity with CO_2. Inspection of the intermediate slices show destabilization of nesquehonite which evolved into hydromagnesite (H) and dypingite (D) (Figure 3-7).

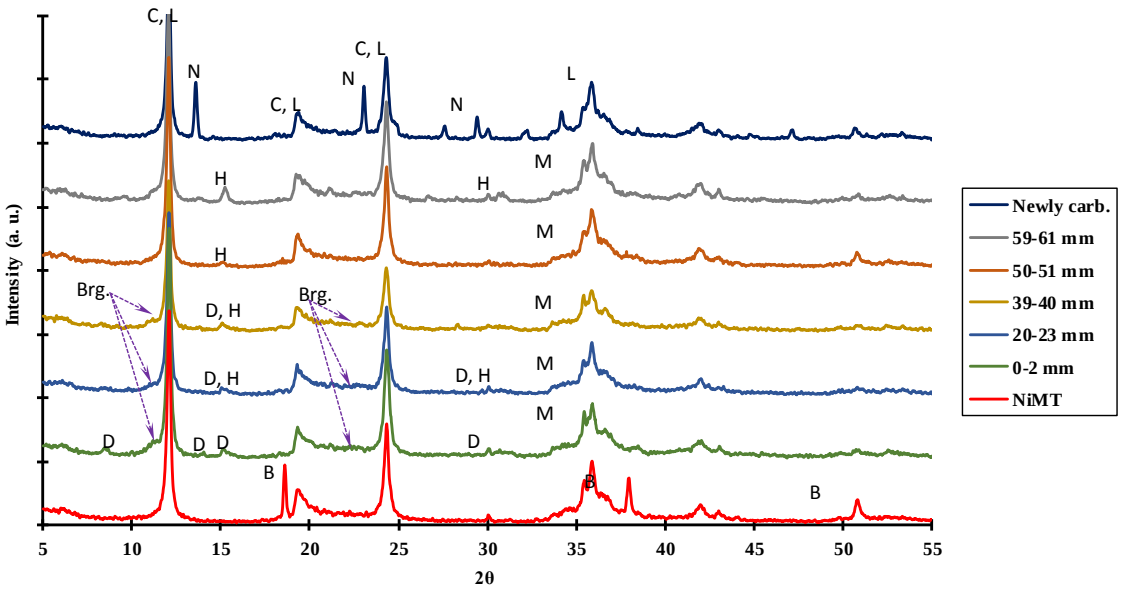

Figure 3-7. X–ray powder diffractograms tracking fate of nesquehonite of spent NiMT materials in contact with atmospheric CO_2 for up to two years. Diffraction peaks of brucite (B), brugnatellite (Brg), chrysotile/lizardite (C,L), dypingite (D), hydromagnesite (H), magnetite (M) and nesquehonite (N).

Dypingite occurred in deeper slices where presumably the larger degrees of water saturation might have inhibited its further dehydration into hydromagnesite. Hydromagnesite prevailed in the upper dryer slices where dypingite dehydration was in all likelihood more active. Recent field observations of an instrumented outdoor cell of ultramafic wastes left to react during 4 years with ambient CO_2 concentrations under natural watering cycles revealed that after cell dismantlement there was no nesquehonite in the core of the cell but instead hydromagnesite was detected as the main carbonate mineral [30]. Interestingly, traces of crystalline brugnatellite (Figure 3-7), an iron–bearing magnesium carbonate ($Mg_6Fe(III)CO_3(OH)_{13}\cdot 4H_2O$), were also detected in our study although it is normally attributed to the hydrothermal alteration of serpentinite [31]. Similar iron-bearing hydrated carbonates such as sjögrenite ($Mg_6Fe(III)_2(CO_3)(OH)_{16}\cdot 4H_2O$) and pyroaurite ($Mg_6Fe(III)_2(CO_3)(OH)_{16}\cdot 4H_2O$) were also evidenced at trace level *via* XRD elsewhere [30].

Unlike XRD, infrared spectroscopy may be employed for identifying amorphous or poorly crystalline materials [32]. Hence, Fourier transform infrared spectroscopy (FTIR) observations of the minerals in the mid–range (4000–400 cm^{-1}) of the infrared spectrum revealed characteristic features (*e.g.*, lattice and molecular vibrations) which can be related to the mineral carbonation evolution of the system. In particular, evidence of long–term evolution of nesquehonite towards more stable carbonate forms was made through attenuated total reflection Fourier transform infrared spectroscopy (ATR FT–IR). For each sample, sixteen scans were performed and averaged. The spectra were corrected against ambient air and the background spectrum was measured both at start and end of the readings. The 650–1500 cm^{-1} "fingerprint region" was used for the identification and differentiation between the different minerals present in such ultramafic complex systems on the basis of the unique combination of bands characterizing each individual mineral [33].

The 59–61 mm deep slice mentioned above was compared to 5 younger NiMT wet carbonation samples obtained from five successive contact cycles as described in section 3.3 above: X1 being the youngest and X5 the oldest. The ATR–FTIR vibrational spectra are illustrated in Figure 3-8 in addition to the spectrum for the as–received NiMT. The nesquehonite infrared band near 850 cm^{-1} corresponds to C–O out-of-plane bend mode $v2$ whereas the $v1$ symmetric C–O stretching mode near 1097 cm^{-1} is seen to almost overlap

with the 1020 cm^{-1} feature pertaining to the asymmetric Si–O–Si stretching band of chrysotile/lizardite. The vibrational features at 1405 cm^{-1}, 1470 cm^{-1} and 1515 cm^{-1} are usually assigned to CO_3^{2-} and HCO_3^- units *v*3 asymmetric stretching vibration [6, 23, 34].

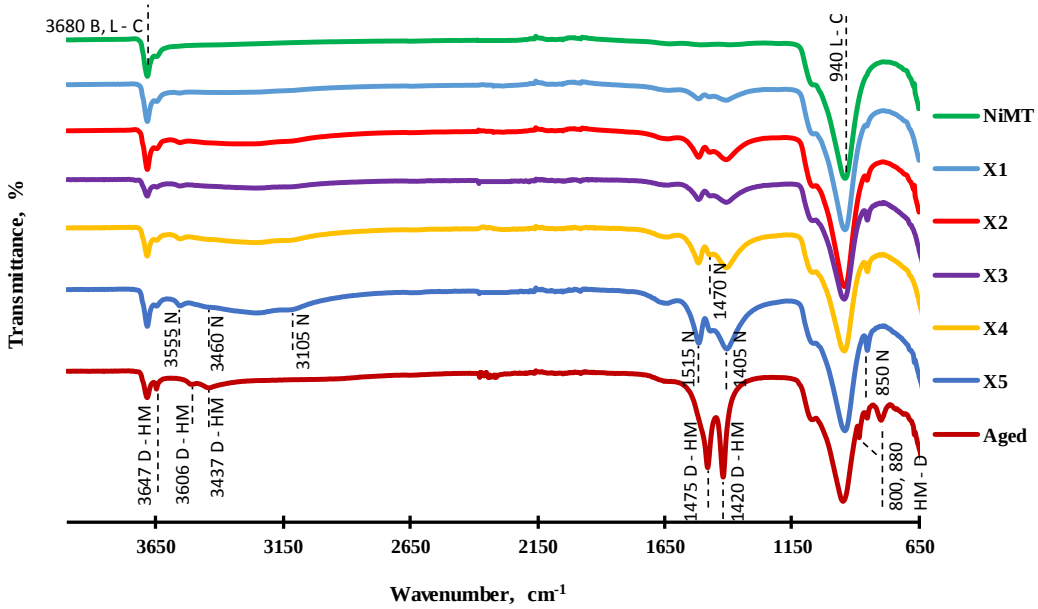

Figure 3-8. ATR–FTIR spectra of as–received NiMT, and carbonated NiMT samples corresponding to 5 carbonation cycles (X1 – X5), and aged NiMT sample corresponding to the 59–61 mm slice. Dotted lines show features pertaining to brucite (B), chrysotile (C), dypingite (D), hydromagnesite (HM), lizardite (L), and nesquehonite (N). The feature near 800-880 cm^{-1} is characteristic of hydromagnesite for aged NiMT sample and suggests that co–nucleation and growth of hydromagnesite (or dypingite) did not occur for the X1-X5 carbonated samples.

These band splits are characteristic of bicarbonate anion suggesting that bicarbonate may be a building block of the nesquehonite structure. As the extent of carbonation progresses further from X1 to X5, broadening of the infrared bands in the 3109–3460 cm^{-1} region corresponds to OH stretching mode of structural water in nesquehonite crystal. The feature at 3555 cm^{-1} has been associated to the stretching mode of the hydroxyl group either in H_2O or hydroxide [23, 35]. The CO_3^{2-} *v*3 asymmetric stretching vibrations of hydromagnesite (and dypingite) manifest as strong bands at *ca*.1420 and 1479 cm^{-1} whereas

the band near 3647 cm^{-1} is reminiscent of the hydromagnesite (and dypingite) hydroxyl groups. Similarly, the weak band split at 3645 cm^{-1} regarded to be OH^- characteristics in nesquehonite due to the inner OH stretch coordinated to $Mg^{2+}Fe^{2+}$ [36]. In contrast to the 59–61 mm deep slice where the 800 and 880 cm^{-1} vibrational features characteristic of hydromagnesite CO_3^{2-} bending vibrations are manifest, their nonappearance for each of the 5 younger NiMT wet carbonation samples is an indirect evidence of the long-term phase transformation of nesquehonite into less hydrated carbonates, e.g., hydromagnesite, as unveiled from the XRD study.

3.4 Conclusion

The formation and stability of nesquehonite as a carbon sink for mineral ambient carbonation of serpentine tailings and mineral wastes from the Dumont open–pit mining project were studied. Wetting/drying and freeze/thaw carbonation cycles, reproduced in laboratory conditions to emulate the behavior of these ultramafic substrates under natural outdoor variabilities, had a significant impact both on their carbonation kinetics and stability of the primary carbonates. Laboratory observations reveal that nesquehonite, formed under wet ambient carbonation, gradually evolves into an amorphous (presumably carbonate) phase when subjected to drying temperatures between 40 and 70°C. Furthermore, the long–term monitoring over 2 years of an already carbonated NiMT which was made up of spent materials carbonated under accelerated wet ambient conditions, revealed the lack of stability of the initial nesquehonite, which evolved into dypingite and hydromagnesite depending on core depth, *i.e.*, age, and wetting/drying history of the slice. As revealed from XRD, nesquehonite was completely transformed into hydromagnesite for the dryer upper slices, whereas dypingite is the more abundant carbonate in the deeper slices. In the intermediate slices, both dypingite and hydromagnesite coexist and such gradation is tentatively linked to the residual water left in the artificial core, with a negative water saturation gradient from the lower wetter to the upper dryer slices. Natural seasonal variations reflecting in wetting/drying and freeze/thaw cycles were shown to stimulate with varying degrees the exfoliation of the carbonated mineral surfaces contributing into rejuvenating reactive surfaces ready to undergo additional carbonation.

3.5 References

[1] D.A.C. Manning, P. Renforth, E. Lopez-Capel, S. Robertson, N. Ghazireh, Carbonate precipitation in artificial soils produced from basaltic quarry fines and composts: An opportunity for passive carbon sequestration, Int. J. Greenhouse Gas Control 17 (2013) 309-317.

[2] J. Pronost, G. Beaudoin, J.-M. Lemieux, R. Hébert, M. Constantin, S. Marcouiller, M. Klein, J. Duchesne, J.W. Molson, F. Larachi, X. Maldague, CO2-depleted warm air venting from chrysotile milling waste (Thetford Mines, Canada): Evidence for in-situ carbon capture from the atmosphere, Geology 40 (2012) 275-278.

[3] E.J. Swanson, K.J. Fricker, M. Sun, A.-H.A. Park, Directed precipitation of hydrated and anhydrous magnesium carbonates for carbon storage, Physical Chemistry Chemical Physics 16 (2014) 23440-23450.

[4] D.W. Ming, W.T. Franklin, Synthesis and Characterization of Lansfordite and Nesquehonite1, Soil Sci. Soc. Am. J. 49 (1985) 1303-1308.

[5] A. Beinlich, H. Austrheim, In situ sequestration of atmospheric CO2 at low temperature and surface cracking of serpentinized peridotite in mine shafts, Chem. Geol. 332–333 (2012) 32-44.

[6] L. Hopkinson, P. Kristova, K. Rutt, G. Cressey, Phase transitions in the system MgO–CO2–H2O during CO2 degassing of Mg-bearing solutions, Geochim. Cosmochim. Acta 76 (2012) 1-13.

[7] V. Ferrini, C. De Vito, S. Mignardi, Synthesis of nesquehonite by reaction of gaseous CO2 with Mg chloride solution: Its potential role in the sequestration of carbon dioxide, Journal of Hazardous Materials 168 (2009) 832-837.

[8] P. Ballirano, C. De Vito, V. Ferrini, S. Mignardi, The thermal behaviour and structural stability of nesquehonite, MgCO3·3H2O, evaluated by in situ laboratory parallel-beam X-ray powder diffraction: New constraints on CO2 sequestration within minerals, Journal of Hazardous Materials 178 (2010) 522-528.

[9] J. Pronost, G. Beaudoin, J. Tremblay, F. Larachi, J. Duchesne, R. Hébert, M. Constantin, Carbon Sequestration Kinetic and Storage Capacity of Ultramafic Mining Waste, Environ. Sci. Technol. 45 (2011) 9413-9420.

[10] G.P. Assima, F. Larachi, G. Beaudoin, J. Molson, Dynamics of carbon dioxide uptake in chrysotile mining residues – Effect of mineralogy and liquid saturation, Int. J. Greenhouse Gas Control 12 (2013) 124-135.

[11] G.P. Assima, F. Larachi, J. Molson, G. Beaudoin, Emulation of ambient carbon dioxide diffusion and carbonation within nickel mining residues, Miner. Eng. 59 (2014) 39-44.

[12] A. Entezari Zarandi, F. Larachi, G. Beaudoin, B. Plante, M. Sciortino, Multivariate study of the dynamics of CO2 reaction with brucite-rich ultramafic mine tailings, Int. J. Greenhouse Gas Control 52 (2016) 110-119.

[13] A.V. Kazakov, M.M. Tikhomirova, V.I. Plotnikova, The system of carbonate equilibria, International Geology Review 1 (1959) 1-39.

[14] P.J. Davies, B. Bubela, The transformation of nesquehonite into hydromagnesite, Chem. Geol. 12 (1973) 289-300.

[15] L. Hopkinson, K. Rutt, G. Cressey, The Transformation of Nesquehonite to Hydromagnesite in the System CaO-MgO-H2O-CO2: An Experimental Spectroscopic Study, The Journal of Geology 116 (2008) 387-400.

[16] W. Cheng, Z. Li, Controlled Supersaturation Precipitation of Hydromagnesite for the MgCl2−Na2CO3 System at Elevated Temperatures: Chemical Modeling and Experiment, Ind. Eng. Chem. Res. 49 (2010) 1964-1974.

[17] A. Botha, C.A. Strydom, Preparation of a magnesium hydroxy carbonate from magnesium hydroxide, Hydrometallurgy 62 (2001) 175-183.

[18] M. Hänchen, V. Prigiobbe, R. Baciocchi, M. Mazzotti, Precipitation in the Mg-carbonate system—effects of temperature and CO2 pressure, Chem. Eng. Sci. 63 (2008) 1012-1028.

[19] K.J. Fricker, A.-H.A. Park, Effect of H2O on Mg(OH)2 carbonation pathways for combined CO2 capture and storage, Chem. Eng. Sci. 100 (2013) 332-341.

[20] J. Suzuki, M. Ito, Nesquehonite from yoshikawa, aichi prefecture, japan: Occurrence and thermal behaviour, The Journal of the Japanese Association of Mineralogists, Petrologists and Economic Geologists 69 (1974) 275-284.

[21] G. Jauffret, J. Morrison, F.P. Glasser, On the thermal decomposition of nesquehonite, J Therm Anal Calorim 122 (2015) 601-609.

[22] J. Lanas, J.I. Alvarez, Dolomitic lime: thermal decomposition of nesquehonite, Thermochim. Acta 421 (2004) 123-132.

[23] B. Morgan, S.A. Wilson, I.C. Madsen, Y.M. Gozukara, J. Habsuda, Increased thermal stability of nesquehonite (MgCO3·3H2O) in the presence of humidity and CO2: Implications for low-temperature CO2 storage, Int. J. Greenhouse Gas Control 39 (2015) 366-376.

[24] G.P. Assima, F. Larachi, G. Beaudoin, J. Molson, CO2 Sequestration in Chrysotile Mining Residues—Implication of Watering and Passivation under Environmental Conditions, Ind. Eng. Chem. Res. 51 (2012) 8726-8734.

[25] G.P. Assima, F. Larachi, J. Molson, G. Beaudoin, Impact of temperature and oxygen availability on the dynamics of ambient CO2 mineral sequestration by nickel mining residues, Chem. Eng. J. 240 (2014) 394-403.

[26] M. Sciortino, J.E. Mungall, J. Muinonen, Generation of High-Ni Sulfide and Alloy Phases During Serpentinization of Dunite in the Dumont Sill, Quebec, Econ. Geol. 110 (2015) 733-761.

[27] R.T. Amos, D.W. Blowes, B.L. Bailey, D.C. Sego, L. Smith, A.I.M. Ritchie, Waste-rock hydrogeology and geochemistry, Appl. Geochem. 57 (2015) 140-156.

[28] G.P. Assima, F. Larachi, J. Molson, G. Beaudoin, Accurate and direct quantification of native brucite in serpentine ores—New methodology and implications for CO2 sequestration by mining residues, Thermochim. Acta 566 (2013) 281-291.

[29] A.L. Harrison, G.M. Dipple, I.M. Power, K.U. Mayer, The impact of evolving mineral–water–gas interfacial areas on mineral–fluid reaction rates in unsaturated porous media, Chem. Geol. 421 (2016) 65-80.

[30] K. Lechat, J.-M. Lemieux, J. Molson, G. Beaudoin, R. Hébert, Field evidence of CO2 sequestration by mineral carbonation in ultramafic milling wastes, Thetford Mines, Canada, Int. J. Greenhouse Gas Control 47 (2016) 110-121.

[31] C. Palache, H. Berman, C. Frondel, Dana's System of Mineralogy, Wiley, New York, 1944.

[32] J. Ji, Y. Ge, W. Balsam, J.E. Damuth, J. Chen, Rapid identification of dolomite using a Fourier Transform Infrared Spectrophotometer (FTIR): A fast method for identifying Heinrich events in IODP Site U1308, Marine Geology 258 (2009) 60-68.

[33] D.G. Henry, J.S. Watson, C.M. John, Assessing and calibrating the ATR-FTIR approach as a carbonate rock characterization tool, Sedimentary Geology (2016).

[34] R.L. Frost, S.J. Palmer, Infrared and infrared emission spectroscopy of nesquehonite Mg(OH)(HCO3)·2H2O–implications for the formula of nesquehonite, Spectrochim. Acta, Part A 78 (2011) 1255-1260.

[35] L. Zhao, L. Sang, J. Chen, J. Ji, H.H. Teng, Aqueous Carbonation of Natural Brucite: Relevance to CO2 Sequestration, Environ. Sci. Technol. 44 (2010) 406-411.

[36] R.L. Frost, B. Jagannadha Reddy, M.J. Dickfos, Raman spectroscopy of the nickel silicate mineral pecoraite—an analogue of chrysotile (asbestos), Journal of Raman Spectroscopy 39 (2008) 909-913.

Chapter 4.

Ambient Mineral Carbonation of Different Lithologies of Mafic to Ultramafic Mining Wastes/Tailings – A Comparative Study

Ali **Entezari-Zarandi**,[1] Faïçal **Larachi**,[*,1] Georges **Beaudoin**,[2] Benoît **Plante**,[3] Michelle **Sciortino**[4]

[1]Department of Chemical Engineering, Université Laval, Québec, QC, Canada G1V 0A6

[2]Department of Geology and Geological Engineering Université Laval, Québec, QC, Canada G1V 0A6

[3]Université du Québec en Abitibi-Témiscamingue, Rouyn-Noranda, Québec, Canada J9X 5E4

[4]Senior Project Geologist, Royal Nickel, Toronto, Ontario, Canada

Abstract

Four lithologies of the Dumont nickel project were studied for assessing the carbonation capacity in ambient conditions of waste rocks and mineral processing tailings consisting of dunite, peridotite, gabbro, and volcanic materials. Mineral carbonation of these mine waste and tailing minerals is contemplated as a premium solution to permanently trap atmospheric CO_2 into solid carbonates using a differential batch carbonation cell and carbonate precipitation columns. The different mafic to ultramafic lithologies of the Dumont nickel project were characterized before and after carbonation by means of X-ray diffraction and thermogravimetry analyses, Fourier transform infrared spectroscopy, optical microscopy, and quantitative evaluation of minerals by scanning electron microscopy. It was found that for identical size fractions, carbonation of rock wastes was quite limited as compared to the tailings. Brucite more abundant in dunite and peridotite substrates was found to be the main reactant involved in carbonation as compared to other less-reactive magnesium silicate minerals. Nesquehonite, the prevalent magnesium carbonate species formed in wet ambient carbonation, remained stable despite prolonged exposition in dry conditions of ambient air. Finally, some design recommendations were formulated to overcome the dilemma due to separate storage of high-permeability brucite-poor (lowly reactive) waste rock stockpiles of finely-ground, and low-permeability brucite-rich (highly reactive) tailings.

Résumé

Quatre lithologies et des rejets de concentrateur provenant du projet Dumont ont été étudiés afin d'évaluer leur capacité de carbonatation dans les conditions ambiantes. Les matériaux étudiés sont composés principalement de dunite, de péridotite, de gabbro et de minéraux d'origine volcanique. La carbonatation minérale des matériaux ultramafiques est considérée comme une solution permanente pour fixer du CO_2 atmosphérique sous formes de carbonates en utilisant des cellules de carbonatation différentielles et des cellules de précipitation des carbonates. Les roches mafiques et ultramafiques ont été caractérisées avant et après les essais de carbonatation en utilisant la diffraction aux rayons X, la thermogravimétrie, la spectrométrie infrarouge à transformée de Fourier, la microscopie optique et une évaluation quantitative par microscopie électronique à balayage. Les résultats suggèrent que pour une granulométrie similaire, la carbonatation des stériles est relativement limitée comparativement aux rejets de concentrateur. La brucite présente dans les échantillons de dunite et de péridotite est le principal minéral impliqué dans la carbonatation comparée aux autres sources de magnésium, moins réactives. La nesquéhonite est le principal carbonate formé dans les conditions ambiantes et est stable malgré la longue durée des essais. Des recommandations ont été proposées afin de pallier aux contraintes liées à l'entreposage séparé des stériles et des rejets de concentrateur. En effet, les stériles sont très perméables, pauvres en brucite et moins réactifs, alors que les rejets de concentrateur sont plus fins, riches en brucite et très réactifs.

4.1 Introduction

The removal of non-economical surrounding materials; overburden and rock, during the mining process leads to the production of so-called “waste rock”. As ore is mined and subjected to comminution processes through a suite of mineral processing operations for the separation of the valuable concentrates produces, a mass of finely ground particles is produced. This process is essential to the liberation of the valuable economic minerals, the non-economic residues of which produces as fine grained mineral mass, termed mine “tailings”. While waste rocks are mainly composed of coarse grained materials, tailings consist of very fine particles potentially offering superior reactivity owing to their larger specific surface area. Therefore, long-term carbon dioxide (CO_2) storage in ultramafic mine tailings and waste rocks is considered as an environmentally and economically viable approach in response to the global warming concerns. Passive mineral carbonation is a thermodynamically favorable process in nature where environmentally-available energy is used to fixate atmospheric carbon dioxide with mafic/ultramafic minerals, the result is secondary carbonate minerals resulting in the storage of CO_2 in the form of stable and environmentally benign carbonates [1].

Starting from mining and industrial residues, tremendous efforts are being deployed to implement and optimize carbon capture and storage solutions at industrial scale and to permanently sequester atmospheric CO_2 as stable mineral carbonates [2-12]. Alkaline waste such as steel slag [13-15], cement kiln dust [2, 16, 17], coal fly ash [18-20], saline waste water [21], and municipal solid wastes [22, 23] are also being evaluated for their usefulness in carbonation, in addition to the role of bacterial activity in mineral carbonation, *i.e.*, carbonate bio-mineralization [24, 25].

Under ambient conditions, different environmental factors such as temperature, CO_2 supply, water availability, and wetting/drying cycles may take part in the formation of meta-stable or secondary carbonates such as lansfordite, nesquehonite or hydromagnesite [10, 26-30]. In-situ formation of these carbonates sometimes has serendipitous advantages such as the ability to cement the reacting particles together to prevent air-borne transport of mineral fires, such as chrysotile. It has been shown that carbonation is sensitive to water saturation

and watering frequency of the soaked mineral specimens while stability of the carbonate products is also tributary of water availability and wetting/drying episodes [27, 31].

The aim of the present study is to gain knowledge on the carbonation behavior of the different mafic to ultramafic lithologies of the Dumont nickel project at ambient temperature and wet conditions. Figure 4-1a shows the location of the Dumont nickel project (DNP) in the Abitibi-Temiscamingue region in North-Western Québec (Canada). DNP is estimated to be the world's fifth largest nickel production site [32] with a target to exploit nickel sulfides, namely, pentlandite, $(Fe,Ni)_9S_8$, and heazlewoodite (Ni_3S_2), as well as nickel-iron alloys in the form of awaruite ($Ni_{2.5-3}Fe$). The Dumont sill consists of a layered mafic-ultramafic intrusion (6800 m in length with average thickness of 700 m) located in the Abitibi greenstone belt (Figure 4-1b). It is composed of variably-serpentinized dunite rocks rich in lizardite with minor amounts of chrysotile, brucite, magnetite and antigorite [33, 34]. The sill is a lower-ultramafic zone comprising dunite and peridotite overlain by a mafic zone of gabbro, quartz gabbro and clinopyroxenite [33]. The sill is hosted in mafic volcanics which form the Abitibi-greenstone belt. Several faults (Figure 4-1c) parallel to the strike of the intrusion have caused offsets in mineralization as well as alteration supported by structural core logging data and airborne magnetometer surveys [34]. The ultramafic zone itself is comprised of upper and lower peridotite and dunite subzones as shown in Figure 4-1d. The nickel deposit is hosted in the dunite subzone.

These four lithologies pertaining to the Dumont nickel project were studied for assessing the carbonation capacity in ambient conditions of their resulting waste rocks and processing tailings. Mineral carbonation was monitored using a differential batch carbonation cell and carbonate precipitation cells aided with an ensemble of characterization techniques before and after carbonation (X-ray diffraction and thermogravimetry analyses, Fourier transform infrared spectroscopy, optical microscopy, and quantitative evaluation of minerals by scanning electron microscopy). Stability of the neo-formed carbonate product was also assessed in terms of mineralogical evolution over time. Finally, some design recommendations are formulated to circumvent limitations inherent to the lower reactivity of waste rocks as opposed to the superior reactivity of the finely-ground and brucite-rich tailings.

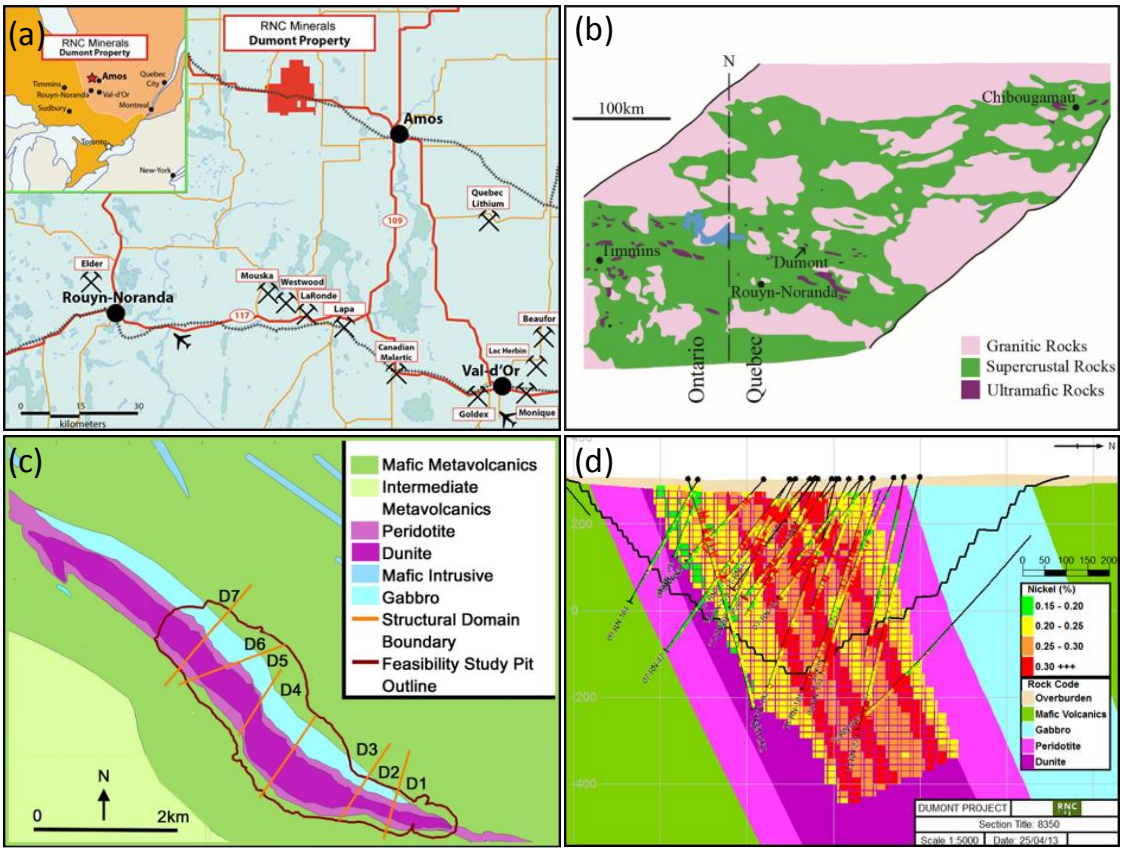

Figure 4-1. Location of Dumont site (a), geologic map of the Dumont sill within the Abitibi greenstone belt (b), geologic map of the Dumont deposit (60-70° dip to NW) (c), cross-sectional view of the Dumont deposit with drill holes showing lithology down drill hole trace (d). (All maps provided by RNC minerals).

4.2 Materials and Methods

4.2.1 Mine Wastes and Tailings

The different lithologies: dunite, peridotite, gabbro, and volcanic take part in the production of waste materials during the mining process. Open-pit mining is planned to start from the extreme southeast of the deposit to access the DNP orebody [32]. Thus, waste rocks resulting from the mining operation as well as the overburden have to be cut out first before being impounded in dump sites located on the hanging wall side of the pit [32].

The ore-bearing zone is the ultramafic dunite body which will feed the processing plant for crushing, milling, flotation and magnetic separation. Hence, the post-processed tailings will consist of finely ground materials, as opposed to the coarsely generated waste rock due to blasting. From a mineralogical point of view, the dunite zone hosts noticeable amounts of brucite which is regarded as the most reactive magnesium mineral in terms of CO_2 sequestration. The whole-rock geochemical analysis of the different DNP lithologies, namely, dunite ([DU]), peridotite ([PD]), gabbro ([GB]), and volcanic ([VO]), is summarized in Table 4-1.

Table 4-1. Whole rock analysis of the different lithologies of the Dumont nickel project

	Lithology sample			
Analytes (wt.%)	**[DU]**	**[PD]**	**[GB]**	**[VO]**
SiO_2	34.5	35.1	47.9	47.0
Al_2O_3	0.48	1.0	11.3	11.7
Fe_2O_3	8.91	9.1	10.3	16.5
CaO	0.05	0.50	13.3	10.3
MgO	41.3	41.0	14.0	5.6
Cr_2O_3	1.02	0.63	0.11	0.01

These lithological samples, provided by RNC Minerals in the form of quarter drill cores, were milled and sieved at different size fractions. For each lithology, the -210+149 μm and -149+105 μm size fractions, referred to as +150 μm and -150 μm, respectively, were isolated and tested for carbonation in this chapter. The major minerals identified from X–ray diffraction (Figure 4-2) as well as some physical properties of each sample are gathered in Table 4-2.

4.2.2 Materials Characterization

X–ray powder diffraction (XRD) and Fourier transform infrared spectroscopy (FTIR) in the attenuated total reflection (ATR) mode were used for mineralogical characterization

in both unreacted and carbonated fractions. A Siemens D5000 diffractometer was employed to identify the crystalline minerals using Cu Kα radiation (λ = 1.54059 Å). The X–ray tube was operated at 40 kV/30 mA and data were collected at a 1°/min angular sweep. The 2θ angular range recorded was 5°–65° with a 0.02° step size. FTIR-ATR determinations were carried out on an iS50 Fourier transform spectrometer (Nicolet) equipped with a mercury cadmium telluride detector cooled with liquid nitrogen and a potassium bromide coated germanium beam splitter. A golden–gate attenuated total reflection module (Specac Ltd.) was used to register attenuated total reflection spectra on a diamond crystal between 750 and 3750 cm^{-1}.

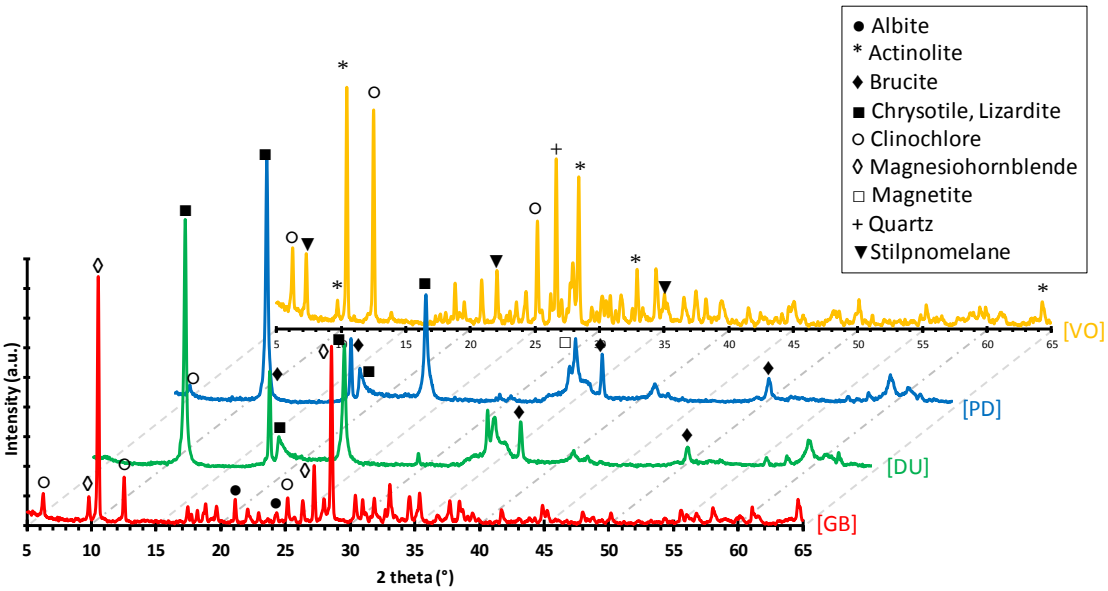

Figure 4-2. X–ray powder diffractograms of [DU], [GB], [PD] and [VO] samples. Diffraction peaks highlighted: albite (●), actinolite (*), brucite (♦), chrysotile/lizardite (■), clinochlore (○), magnesiohornblende (◊), magnetite (□), quartz (+) and stilpnomelane (▼).

The specific surface areas of dried (at 110°C overnight under N_2 stream) and weighed sieved fractions were determined from nitrogen adsorption/desorption at 77K (-196.15°C) on a Micromeritics Tristar 3000 instrument using the Brunauer–Emerett–Teller (BET) adsorption isotherm method. Bulk specific gravities were determined by an Ultrapyc 1200e gas pycnometer (Quatachrome Instruments) using N_2 and averaging three repeat tests. The

content of native brucite in each lithological fraction was determined using a coupled thermogravimetry-mass spectrometry method developed by our group [35] (TGA-MS, Perkin Elmer Pyris Diamond TGA-DTA and Thermostar Prisma QMS200, Pfeiffer Vacuum). The mass loss of unreacted samples over the 250-375°C temperature range (Appendix C, Figure S1) was stoichiometrically related to brucite dehydroxylation [35].

Table 4-2. Major minerals and properties of the different lithologies of the Dumont nickel project for the -149+105 μm size fractions

	Lithology sample			
Properties	[DU]	[PD]	[GB]	[VO]
Density (g/cm^3)	2.67	2.66	3.04	2.98
BET area (m^2/g)	4.95	4.26	16.35	3.58
Organic Carbon (%)	<0.1	<0.1	<0.1	<0.1
Native brucite (%)*	8.5	8.9	0.41	0.62
Major minerals				
Lizardite	✓	✓		
Chrysotile	✓	✓		
Magnetite	✓	✓		
Brucite	✓	✓		
Magnesiohornblende			✓	
Clinochlore		✓	✓	✓
Ferrosilite			✓	
Quartz			✓	✓
Actinolite				✓
Stilpnomelane				✓

* See also Figure S1 (Appendix C).

4.2.3 Differential Batch Carbonation Cell

Carbonation monitoring of samples from the different lithologies was carried out in a differential thin–layer carbonation batch cell [6, 26, 27, 36]. The carbonation cell involves three main elements: a gas reservoir containing CO_2/N_2 mixtures with varying mole fractions, a sample holder for supporting the thin mineral layer, and a diffusion compartment (Figure 4-3a). Batch carbonation tests were performed upon diffusion of CO_2-containing gas across a 10-12 mm thin mineral layer, typically *ca*. 35 g of material, for the +150µm and -150µm fractions for each type of lithology. Repeated gentle hand–tapping on the body of the sample holder helped elimination of the cavities and trapped air in the thin layer as well as leveling off of the sample free surface. Before carbonation, the samples were systematically soaked in water by stepwise addition of controlled amounts of deionized water until an overall liquid saturation of 50 % v/v was attained. This saturation was shown to be the optimal wetting degree to achieve the highest capacities and fastest rates of carbonation [6, 36].

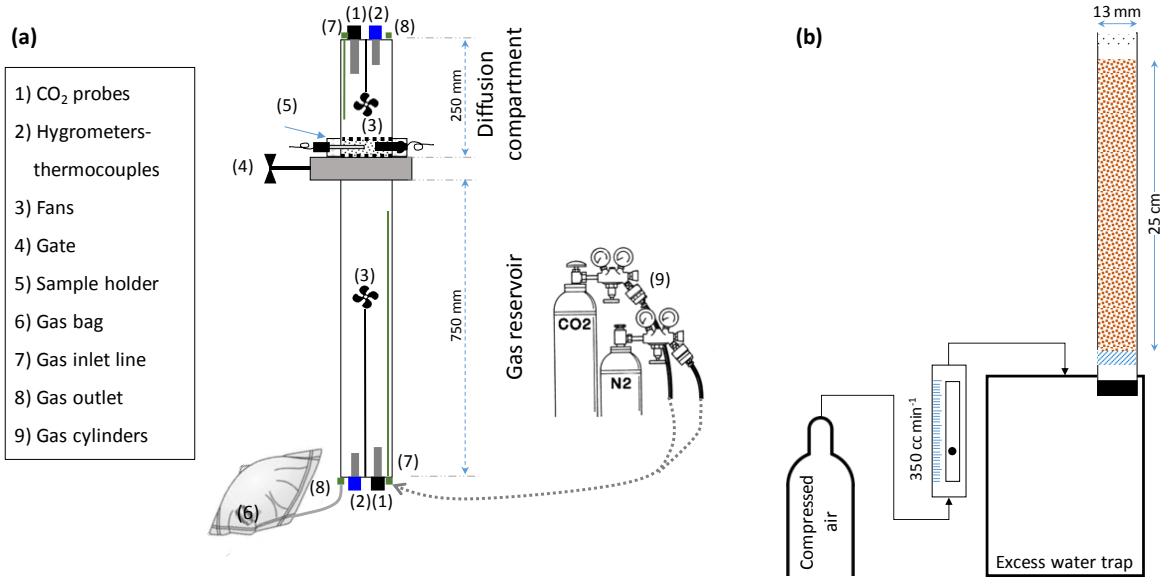

Figure 4-3. Diagrams of the experimental setups used for monitoring passive carbonation in a differential thin–layer carbonation batch cell (a), and for carbonate accumulation in carbonate precipitation columns (b).

Each test started by contacting the wetted layer with CO_2–rich gas mixtures (10%v/v CO_2, balance N_2) until all the CO_2 contained in the gas reservoir was consumed. For additional operational details on the carbonation cell, readers are referred to [36] and [6].

4.2.4 Carbonate Precipitation Cell

To emulate field drainage from ultramafic waste piles and subsequent carbonate precipitation thereof, a stream of ambient air delivered at room temperature and atmospheric pressure from a compressed-air cylinder was circulated upward through two identical columns each hosting approximately 45 g of [DU] and [PD] samples (Figure 4-3b). Coarser sample fractions (-354+297 μm) were used in order to prevent excessive pressure drops and material entrainment out of the cells due to air flow. The two columns were transparent plastic tubes 280 mm long with an inner diameter of 13 mm. They were terminated with a fritted disc at the bottom serving both as a sample holder and a gas distributor, and a metallic mesh at the top for ensuring a uniform radial distribution of the trickling water. Addition from the top of the column of random amounts of deionized water maintained the cell inventory *temporarily* wet owing to capillary holdup while excess amounts of water, approximately 30 mL, were drained and accumulated at the bottom in an excess water trap (Figure 4-3b). Due to continuous air flow, both capillary water across sample and excess water from trap gradually evaporated leaving behind, after several watering-evaporation cycles, white fine-grained crystalline needle-like precipitates (Appendix C, Figure S2). Post-mortem analyses of these precipitates were done once after no water was added but the air stream was kept in circulation across the setup for two more weeks. The white deposits thus formed were collected immediately for FTIR-ATR and XRD analyses. For the sake of assessment of precipitate stability, the materials collected from the excess water trap were stored in an open container for a period of 18 months before re-analyzing their mineralogical structure by ATR-FTIR. Care was taken to prevent contamination with foreign substances of the open container.

4.3 Results and Discussion

4.3.1 Carbonation of Sample Lithologies in Differential Batch Cell

A LabView monitoring interface was customized for multiple-sensor data acquisition of the instantaneous evolutions of CO_2 mole fractions in gas reservoir and diffusion compartment shown in Figure 4-3a, and of pH and pore water electrical conductivity of the carbonating mine waste samples at ambient temperature (Figure 4-4). Temperature, hygrometric, and total diffuse reflectance instrumentation was also available for comprehensive monitoring of the dynamic evolution in the three cell sections [27].

The dunite and peridotite samples exhibited similar carbonation patterns as they feature highly reactive materials vis-à-vis carbonation for both tested fractions (Figures 4-4a1,b1). This was unlike the carbonation of gabbro and volcanic samples which was comparatively slow (Figures 4-4c1,d1). For instance, the carbonation reactivity was in the order [VO] < [GB] < [DU] < [PD] for the -150 μm size fractions.

As expected, the reactivity of the finer size fraction outpaced that of the coarser for each lithology, though the difference was more pronounced in the case of [DU] and [PD] samples. In addition to size fraction, there is also a connection between pH and carbonation reactivity (Figures 4a2-d2). Specifically, in the case of [DU] and [PD] samples, finer particle size led to faster restoration of pH toward the initial value.

One may also note that the higher the medium pH, the faster the carbon dioxide exhaustion. The time evolution of electrical conductivity (ECp) of pore water simultaneously registered with CO_2 uptake and pH variations is illustrated in Figures 4-4a3-d3 for the four lithologies. [DU] and [PD] ECp readings increase significantly over the early minutes of carbonation before reaching a maximum. This maximum is more prominent for the coarser (+150 μm) than for the finer (-150 μm) size fractions. This suggests that the electrical conductivity is impacted more by proton production from the acidic absorption of CO_2 than from leaching of magnesium cations as their concentrations are lower in coarser size fractions. Another non-exclusive interpretation could be that the higher carbonation reactivity associated with the -150 μm size fraction implies faster consumption of metal cations and bicarbonate/carbonate species, thereby generating lower ECp.

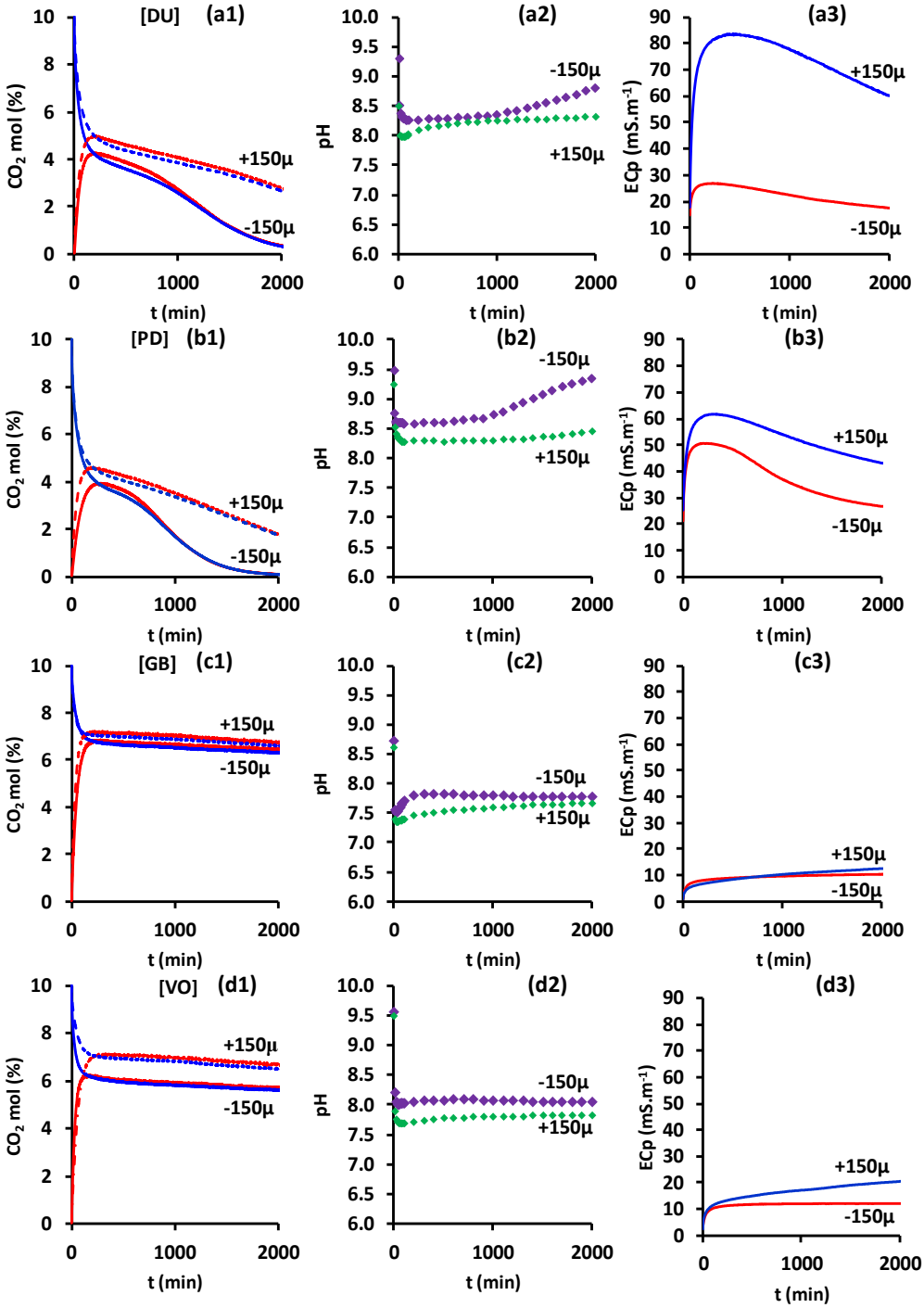

Figure 4-4. Instantaneous evolutions of CO_2 mole fractions in gas reservoir and diffusion compartment, and of pH and poral water electrical conductivity (ECp) during the wet carbonation of dunite [DU] (a1-3), peridotite [PD] (b1-3), gabbro [GB] (c1-3) and volcanic [VO] (d1-3) samples.

The above carbonation behaviors stem from the different mineralogy and texture of the tested samples as indicated in Tables 4-1,4-2. Furthermore, quantitative evaluation of minerals by scanning electron microscopy (QEMSCAN) maps of [DU] and [PD] drill cores (Figure 4-5) reveal the presence of fine grained brucite particles locked in the main serpentine matrix. This is especially remarkable in the case of brucite, which is detected in the form of numerous tiny inclusions in dunite (Figure 4-5a). As comminution towards finely ground particles is tantamount to the liberation of increased brucite inclusions, higher carbonation rates are expected for the -150 μm size fractions *versus* +150 μm size fractions, as confirmed form Figure 4-4. [DU] and [PD] QEMSCAN analyses sorted as a function of mass fraction and corresponding mean particle size for the detected minerals are summarized in Table S1 (Appendix C).

It can be seen that brucite particles, typically 7 to 8 μm in size, and more abundant in dunite than in peridotite, are interspersed in serpentinic bulk. The analyses also indicate the presence of Mg serpentine, mainly lizardite and chrysotile (Table 4-2), in significant amounts in both sample matrices implying completely serpentinized rocks (0-0.1% olivine content), whereas clinopyroxene, chlorite, and magnetite are more abundant in the [PD] sample (Appendix C, Table S1).

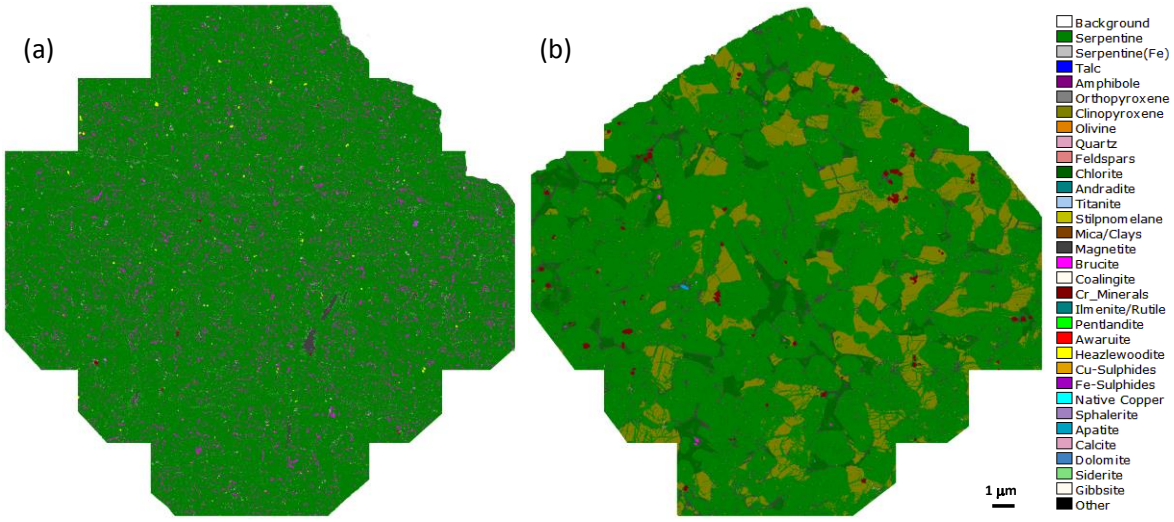

Figure 4-5. QEMSCAN mineral assays of polished sections of [DU] (a) and [PD] (b) samples.

According to Table 4-2, quantification of native brucite led to comparable levels near 8.5-8.9 % for dunite and peridotite. Such levels are typically an order of magnitude higher than the amounts of brucite assayed in gabbro and the volcanic rock samples and are coherent with the more pronounced [DU] and [PD] reactivity *versus* that of [GB] and [VO] (Figure 4-4). Note that the brucite concentration within peridotite as revealed from QEMSCAN (Appendix C, Table S1) and that derived from thermogravimetry-mass spectrometry method (Table 4-2) are not the same. This might be ascribed to variabilities inherent to the different sampled cores which is in turn due to field inhomogeneity. In addition, [GB] and [VO] samples contain much less magnesium than [DU] and [PD] while calcium is in higher amounts in the former than in the latter sample pairs (Table 4-1). Calcium, unlike the samples free brucitic magnesium, is not present in its free $CaO/Ca(OH)_2$ forms but is rather incorporated into the structures of actinolite, magnesiohornblende, and stilpnomelane. In ambient conditions, these minerals are not prone to leach as easily as chrysotile and lizardite [37-39].

4.3.2 Nesquehonite Precipitation and Stability

Over the time intervals shown in Figure 4-4, the carbonation kinetics is mainly tributary to the content of brucite in the tested lithologies. Protons produced during acidification of the pore water through CO_2 absorption (R1) are mitigated by the leaching of brucite (R2) to counter acidification of the medium. These two reactions progress favor dissolution of brucite as long as gaseous CO_2 is available in the gas reservoir (Figure 4-3a) until Mg^{2+} supersaturation conditions emerge and favor nucleation and then crystallization and/or precipitation of solid magnesium carbonates. The pH of these processes varies from 7.5 to 9 (Figures 4b1-d1) and suggests that crystallization/precipitation involves bicarbonates rather than aqueous carbonates. The reaction stoichiometry for formation of nesquehonite, as an example of hydrated carbonate, is given as (R3):

$$CO_2 + H_2O \rightarrow HCO_3^- + H^+ \quad \text{(R1)}$$

$$Mg(OH)_2 + 2H^+ \rightarrow Mg^{2+} + 2H_2O \quad \text{(R2)}$$

$$Mg^{2+} + 2HCO_3^- + 3H_2O \rightarrow Mg(HCO_3)(OH)\cdot 2H_2O + HCO_3^- + H^+ \quad \text{(R3)}$$

The white-colored needle-like precipitate collected as described in section 4.2.4 is mainly composed of nesquehonite, as revealed by XRD and FTIR-ATR (Appendix C, Figure S3). The collected precipitates from the [DU] cell was not sufficient for X-ray analysis, thus XRD was performed only on the material collected from the [PD] cell, while both samples were analyzed with ATR-FTIR. Optical microscopy images of the precipitates (Appendix C, Figure S2) likewise suggest nesquehonite in the form of elongated needle-like crystals. The time evolution of pH of the draining water collected in the excess water trap (Figure 4-3a) following the watering episodes of the carbonate precipitation cells was also monitored for both [PD] and [DU] columns. Drainage alkalization after the drained liquor was contacted with the [PD] powder was slightly higher than that from the [DU] (Figure 4-6). Such differences in alkalinity can be correlated to the larger amounts of brucite being leached from the [PD] sample in agreement both with the (R2) attenuated acidity and higher pH values registered for [PD] *versus* [DU] (Figures 4-4 a2,b2). Similarly, assuming oversaturation conditions met by the leached magnesium, formation of more nesquehonite in the case of the [PD] column *via* (R3) would explain the higher conversion of CO_2, regardless of size fractions, for the [PD] than for the [DU] sample, in agreement with Figures 4-4 a1,b1.

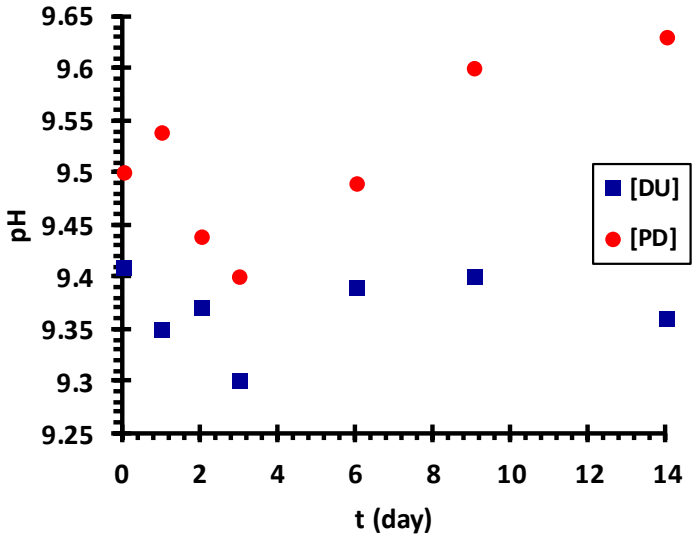

Figure 4-6. Change in pH as a function of time for [DU] and [PD] sample pulp solutions.

The FTIR-ATR transmittance spectra over the 1700 – 700 cm^{-1} wavenumber range for the [DU] and [PD] samples were collected from the top and bottom of each column (Figures 4-7a,b). The infrared band near 850 cm^{-1}, corresponding to C–O out-of-plane bend mode *v*2, and the vibrational features at 1405 cm^{-1}, 1470 cm^{-1}, and 1515 cm^{-1}, corresponding respectively to CO_3^{2-} and HCO_3^- *v*3 asymmetric stretching mode, become clearly visible for both top and bottom column carbonated samples. These features are not visible in the unreacted samples, the vibrational spectra of which are also shown for comparative purposes.

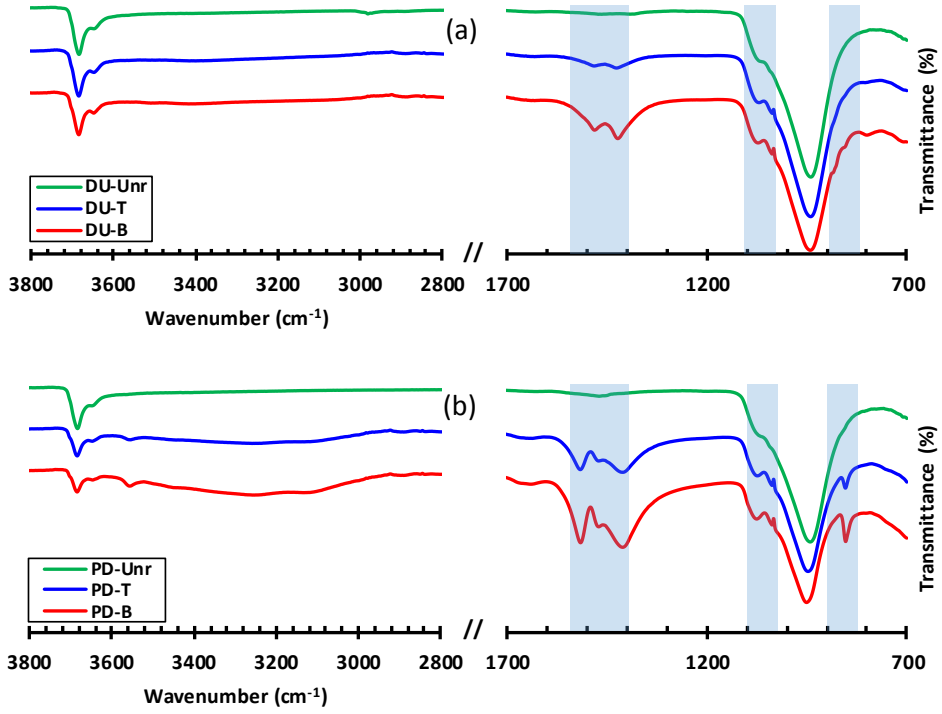

Figure 4-7. FTIR-ATR spectra of samples taken from [DU] (a) and [PD] (b) cells corresponding to samples from column top (DU-T and PD-T) and samples from column bottom (DU-B and PD-B) along with unreacted samples (DU-Unr and PD-Unr) shown for comparison.

Similarly, the 3109–3460 cm^{-1} region featured a broad vibrational content in the case of the [PD] sample, especially from the bottom one, corresponding to the OH stretching mode of structural water in nesquehonite crystals. This observation implies that carbonation conditions were met more favorably at the bottom of the column. Water addition, on the one

hand, facilitates leaching of magnesium minerals (R2). On the other hand, the gravity-driven downward transport of pore water tends to concentrate Mg towards the lower section of the column, leading to more carbonation towards the bottom exit of the column. The lower degree of water saturation near the column top limits both dissolution and precipitation reactions [27, 40, 41].

Nesquehonite was observed to gradually evolve into less hydrated dypingite and then hydromagnesite (on Mg-atom basis) upon its exposure to periodic wetting/drying cycles at room temperature over prolonged periods of time [27]. However, our current FTIR-ATR spectral observations after 18 months of exposure to the atmosphere (temperature and humidity) of the white-colored needle-like precipitate collected described above suggest that nesquehonite is stable in dry conditions. In other words, the kinetics of nesquehonite transformation into other thermodynamically stable carbonate phases is so slow that no meaningful changes could be witnessed from the FTIR-ATR spectra. This finding is in agreement with literature observations where thermal stability of nesquehonite was proven at least for a storage duration of 3 years with no decomposition [42].

4.3.3 Carbonation Differences of Waste Stockpiles *vs.* Tailings Ponds

As discussed earlier, the dunite and peridotite lithologies exhibited comparable carbonation behaviors while outpacing those of the gabbro and volcanic materials. Therefore, it is clear that the waste and tailing storage methods to be selected will affect the global potential of the disposed materials vis-à-vis passive mineral carbonation. From a mining engineering perspective, these four lithologies undergo different operations during the mine's life time. As a consequence of blasting operations during mine operations, the waste rock material produced out of the [GB] and [VO] lithologies is coarse grained and is stockpiled in the mine's vicinity. However, particularly important is the fact that nickel occurrence within the dunite body [33, 34], and to a lesser extent [PD], makes these two lithologies of interest for further mineral processing operations by turning their materials into very fine particle sizes for nickel liberation. After separation of the valuable nickel minerals, the fine-grained tailings, which consist of a dense pulp, are routed for storage in tailing ponds. If the [GB] and [VO] waste stockpiles possess high porous-medium permeability which facilitates atmospheric CO_2 transport and water percolation, the very fine-grained tailing ponds

containing [DU] and [PD] with varying degrees of water saturation exhibit particularly limited carbonation uptakes mainly due to the lower in-depth penetration of CO_2. These observations are in agreement with 5 year filed cell monitoring of DNP residues [43].

4.3.4 Waste Stockpile and Tailing Pond Design Issues

There is an obvious dilemma where the high-permeability stockpiles present poor carbonation potential whereas the high-carbonation potential of the tailings, due to higher brucite content and larger liquid-solid contact area between brucite and Mg serpentines and carbon ($CO_{2(g,aq)}$, $HCO_3^-{}_{(aq)}$, $CO_3^{2-}{}_{(aq)}$), is under-utilized in the pond configurations. One possible approach to overcome this limitation could be offset by new stockpiles designs incorporating combinations of fine-grained pulp and coarse grained waste rocks in such a way that tailings form stable thin coatings over the waste rock particles. This proposed method has similarities with the GEOCOAT® process [44] or the co-disposal technique of Golder Associates Ltd [45]. Furthermore, a number of mixing/coating strategies may be implanted on the site with an aim to mix and transfer material on conveyors or release paste at the edge of the dump to mix it on the stockpile face. Spraying the fine-grained pulp over coarse-grained waste rock as shown in Figure 4-8 could be an example. In this manner, the general problem associated with low CO_2 permeability into depth of tailing ponds is addressed. From another perspective, it is well known that carbonation results in cementing the particles together [27], thus carbonation similarly improves the (mechanical) structure stability of the waste stockpiles.

4.3.5 Conclusion

Different mafic to ultramafic lithologies forming mine tailings and waste rock sites were compared in terms of mineral carbonation capacities. It is concluded that carbonation of rock wastes is limited with regard to their mineralogical composition. However, brucite, a minor mineral in ultramafic rocks, found especially in dunite and peridotite substrates, was the main reactant involved in carbonation as compared to major magnesium silicate minerals which are harder to carbonate in ambient conditions. The prevalent magnesium carbonate product which formation is dictated by the availability of water was nesquehonite. Once

formed, the stability of nesquehonite was barely affected upon its subsequent exposure to non-humid environmental conditions over prolonged periods of times.

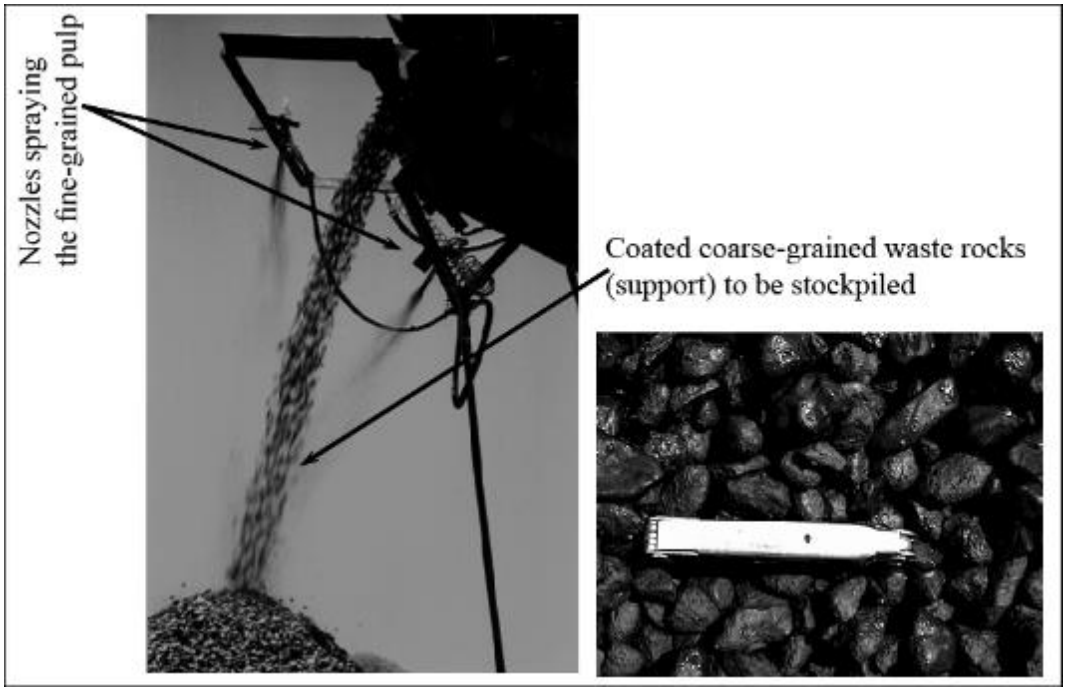

Figure 4-8. Spraying fine-grained pulp over coarse-grained waste rocks to enhance carbonation reactivity of waste rock/tailings stockpile (Reproduced from Harvey et al. (2002) with permission of Elsevier).

4.4 References

[1] D.A.C. Manning, P. Renforth, E. Lopez-Capel, S. Robertson, N. Ghazireh, Carbonate precipitation in artificial soils produced from basaltic quarry fines and composts: An opportunity for passive carbon sequestration, International Journal of Greenhouse Gas Control 17 (2013) 309-317.

[2] D.N. Huntzinger, J.S. Gierke, L.L. Sutter, S.K. Kawatra, T.C. Eisele, Mineral carbonation for carbon sequestration in cement kiln dust from waste piles, Journal of Hazardous Materials 168 (2009) 31-37.

[3] G.P. Assima, F. Larachi, J. Molson, G. Beaudoin, Impact of temperature and oxygen availability on the dynamics of ambient CO2 mineral sequestration by nickel mining residues, Chemical Engineering Journal 240 (2014) 394-403.

[4] F. Bodénan, F. Bourgeois, C. Petiot, T. Augé, B. Bonfils, C. Julcour-Lebigue, F. Guyot, A. Boukary, J. Tremosa, A. Lassin, E.C. Gaucher, P. Chiquet, Ex situ mineral carbonation for CO2 mitigation: Evaluation of mining waste resources, aqueous carbonation processability and life cycle assessment (Carmex project), Minerals Engineering 59 (2014) 52-63.

[5] M. Bodor, R. Santos, T. Van Gerven, M. Vlad, Recent developments and perspectives on the treatment of industrial wastes by mineral carbonation — a review, Central European Journal of Engineering 3 (2013) 566-584.

[6] A. Entezari Zarandi, F. Larachi, G. Beaudoin, B. Plante, M. Sciortino, Multivariate study of the dynamics of CO2 reaction with brucite-rich ultramafic mine tailings, International Journal of Greenhouse Gas Control 52 (2016) 110-119.

[7] A.L. Harrison, I.M. Power, G.M. Dipple, Accelerated Carbonation of Brucite in Mine Tailings for Carbon Sequestration, Environmental Science & Technology 47 (2013) 126-134.

[8] C. Julcour, F. Bourgeois, B. Bonfils, I. Benhamed, F. Guyot, F. Bodénan, C. Petiot, É.C. Gaucher, Development of an attrition-leaching hybrid process for direct aqueous mineral carbonation, Chemical Engineering Journal 262 (2015) 716-726.

[9] N.A. Meyer, J.U. Vögeli, M. Becker, J.L. Broadhurst, D.L. Reid, J.P. Franzidis, Mineral carbonation of PGM mine tailings for CO2 storage in South Africa: A case study, Minerals Engineering 59 (2014) 45-51.

[10] H.C. Oskierski, B.Z. Dlugogorski, G. Jacobsen, Sequestration of atmospheric CO2 in chrysotile mine tailings of the Woodsreef Asbestos Mine, Australia: Quantitative mineralogy, isotopic fingerprinting and carbonation rates, Chemical Geology 358 (2013) 156-169.

[11] A.-H.A. Park, L.-S. Fan, mineral sequestration: physically activated dissolution of serpentine and pH swing process, Chemical Engineering Science 59 (2004) 5241-5247.

[12] J. Pronost, G. Beaudoin, J. Tremblay, F. Larachi, J. Duchesne, R. Hébert, M. Constantin, Carbon Sequestration Kinetic and Storage Capacity of Ultramafic Mining Waste, Environmental Science & Technology 45 (2011) 9413-9420.

[13] O. Capobianco, G. Costa, L. Thuy, E. Magliocco, N. Hartog, R. Baciocchi, Carbonation of stainless steel slag in the context of in situ Brownfield remediation, Minerals Engineering 59 (2014) 91-100.

[14] A. Kirchofer, A. Becker, A. Brandt, J. Wilcox, CO2 Mitigation Potential of Mineral Carbonation with Industrial Alkalinity Sources in the United States, Environmental Science & Technology 47 (2013) 7548-7554.

[15] M. Salman, Ö. Cizer, Y. Pontikes, R.M. Santos, R. Snellings, L. Vandewalle, B. Blanpain, K. Van Balen, Effect of accelerated carbonation on AOD stainless steel slag for its valorisation as a CO2-sequestering construction material, Chemical Engineering Journal 246 (2014) 39-52.

[16] D.N. Huntzinger, J.S. Gierke, S.K. Kawatra, T.C. Eisele, L.L. Sutter, Carbon Dioxide Sequestration in Cement Kiln Dust through Mineral Carbonation, Environmental Science & Technology 43 (2009) 1986-1992.

[17] C.W. Noack, D.A. Dzombak, D.V. Nakles, S.B. Hawthorne, L.V. Heebink, N. Dando, M. Gershenzon, R.S. Ghosh, Comparison of alkaline industrial wastes for aqueous mineral carbon sequestration through a parallel reactivity study, Waste Management 34 (2014) 1815-1822.

[18] M.C. Mayoral, J.M. Andrés, M.P. Gimeno, Optimization of mineral carbonation process for CO2 sequestration by lime-rich coal ashes, Fuel 106 (2013) 448-454.

[19] G. Montes-Hernandez, R. Pérez-López, F. Renard, J.M. Nieto, L. Charlet, Mineral sequestration of CO2 by aqueous carbonation of coal combustion fly-ash, Journal of Hazardous Materials 161 (2009) 1347-1354.

[20] J.-H. Wee, A review on carbon dioxide capture and storage technology using coal fly ash, Applied Energy 106 (2013) 143-151.

[21] R.M. Dilmore, B.H. Howard, Y. Soong, C. Griffith, S.W. Hedges, A.D. DeGalbo, B. Morreale, J.P. Baltrus, D.E. Allen, J.K. Fu, Sequestration of CO2 in Mixtures of Caustic Byproduct and Saline Waste Water, Environmental Engineering Science 26 (2009) 1325-1333.

[22] N. Um, S.-Y. Nam, J.-W. Ahn, Effect of Accelerated Carbonation on the Leaching Behavior of Cr in Municipal Solid Waste Incinerator Bottom Ash and the Carbonation Kinetics, MATERIALS TRANSACTIONS 54 (2013) 1510-1516.

[23] C.-L. Washbourne, E. Lopez-Capel, P. Renforth, P.L. Ascough, D.A.C. Manning, Rapid Removal of Atmospheric CO2 by Urban Soils, Environmental Science & Technology 49 (2015) 5434-5440.

[24] I.A. Bundeleva, L.S. Shirokova, P. Bénézeth, O.S. Pokrovsky, E.I. Kompantseva, S. Balor, Calcium carbonate precipitation by anoxygenic phototrophic bacteria, Chemical Geology 291 (2012) 116-131.

[25] I.A. Bundeleva, B. Ménez, T. Augé, F. Bodénan, N. Recham, F. Guyot, Effect of cyanobacteria Synechococcus PCC 7942 on carbonation kinetics of olivine at 20 °C, Minerals Engineering 59 (2014) 2-11.

[26] G.P. Assima, F. Larachi, J. Molson, G. Beaudoin, Comparative study of five Québec ultramafic mining residues for use in direct ambient carbon dioxide mineral sequestration, Chemical Engineering Journal 245 (2014) 56-64.

[27] A. Entezari Zarandi, F. Larachi, G. Beaudoin, B. Plante, M. Sciortino, Nesquehonite as a carbon sink in ambient mineral carbonation of ultramafic mining wastes, Chemical Engineering Journal 314 (2017) 160-168.

[28] A.L. Harrison, G.M. Dipple, I.M. Power, K.U. Mayer, Influence of surface passivation and water content on mineral reactions in unsaturated porous media: Implications for brucite carbonation and CO2 sequestration, Geochimica et Cosmochimica Acta 148 (2015) 477-495.

[29] S.A. Wilson, A.L. Harrison, G.M. Dipple, I.M. Power, S.L.L. Barker, K. Ulrich Mayer, S.J. Fallon, M. Raudsepp, G. Southam, Offsetting of CO2 emissions by air capture in mine tailings at the Mount Keith Nickel Mine, Western Australia: Rates, controls and prospects for carbon neutral mining, International Journal of Greenhouse Gas Control 25 (2014) 121-140.

[30] L. Zhao, L. Sang, J. Chen, J. Ji, H.H. Teng, Aqueous Carbonation of Natural Brucite: Relevance to CO2 Sequestration, Environmental Science & Technology 44 (2010) 406-411.

[31] G.P. Assima, F. Larachi, G. Beaudoin, J. Molson, CO2 Sequestration in Chrysotile Mining Residues—Implication of Watering and Passivation under Environmental Conditions, Industrial & Engineering Chemistry Research 51 (2012) 8726-8734.

[32] L.P. Staples, J.M. Bowen, S.B. Bernier, D.A. Warren, C.C. Scott, J.F. Duncan, B.A. Murphy, V.J. Bertrand, K.C. Scott, S. Latulippe, Technical Report on the Dumont Ni Project, Launay and Trécesson Townships, Quebec, Canada, Royal Nickel Corporation, 2013, pp. 432.

[33] J. Duke, Petrology and economic geology of the Dumont sill: an Archean intrusion of komatiitic affinity in northwestern Quebec, Geological Survey of Canada, 1986.

[34] M. Sciortino, J.E. Mungall, J. Muinonen, Generation of High-Ni Sulfide and Alloy Phases During Serpentinization of Dunite in the Dumont Sill, Quebec, Economic Geology 110 (2015) 733-761.

[35] G.P. Assima, F. Larachi, J. Molson, G. Beaudoin, Accurate and direct quantification of native brucite in serpentine ores—New methodology and implications for CO2 sequestration by mining residues, Thermochimica Acta 566 (2013) 281-291.

[36] G.P. Assima, F. Larachi, J. Molson, G. Beaudoin, Emulation of ambient carbon dioxide diffusion and carbonation within nickel mining residues, Minerals Engineering 59 (2014) 39-44.

[37] J.R. Gronow, The dissolution of asbestos fibers in water, Clay minerals 22 (1987) 21-35.

[38] S. Hu, R. Zhang, X. Zhang, Study on mineral surface reacted with water at temperatures above 300°C and 23 MPa, Research on Chemical Intermediates 37 (2011) 503-514.

[39] R. Zhang, S. Hu, X. Zhang, W. Yu, Dissolution Kinetics of Dolomite in Water at Elevated Temperatures, Aquatic Geochemistry 13 (2007) 309-338.

[40] G.P. Assima, F. Larachi, G. Beaudoin, J. Molson, Dynamics of carbon dioxide uptake in chrysotile mining residues – Effect of mineralogy and liquid saturation, International Journal of Greenhouse Gas Control 12 (2013) 124-135.

[41] A.L. Harrison, G.M. Dipple, I.M. Power, K.U. Mayer, The impact of evolving mineral–water–gas interfacial areas on mineral–fluid reaction rates in unsaturated porous media, Chemical Geology 421 (2016) 65-80.

[42] P. Ballirano, C. De Vito, V. Ferrini, S. Mignardi, The thermal behaviour and structural stability of nesquehonite, MgCO3·3H2O, evaluated by in situ laboratory parallel-beam X-ray powder diffraction: New constraints on CO2 sequestration within minerals, Journal of Hazardous Materials 178 (2010) 522-528.

[43] A. Gras, G. Beaudoin, J. Molson, B. Plante, B. Bussière, J.M. Lemieux, P.P. Dupont, Isotopic evidence of passive mineral carbonation in mine wastes from the Dumont Nickel Project (Abitibi, Quebec), International Journal of Greenhouse Gas Control 60 (2017) 10-23.

[44] T.J. Harvey, W. Van Der Merwe, K. Afewu, The application of the GeoBiotics GEOCOAT® biooxidation technology for the treatment of sphalerite at Kumba resources' Rosh Pinah mine, Minerals Engineering 15 (2002) 823-829.

[45] A. Li, B. Andruchow, I. Wislesky, E. Olson, Field testing of co-disposal techniques for acid generating tailings and waste rock at Cerro de Maimón mine, Tailings and mine waste '11, Norman B. Keevil Institute of Mining Engineering, Vancouver, 2011.

Chapter 5.

Ambient Mineral Carbonation of Québec Ultramafic Mining Wastes

Ali **Entezari-Zarandi**,[1] Faïçal **Larachi**,[*,1] Georges **Beaudoin**,[2] Benoît **Plante**,[3] Bruno **Bussière**,[3] Michelle **Sciortino**[4]

[1]Department of Chemical Engineering, Université Laval, Québec, QC, Canada G1V 0A6

[2]Department of Geology and Geological Engineering Université Laval, Québec, QC, Canada G1V 0A6

[3]Université du Québec en Abitibi-Témiscamingue, Rouyn-Noranda, Québec, Canada J9X 5E4

[4]Senior Project Geologist, Royal Nickel, Toronto, Ontario, Canada

Abstract

Research is rapidly developing a variety of novel solutions that can help to mitigate the accumulation of CO_2 in the atmosphere. Mineral carbonation of mine wastes is quickly becoming one of the most attractive of these new solutions, primarily because of its relative simplicity, use of otherwise valueless materials, and its ability to be implemented passively and at a large-scale. Furthermore, the products of mineral carbonation are considered to be environmentally-benign and stable. The province of Québec is the perfect location to assess the proof-of-concept of mineral carbonation given its long-standing history with mining industry and its projected and current production of ultramafic wastes from the exploitation of mineral resources. In this chapter, some of the salient findings from the research on ambient carbonation of ultramafic mining residues will be reviewed.

Résumé

La recherche développe rapidement une variété de solutions novatrices qui peuvent aider à atténuer l'accumulation de CO_2 dans l'atmosphère. La carbonatation minérale des déchets de mines devient rapidement l'une des plus attrayantes de ces nouvelles solutions, principalement en raison de sa simplicité relative, de l'utilisation de matériaux autrement sans valeur et de sa capacité à être mise en œuvre de façon passive et à grande échelle. En outre, les produits de la carbonatation minérale sont considérés comme respectueux de l'environnement et stables. La province de Québec est l'endroit idéal pour évaluer la preuve de concept de la carbonatation minérale, compte tenu de son histoire ancienne avec l'industrie minière et de la production projetée et actuelle de déchets ultramafices de l'exploitation des ressources minérales. Dans ce chapitre, certains des résultats remarquables de la recherche sur la carbonatation ambiante des résidus miniers ultramafices seront examinés.

5.1 Carbon Mineralization

In response to growing concerns over climate change, new technologies are being intensively researched with the goal of developing robust and reliable strategies for the long-term storage of carbon emissions.

Carbon mineralization of alkaline, mafic and ultramafic minerals is a naturally-occurring kinetically slow weathering phenomenon during which Ca/Mg-rich rocks gently react with the atmospheric CO_2 that is dissolved in rain droplets. While the removal of CO_2 from the atmosphere by natural carbon mineralization is too slow to match the rapid rate of anthropogenic emissions, accelerated carbon mineralization might allow for greater control over the concentration of atmospheric CO_2 while also allowing mining operations to sum up with a positive carbon balance.

Particle size, and thus, specific surface area, is a critical factor that affects carbon mineralization by controlling the leaching rate of the reactive metal ions, the sibling moiety involved in solid carbon storage. While comminution is an essential part of the mining process because it allows for the liberation of key metal-containing minerals from the surrounding rock, it also advantageously produces tailings with specific surface areas that are large enough to increase weathering by carbon mineralization.

Mg-rich mine waste, which consist of either coarse-grained waste rocks, or fine-grained mineral processing tailings, can therefore be considered to represent some of the largest man-made chemical reactors that accelerate CO_2 sequestration from the atmosphere. Such reactors exhibit highly heterogeneous spatiotemporal reactivity patterns which depend upon their contact with meteoric water, wind and exposure to solar radiation. The variability of these factors can result in the creation of dry, semi-saturated, and fully-saturated zones at different temperatures. Understanding the carbonation behavior in correlation with the conditions prevailing in each zone is therefore a prerequisite to the precise quantification of the carbonation efficiency of mining wastes.

Several chrysotile mine tailing sites in southern Québec (e.g., Black Lake and Thetford Mines) are good examples of passive carbon mineralization reactors currently active. It is estimated that two billion metric tonnes of chrysotile mining residues in Québec

have the potential to capture ~700 million metric tonnes of atmospheric CO_2 [1]. The Dumont Nickel Project (DNP), located in northwestern Québec, is predicted to be the fifth largest nickel sulfide producer worldwide and will involve mining a ~1.4×10^9 m^3 ultramafic sill. Over its 31-year lifetime, the DNP will mine and mill ~1.18 billion metric tonnes of serpentinized ores, which will be disposed of as brucite-rich lizardite/chrysotile mineral processing tailings [2,3], in addition to the ~1.16 billion metric tonnes of peridotite/gabbro waste rocks that will be excavated to access the nickel-rich dunite ore.

5.2 Ambient Carbon Mineralization of Nickel Mine Tailings

The research conducted in our group to date shows that carbon mineralization is sensitive to pore water saturation and also to the watering frequency of the mining waste [4,5]. Virtually no sign of carbonation is observed when desiccated tailing materials – mined and milled wastes alike – are contacted at ambient temperature with moisture-free CO_2-containing gas. At the opposite end of the spectrum, carbonation of *fully* wetted tailings is also barely active as a result of the slow CO_2 diffusion rate in stagnant waters, which is a few orders of magnitude slower than its gas phase analog. On the contrary, relatively high CO_2 uptake rates are measured for *partially* wetted materials where the degree of carbonation is prompted by the acidity of the solution which drives metal leaching and by the minerals alkalinity which promotes the precipitation of (hydrated) carbonate minerals. Typical kinetic trends of the CO_2 uptake behavior of the DNP tailings are illustrated in Figure 5-1 along with the dynamic evolution of the solution pH over the course of multiple carbonation cycles. The reactivity of the tailings diminishes from cycle 1 to cycle 5 (Figure 5-1a); this is mirrored by the material's dwindling ability to alkalinize the pore water (Figure 5-1b). These observations are in accord with the fact that brucite, and, to a lesser extent, chrysotile, react primarily with CO_2 and water to produce nesquehonite ($MgCO_3{\cdot}3H_2O$).

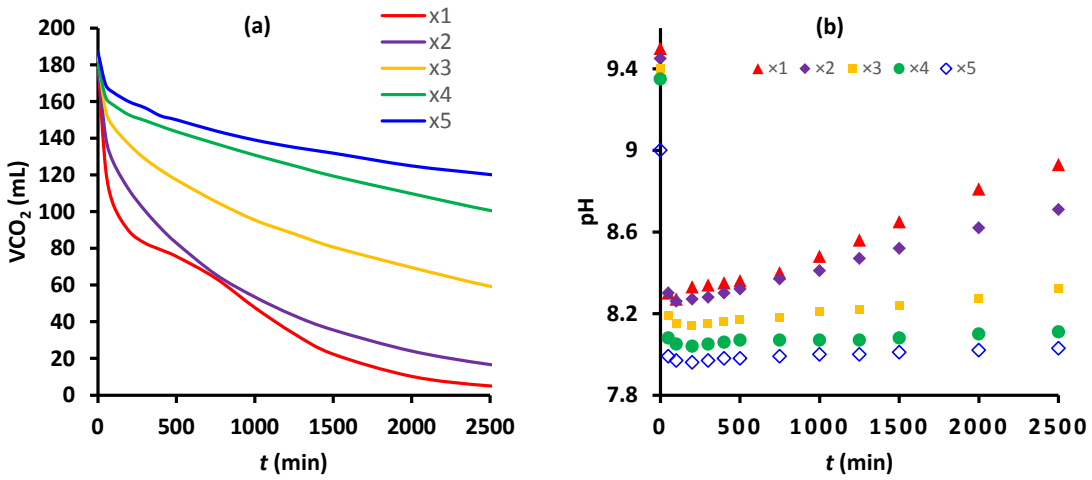

Figure 5-1. Carbon mineralization behavior of the DNP tailings (50% water saturation) at ambient temperature and pressure across multiple carbonation cycles: (a) volumetric consumption of CO_2 over time (b) transient evolution of the pH of the pore water.

Interestingly, an unanticipated outcome of carbon mineralization in terms of run-off water alkalinization and metal content could reflect in lowering, in the long-term, the mine environmental impact as alkaline mine drainage is expected to be attenuated by carbonation of the waste piles. Contrary to the well-known problem of acid mine drainage, in mines that exploit ultramafic bodies, there is an unavoidable risk of producing alkaline mine drainage. Although high alkalinity is essential for the formation of solid carbonated species, high pH run-off waters can be harmful to the environment because metal hydroxide compounds (e.g., $Al(OH)_3$) known to be sparingly soluble in neutral water may become soluble in alkaline media, while some neutral pH soluble metals can precipitate as hydroxide (e.g., $Co(OH)_2$, $Ca(OH)_2$ and $Cu(OH)_2$) [6].

Temperature is another crucial factor that impacts carbon mineralization, and is especially relevant for disposal sites in Québec which are exposed to long, cold winters and short, but hot, summers. There are two short transitional periods during the spring and fall which are characterized by moderate temperatures and an abundance of rain showers. Though sparingly soluble in water, CO_2 increases in solubility in colder conditions, thus resulting in

a stronger acidification. This serves to partially offset the decline in silicate mineral dissolution that positively correlates with temperature (Figure 5-2).

Laboratory observations emulating outdoor conditions suggest that carbonation virtually never stops even under very cold conditions (e.g., −5°C), whereas the carbonation rates are notably stimulated (up to 40°C), provided that pore water is present, under warmer conditions [4,7]. These observations agree with the field tests conducted by our group during winter where warm (~14°C) vents of CO_2-depleted air were detected at the surface of mine waste heaps through a relatively thick snow cover with a background air temperature around -20°C [8].

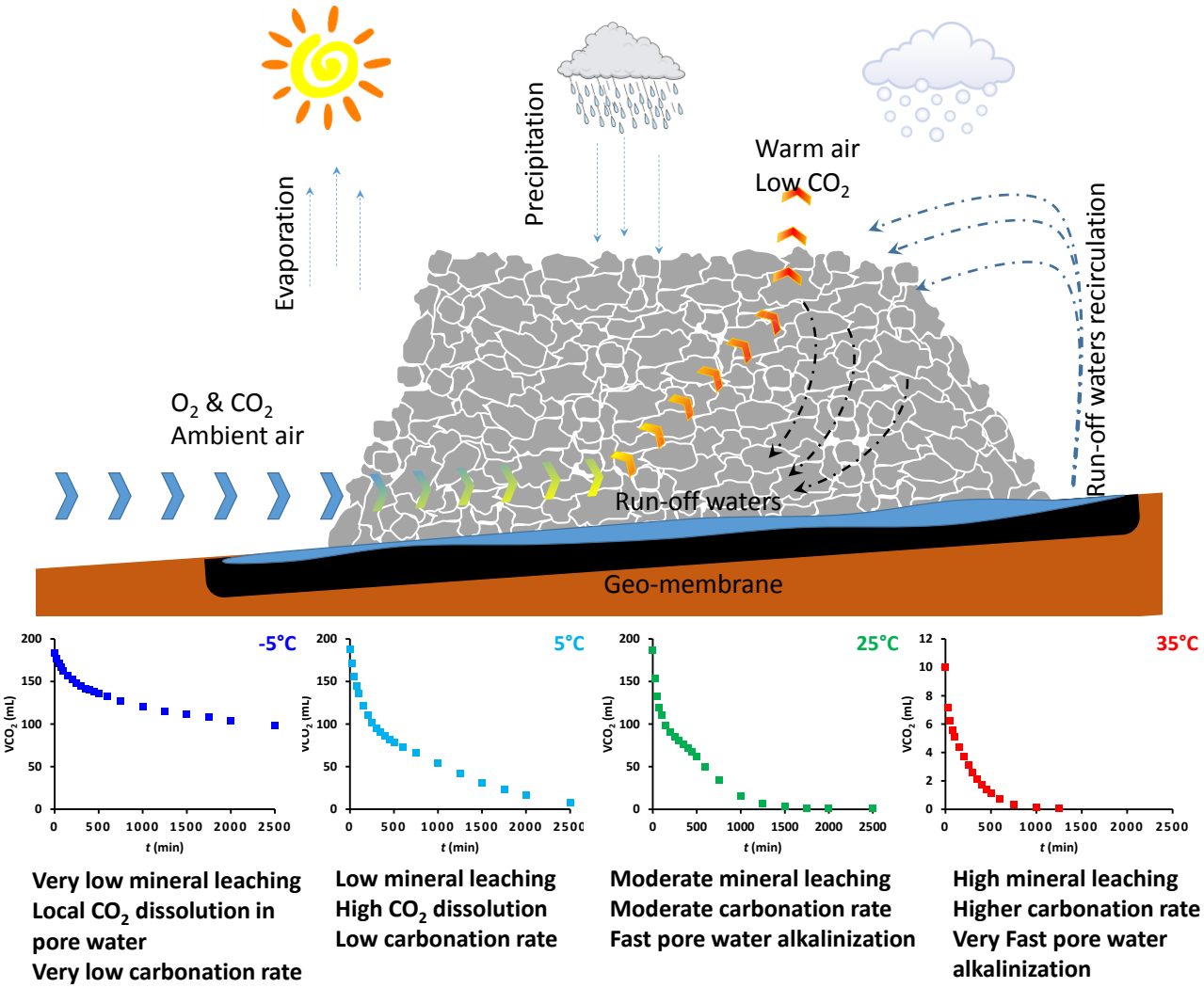

Figure 5-2. Schematic representation of the impact of temperature on the carbon mineralization of ultramafic nickel tailings in outdoor conditions. Variations in seasonal temperatures as well as the volume of precipitation will greatly affect the carbonation rates.

5.3 Bottom Line

Mineral carbonation of mine wastes can be considered as an immediate tool to withdraw carbon dioxide from the atmosphere where the presence of pore water in the heaps is increasingly documented in the literature as being a crucial participant in the carbon mineralization processes [9].

1- Geo-engineered solutions applied at scale of mine waste dumps and highly-reactive tailing ponds can provide pathways to further intensify air and water circulation and, thus ensure optimal degrees of water saturation and CO_2 availability across the entire inner structure of the piles.

2- A further improvement could be realized by taking advantage of the heat released due to carbonation within a structure's core. This heat can be recovered and used to pre-warm, prior to their injection, CO_2–containing streams, such as those resulting from pre-/or post-combustion flue gases, thus further accelerating the carbonation reaction.

3- Canada's metal mining effluent regulations (MMER) forbid discharge of waters with pH > 9.5. Carbon mineralization consumes both metal and hydroxide ions in order to form hydrated metal carbonates. Optimal geo-engineered designs of a tailings site will not only withdraw substantial amounts of CO_2 from the atmosphere, but will also contribute to producing environmentally benign minerals that can mitigate the alkalinity of the run-off waters as well as their dissolved metal content.

5.4 References

[1] J. Pronost, G. Beaudoin, J. Tremblay, F. Larachi, J. Duchesne, R. Hébert, et al., Carbon Sequestration Kinetic and Storage Capacity of Ultramafic Mining Waste. Environmental Science & Technology 45 (2011) 9413-9420.

[2] L. P. Staples, J. M. Bowen, S. B. Bernier, D. A. Warren, C. C. Scott, J. F. Duncan, et al., Technical Report on the Dumont Ni Project, Launay and Trécesson Townships, Quebec, Canada. Royal Nickel Corporation. July 2013.

[3] M. Sciortino, J. E. Mungall, and J. Muinonen, Generation of High-Ni Sulfide and Alloy Phases During Serpentinization of Dunite in the Dumont Sill, Quebec. Economic Geology 110 (2015) 733-761.

[4] G. P. Assima, F. Larachi, J. Molson, and G. Beaudoin, Impact of temperature and oxygen availability on the dynamics of ambient CO_2 mineral sequestration by nickel mining residues. Chemical Engineering Journal 240 (2014) 394-403.

[5] G. P. Assima, F. Larachi, G. Beaudoin, and J. Molson, Dynamics of carbon dioxide uptake in chrysotile mining residues – Effect of mineralogy and liquid saturation. International Journal of Greenhouse Gas Control 12 (2013) 124-135.

[6] C. A. Cravotta III, Dissolved metals and associated constituents in abandoned coal-mine discharges, Pennsylvania, USA. Part 2: Geochemical controls on constituent concentrations. Applied Geochemistry 23 (2008) 203-226.

[7] G. P. Assima, F. Larachi, J. Molson, and G. Beaudoin, New tools for stimulating dissolution and carbonation of ultramafic mining residues. The Canadian Journal of Chemical Engineering 92 (2014) 2029-2038.

[8] J. Pronost, G. Beaudoin, J.-M. Lemieux, R. Hébert, M. Constantin, S. Marcouiller, M. Klein, J. Duchesne, J.W. Molson, F. Larachi, X. Maldague, CO_2-depleted warm air venting from chrysotile milling waste (Thetford Mines, Canada): Evidence for in-situ carbon capture from the atmosphere. Geology 40 (2012) 275-278.

[9] K. Lechat, J.-M. Lemieux, J. Molson, G. Beaudoin, R. Hébert, Field evidence of CO_2 sequestration by mineral carbonation in ultramafic milling wastes, Thetford Mines, Canada. International Journal of Greenhouse Gas Control 47 (2016) 110-121.

Chapter 6.

Thesis Conclusion and Recommendations

Dynamics of passive mineral carbonation in ultramafic mining wastes and tailings of Dumont Nickel Project was investigated in this PhD thesis. Mineral carbonation in ambient conditions received little attention and research is yet at the laboratory to pilot-scale while it is the only "in service" strategy for capturing atmospheric CO_2. However, more work is still required before it can be employed in real carbon capture and storage strategies.

6.1 Key contributions

Chapter 2 was devoted to the understanding of ambient environmental controls where these mining wastes are to be stored. Mimicking environmental conditions of northern Québec, temperature dependent carbonation tests were performed in the ranges of extremely hot summer days (dark rock surfaces) (35 ± 1 °C), laboratory (warm summer days) (23 ± 2 °C), low (spring and fall) (5 ± 1 °C), and freezing (-5 ± 2 °C) conditions. Although temperature was found to have a remarkable effect on the carbonation kinetics, yet the experimental results suggested that even in freezing conditions of winter mineral carbonation proceeds though in a much slower rate. A porous flaky carbonate phase was observed to form mainly on the brucite surfaces which was gradually replaced by denser elongated nesquehonite crystals upon further carbonation. Nevertheless, unreacted brucite cores could be liberated employing surface abrasion strategies.

The focus of chapter 3 was mainly on the stability of ambient carbonation products. Nesquehonite the predominant form of magnesium carbonate in ambient conditions is known to be a metastable carbonate. A wetting/drying cycle was designed to subject the primary

carbonates and evaluate their stability upon temperature oscillations (25–70°C). The study of this phenomenon coupled by freeze/thaw cycles is of great importance to mimic the natural weathering scenarios. The cycles found to be the origin of a thermomechanical stresses leading to a "peel-off" effect which inflicted micro–fractures to the carbonate product layers enabling water and gas to reach and react with fresh, unearthed mineral sites. Furthermore, the long–term monitoring of an already carbonated NiMT (over 24 months) revealed that the initial nesquehonite product evolved into dypingite and hydromagnesite depending on the depth, *i.e*., age, and wetting/drying history of the slice.

Likewise, in chapter 4, a high pure nesquehonite product was precipitated from major brucite reach lithologies of Dumont project (*i.e*. dunite and peridotite). It was found that Nesquehonite tends to remain unchanged over prolonged times (an 18 months monitoring was performed) if not being subjected to subsequent wetting/drying cycles or humid conditions. Four lithologies of the Dumont nickel project (*i.e*. dunite, peridotite, gabbro, and volcanic) were assessed in terms of carbonation capacity in ambient conditions. These lithologies are engaged in production of mining operation waste rocks (gabbro, and volcanic) and mineral processing tailings (dunite and peridotite). It was found that for identical size fractions, carbonation of rock wastes was quite limited as compared to the tailings. Brucite more abundant in dunite and peridotite substrates was found to be the main reactant involved in carbonation as compared to other less-reactive magnesium silicate minerals. Engineering recommendations were made to overcome the dilemma due to high-permeability yet low-reactive (brucite-poor) coarse-grained waste rock stockpiles, and low-permeability however high-reactive (brucite-rich) tailings.

6.2 Recommendations for future work

The proposed “co-disposal” of mining operation waste rocks and mineral processing tailings (section 4.3.3) in the form of engineered heaps needs deeper experimental work and study. The idea is quite interesting as it has positive effects both on mineral carbonation capacity and structural stability of the heap (due to the cementing effect of carbonation).

Development of a reactive transport kinetics model seems quite essential to be coupled with our experimental work describing the passive carbonation of mafic-ultramafic material under environmental conditions.

Effects of the heating rate, particle size, and atmospheric conditions on the decomposition of hydrated carbonates are needed to be scrutinized in more details to provide a more comprehensive understanding of the decomposition process as well as possible determination of unfamiliar phases observed during thermal analysis by employing TG-MS technique.

Appendix A

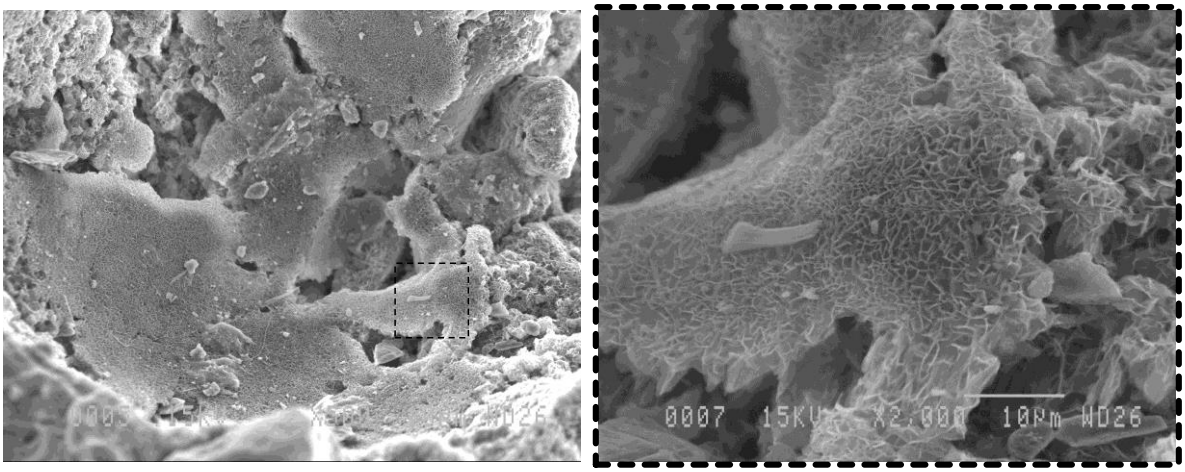

Figure S1. Flaky magnesium carbonates covering the surface of NiMT particles.

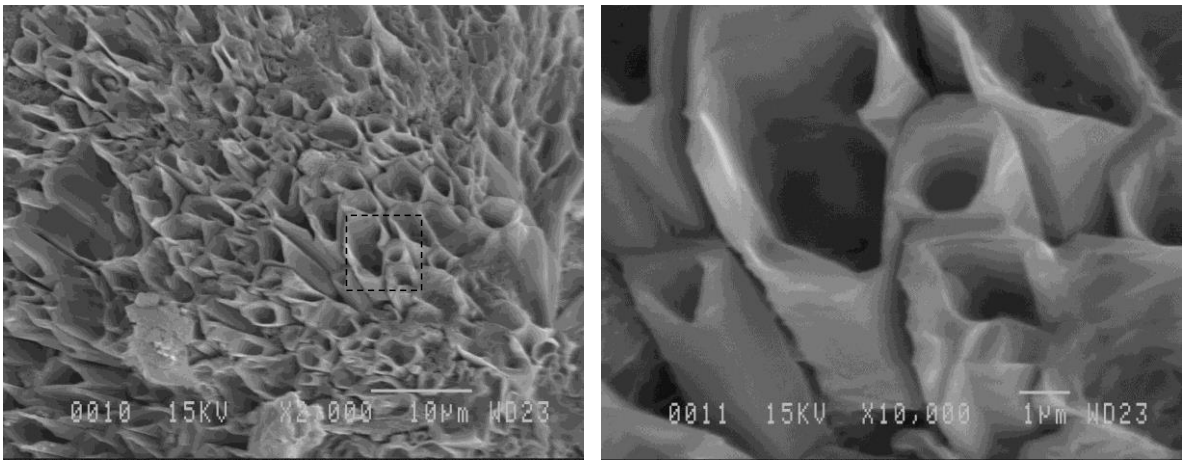

Figure S2. Strange magnesium carbonate formations presenting hollow-fiber structures.

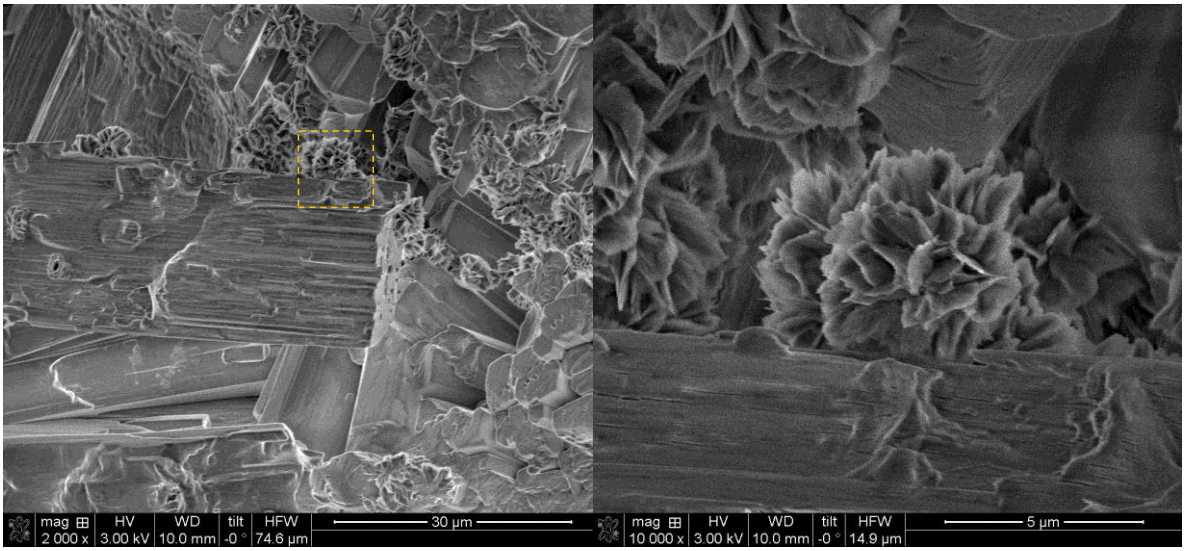

Figure S3. Rosette-like formations (probably dypingite) precipitated on prismatic crystals of silica sand.

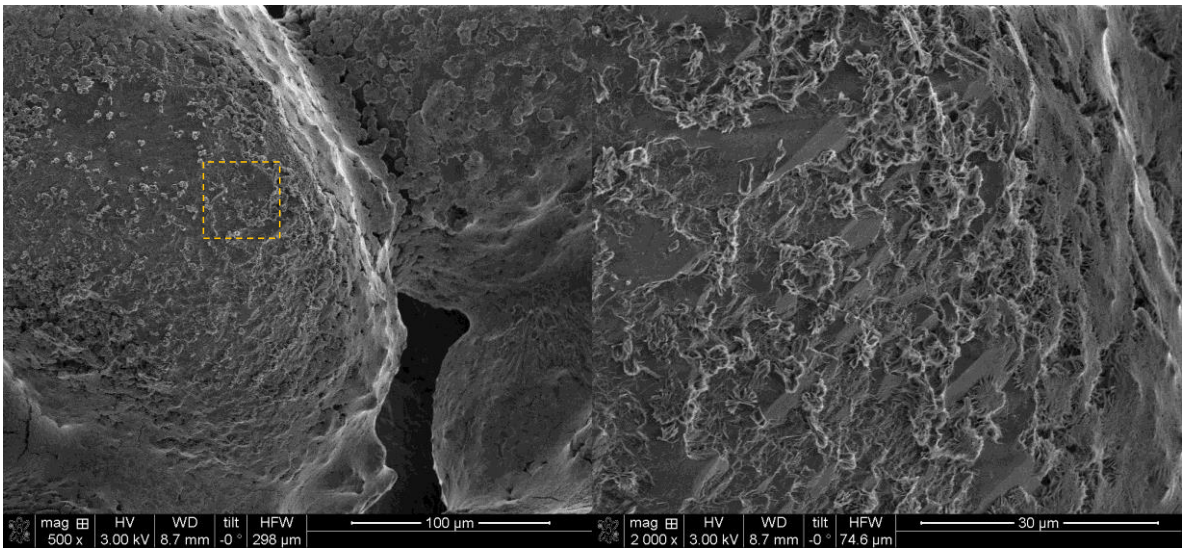

Figure S3. After carbonation micrograph presenting silica particles covered with a pulp of pure brucite. Tiny flakes and needles are detectable forming collections similar to rosettes of dypingite.

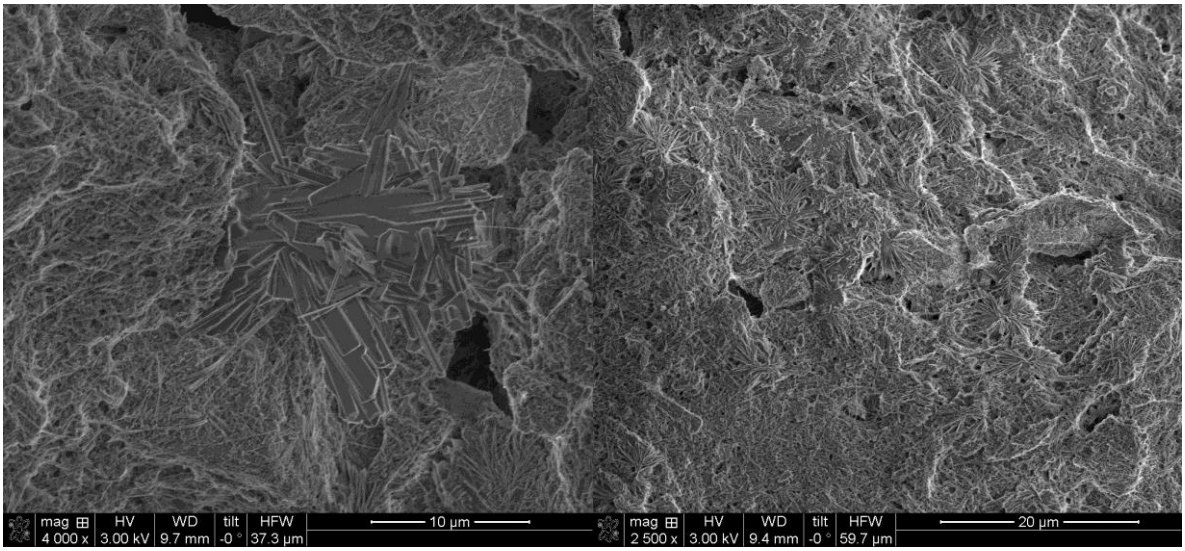

Figure S4. SEM micrographs of the Nesquehonite. Note the radial collections of needle-like nesquehonite crystals in right and elongated prismatic crystals in left.

Appendix B

Table S1. Details of experimental campaign on mineral carbonation under ambient conditions.

No.	Material	Size (μm)	W. (g)	T. (°C)	CO_2 conc. (%)	W.S. (%)	Water	Duration (min)	Contacts
1	NiMT	-106	35	22	7	60	DI	5000	1
2	NiMT	-106	35	22	7	40	DI	5000	1
3	NiMT	-106	35	22	7	80	DI	5000	1
4	NiMT	-212 +180	35	22	7	80	DI	5000	1
5	NiMT	-212 +180	35	22	7	60	DI	5000	1
6	NiMT	-212 +180	35	22	7	40	DI	5000	1
7	NiMT	-212 +180	35	22	7	80	DI	5000	1
8	NiMT	-180 +106	35	22	7	80	DI	5000	1
9	NiMT	-180 +106	35	22	7	60	DI	5000	1
10	NiMT	-180 +106	35	22	7	40	DI	5000	1
11	NiMT	-106	35	22	10	80	PR.	5000	1
12	NiMT	-106	35	22	10	80	PR.	5000	1
13	NiMT	-106	35	22	10	60	PR.	5000	1
14	NiMT	-106	35	22	10	40	PR.	5000	1
15	NiMT	140	35	22	10	60	DI	4000	1
16	Gabbro	140	35	22	10	80	DI	4000	1
17	NiMT (Mag. Sep.)*	-106	35	22	10	60	lab	4000	1
18	NiMT (Mag. Sep.)	-106	35	22	10	60	DI	4000	1
19	NiMT (Mag. Sep.)	-106	35	22	0	60	DI	2500	1
20	NiMT	-106	35	22	10	60	DI	4000	1
21	Silica sand	140	35	22	10	80	DI	2500	1
22	Chrysotile	+75 -106	30	22	10	60	DI	5000	1

23	Chrysotile	+38 -53	30	22	10	60	DI	5000	1
24	Peridotite	106	35	22	10	60	DI	4000	1
25	NiMT	140	35	22	10	60	DI	3000	2
26	Brucite + silica**	75	30	22	10	60	DI	3000	2
27	Dunite	106	35	22	10	60	DI	3000	1
28	Dunite + pyrite***	106	35	22	10	60	DI	3000	1
29	Dunite	106	40	22	10	60	pH 4	3000	1
30	Dunite	106	40	22	10	60	pH 2	3000	1
31	NiMT	-106	50	22	10	50	DI	4000	1
32	NiMT	-106	50	22	10	50	pH 2	4000	5
33	NiMT	-106	30	15	10	30	DI	4000	1
34	NiMT	-106	30	15	10	50	DI	5000	1
35	NiMT	-106	30	12	10	50	DI	5000	3
36	NiMT	-106	30	10	10	50	DI	5000	1
37	NiMT (Sonicated)+	140	35	22	10	50	DI	5000	1
38	NiMT (Sonicated)	140	35	22	10	50	DI	5000	1
39	NiMT	140	35	22	10	50	DI	5000	2
40	NiMT	140	40	5	10	50	DI	5000	1
41	NiMT	140	35	5	10	50	DI	5000	1
42	NiMT	140	35	0	10	50	DI	5000	1
43	NiMT	140	40	0	10	75	DI	5000	1
44	NiMT	140	35	10	10	50	DI	5000	5
45	NiMT	140	35	22	10	50	DI	5000	2
46	NiMT	140	35	1	10	50	DI	5000	1
47	NiMT	140	35	35	10	50	DI	3000	2
48	Brucite + silica	75	35	22	10	60	DI	3000	2
49	NiMT	140	35	22	10	0	-	2500	1
50	NiMT	140	35	22	7	0	-	2500	1
51	NiMT	140	35	22	10	0	-	2500	1

52	NiMT	140	35	-5	10	50	DI	2500	1
53	NiMT	140	35	22	10	50	DI	2500	1
54	Brucite + silica	75	45	-5	10	50	DI	2500	1
55	Brucite + silica	75	45	0	10	50	DI	2500	1
56	Brucite + silica	75	45	5	10	50	DI	2500	1
57	Brucite + silica	75	40	22	10	40	DI	2500	1
58	Brucite + silica	75	40	22	10	60	DI	2500	1
59	Brucite + silica	75	40	22	10	80	DI	2500	1
60	NiMT	140	35	22	10	40	DI	5000	1
61	NiMT	140	35	22	10	60	DI	5000	1
62	Brucite + silica	75	40	22	10	40	DI	2500	1
63	Brucite + silica	75	40	22	10	60	DI	2500	1
64	Brucite + silica	75	40	22	10	80	DI	2500	1
65	NiMT (al. carb.)++	140	35	22	10	50	DI	5000	1
66	NiMT	140	80	22	10	60	DI	5000	3
67	NiMT	140	35	22	10	50	DI	5000	1
68	NiMT (50% al. carb.)+++	140	35	22	10	50	DI	5000	1
69	NiMT (25% al. carb.)-	140	35	22	10	50	DI	5000	1
70	NiMT (3% brucite)--	140	35	22	10	50	DI	5000	1
71	NiMT	140	70	22	10	50	DI	2500	9
72	NiMT	140	140	22	10	50	DI	2500	5

*	Magnetic particles removed prior to carbonation.
**	11 wt. % pure brucite diluted in pure silica sand.
***	20 wt.% pyrite added to dunite.
+	Material was sonicated for 30 minutes prior to carbonation.
++	Carbonated material was dried overnight in an oven and inserted into the sample holder for re-carbonation.
+++	A mixture of 50 w. %. of un-reacted NiMT and 50 w. %. of already carbonated material.
-	A mixture of 75 w. %. of un-reacted NiMT and 25 w. %. of already carbonated material.
--	A mixture of 3 w. %. of pure brucite mineral and 97 w. %. of un-reacted NiMT.

DI: De-ionized Water, PR.: Process watter, Lab: laboratory general water.

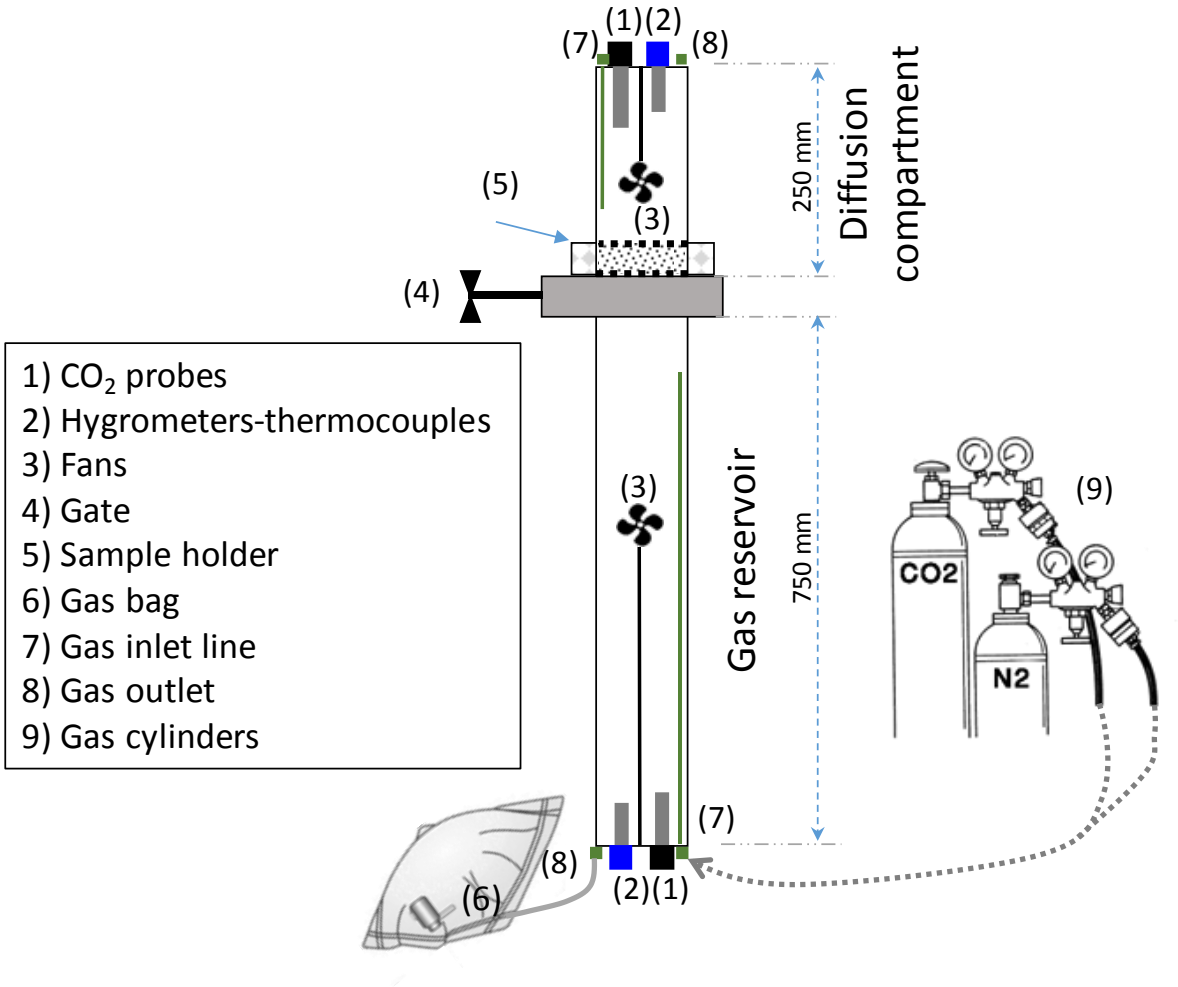

Figure S1. Schematic diagram of the batch differential thin-bed diffusive carbonation cell (Assima et al., 2014a; Entezari Zarandi et al., 2016).

Figure S2. Photograph of spent NiMT progressively accumulated over 2 years from the diffusive batch cell and representing *ca*. 70 room-temperature wet carbonation runs to evaluate the long-term stability of the carbonates. The samples were left open in laboratory conditions.

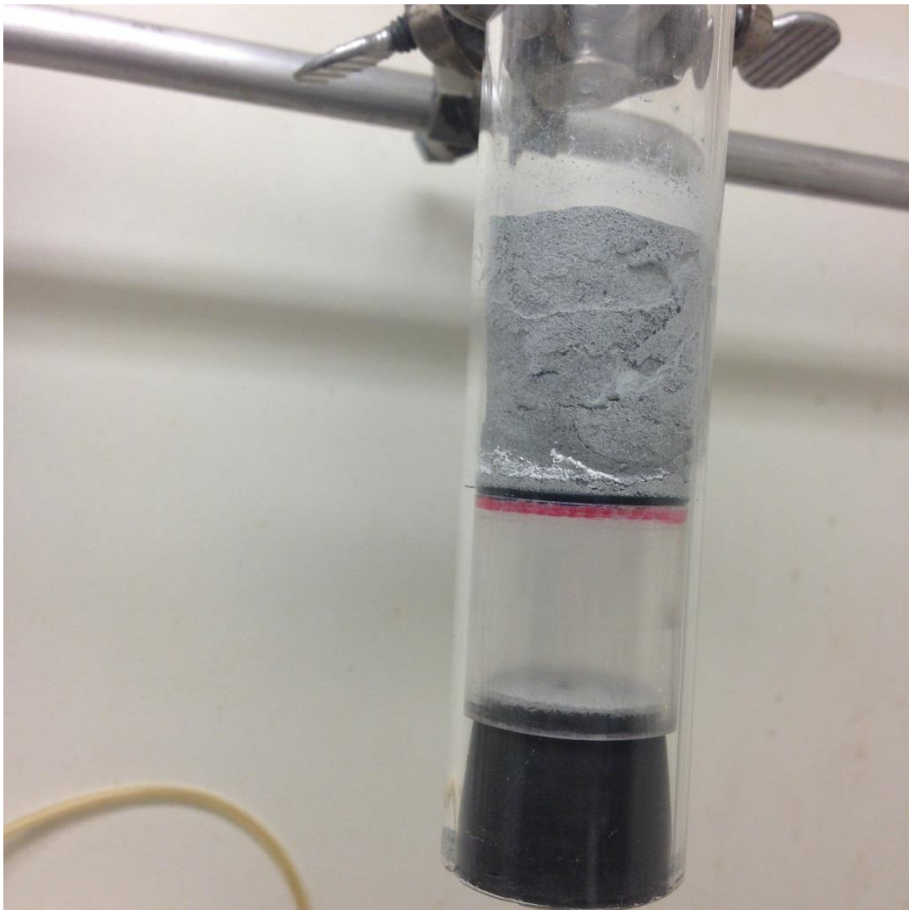

Figure S3. Formation of white deposits, probably carbonates, at the bottom of the NiMT layer after 14 days carbonation with atmospheric CO_2 stream.

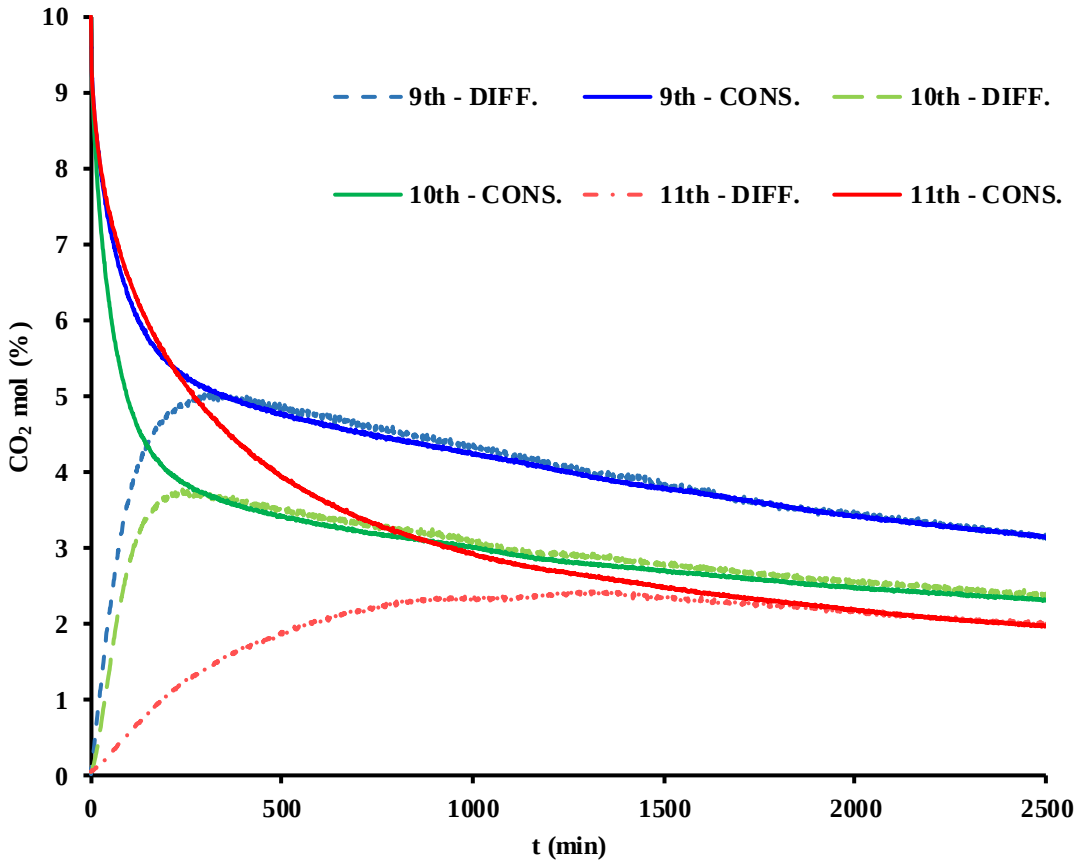

Figure S4. Comparison of CO_2 consumption and diffusion profiles of NiMT layer during 9th contact with fresh CO_2 load, oven dried (40°C) product (10th contact) and product after 10 freeze/thaw cycles. Consumption and diffusion profiles were measured, respectively, in gas reservoir and diffusion compartments of the reactor depicted in figure S1.

Appendix C

Table S1. Mineral content of [DU] and [PD] samples based on quantitative evaluation of minerals by scanning electron microscopy (QEMSCAN). Data were provided by RNC Minerals.

Mineral	[DU]		[PD]	
	Mass* (%)	Size** (µm)	Mass (%)	Size (µm)
Serpentine	85.1	13	57.6	10
Fe-Serpentine	2.01	4	6.74	5
Orthopyroxene	0.00	6	0.01	9
Clinopyroxene	2.70	7	12.1	15
Olivine	0.03	8	0.09	5
Quartz	0.03	12	0.01	5
Feldspars	0.01	13	0.02	10
Chlorite	0.16	3	9.12	7
Mica/Clays	0.01	5	0.05	5
Magnetite	4.09	10	12.5	12
Brucite	2.98	8	0.11	7
Cr_Minerals	0.01	6	1.39	16

* Based on 100% mineral mass normalization; ** Based on mean grain size by frequency

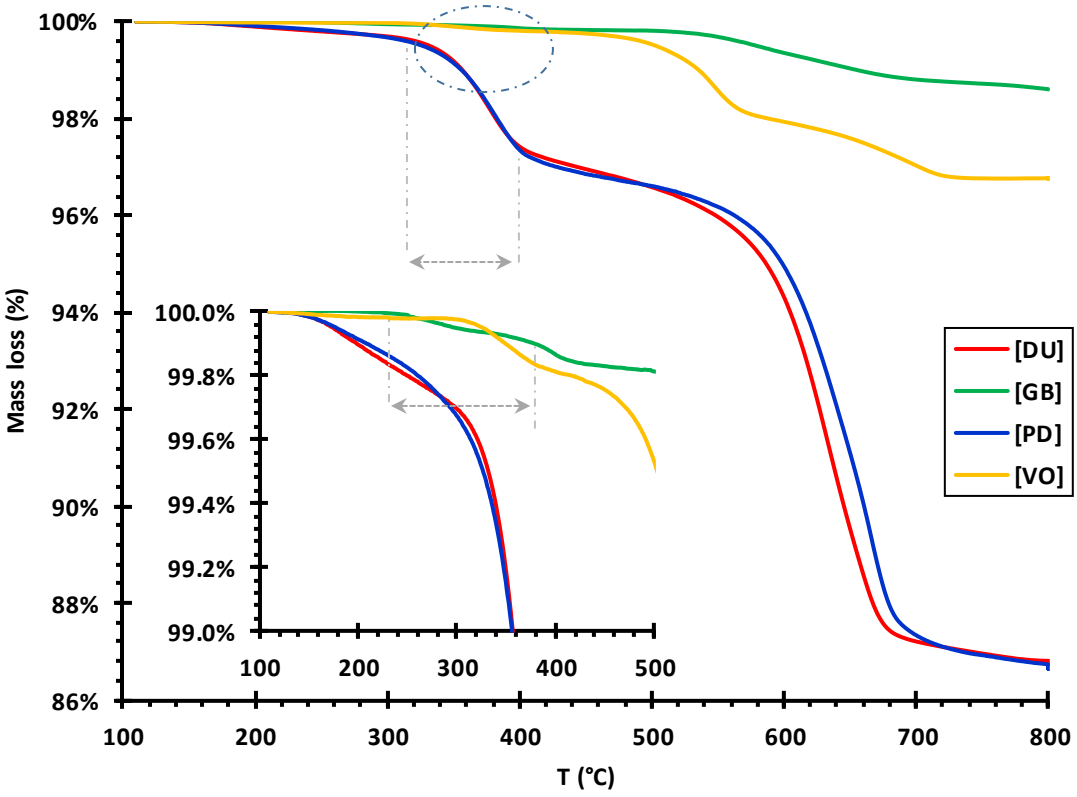

Figure S1. Thermogravimetric data monitoring of [DU], [GB], [PD] and [VO] samples in terms of weight loss (%) due to thermal decomposition. Heating rate = 10 °C/min from room temperature to 110 °C, samples were then kept at 110 °C for 30 min to ensure removal of physically-bound water. Heating rate = 10 °C/min applied from 110 °C to 800 °C under N_2 flow rate = 50mL/min. Inset zooms out in region where [GB] and [VO] decomposition is assigned to dehydroxylation of their brucite component.

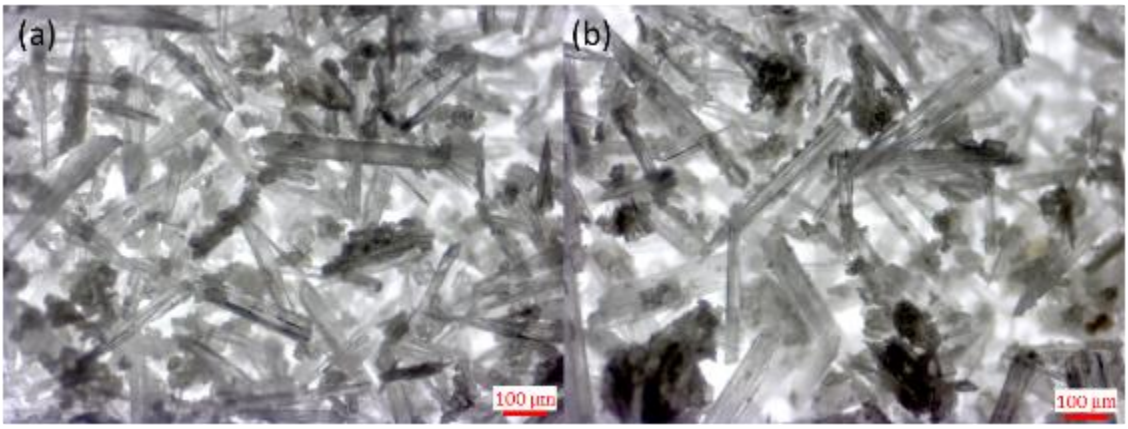

Figure S2. Optical microscopy image of magnesium carbonate crystals (nesquehonite) formed after multiple evaporations of excess water: [DU] (a) and [PD] (b) cells.

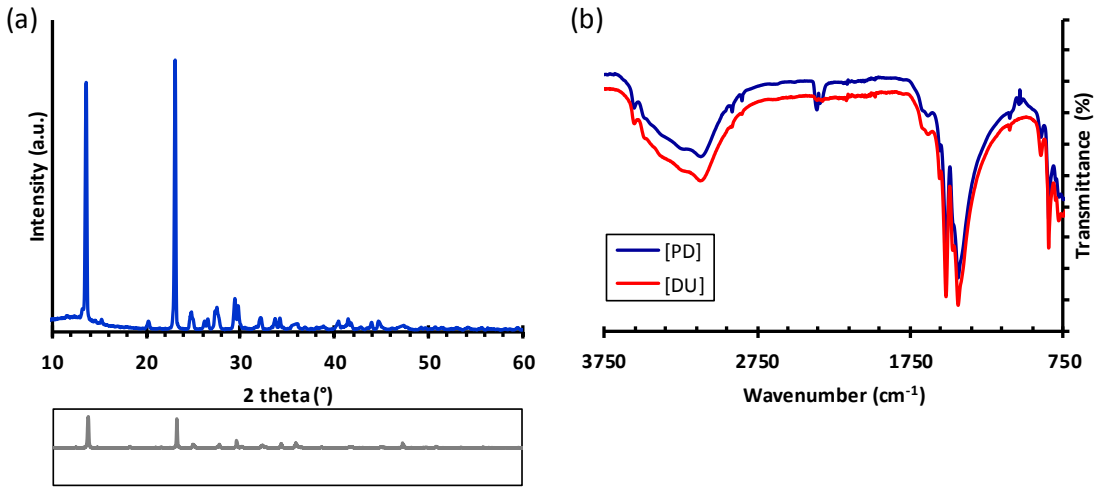

Figure S3. XRD spectrum of white deposits collected from [PD] cell shows major peaks assigned to nesquehonite (a), FTIR spectra of [DU] and [PD] samples between 750 and 3750 cm^{-1}. Note that XRD pattern is in good agreement with nesquehonite ($MgCO_3 \cdot 3H_2O$) reference data (http://rruff.info/nesquehonite/R050639), spectrum drawn in gray color right below figure (a).